

**INTEGRATED NUMERICAL MODELING APPLYING  
STRATIFORM HYDROGEOLOGICAL  
CONCEPTUAL MODEL, SARDON  
CATCHMENT STUDY CASE, SPAIN**

MEHRETEAB YOHANNES WELDEMICHAEL  
February, 2016

SUPERVISORS:  
Dr. Maciek W. Lubczynski  
Drs. Robert Becht



# **INTEGRATED NUMERICAL MODELING APPLYING STRATIFORM HYDROGEOLOGICAL CONCEPTUAL MODEL, SARDON CATCHMENT STUDY CASE, SPAIN**

**MEHRETEAB YOHANNES WELDEMICHAEL**  
Enschede, The Netherlands, February, 2016

Thesis submitted to the Faculty of Geo-Information Science and Earth Observation of the University of Twente in partial fulfilment of the requirements for the degree of Master of Science in Geo-information Science and Earth Observation.  
Specialization: Water Resources and Environmental Management (WREM)

**SUPERVISORS:**  
Dr. Maciek W. Lubczynski  
Drs. Robert Becht

**THESIS ASSESSMENT BOARD:**  
Prof. Dr. Z. Su (Chair)  
Dr. A. (Alain) Frances (External Examiner, National Laboratory for Energy and Geology (LNEG))



#### DISCLAIMER

This document describes work undertaken as part of a programme of study at the Faculty of Geo-Information Science and Earth Observation of the University of Twente. All views and opinions expressed therein remain the sole responsibility of the author and do not necessarily represent those of the Faculty.

**THIS WORK IS DEDICATED TO MY BELOVED FAMILY**

## ABSTRACT

Hard-rock aquifers are complex due to their heterogeneity, anisotropy and discontinuity of flow system. These hard-rock aquifers attract attention as they cover large areas and are major sources of water supply in water scarce arid and semi-arid areas. The use of stratiform hydrological conceptual model of hard-rock aquifers developed recently, creates a hope for better results of water resources exploration and evaluation than the classical conceptual model developed previously.

The overall objective of the study is to understand dynamics of surface-groundwater interactions in hard-rock aquifers applying stratiform hydrological conceptual model into integrated hydrological numerical model of Sardon Catchment (~80 km<sup>2</sup> in Spain) of hard rock aquifer, calibrated on daily basis throughout 7-year period. The model was developed using MODFLOW-NWT code under the ModelMuse Graphical User Interface, where surface-groundwater interactions through unsaturated zone were simulated using Stream Flow Routing (SFR2) and Unsaturated-Zone Flow (UZFI) MODFLOW packages.

Steady-state and transient models were calibrated and validated using 7 years of daily hydraulic heads. In the steady-state calibration: gross recharge, contributed 81.4% and stream leakage 18.6% of the total groundwater inflow. The groundwater outflow consisted of groundwater evapotranspiration 46.8%, stream leakage 40.2%, and groundwater exfiltration 11.3% and lateral outflow at the northern boundary 1.7%.

In transient model simulation: gross recharge contributed 52.2%, stream leakage 43.3% and groundwater storage gain 43% of the total groundwater inflow. Regarding groundwater outflow, groundwater evapotranspiration contributed 24.8 %, stream leakage 23.3%, groundwater exfiltration 12.4% and loss from groundwater storage 37.8% of the total groundwater outflow. When comparing to precipitation,  $R_g = 0.73 \text{ mm day}^{-1}$  represented 49.3 %,  $ET_g = 0.35 \text{ mm day}^{-1}$  - 23.7 %,  $Exf_{gw} = 0.17 \text{ mm day}^{-1}$  - 11.5 %,  $R_n = 0.21 \text{ mm day}^{-1}$  - 14.2 %,  $\Delta S = 0.08 \text{ mm day}^{-1}$  - 5.4% and  $q_g = 0.02 \text{ mm day}^{-1}$  -1.4 % of precipitation.

The calibrated transient model showed temporally and spatially variable patterns of groundwater fluxes. Regarding temporal patterns:  $4.5 \times 10^{-5}$  (September) to  $12.8 \text{ mm day}^{-1}$  (October) with an average of  $0.73 \text{ mm day}^{-1}$ ;  $Exf_{gw}$  from  $0.01 \text{ mm day}^{-1}$  (August) to  $3.15 \text{ mm day}^{-1}$  (February),  $ET_g$  from  $0.03 \text{ mm day}^{-1}$  (November) to  $1.34 \text{ mm day}^{-1}$  (June),  $ET_{un}$  from  $0 \text{ mm day}^{-1}$  (June-October) to  $2.68 \text{ mm day}^{-1}$  (August) and  $R_n$  from  $-1.1 \text{ mm day}^{-1}$  (May) to  $10.1 \text{ mm day}^{-1}$  (October) with an average of  $0.21 \text{ mm day}^{-1}$ . The groundwater flux variability corresponds mainly with seasonal variability of driving forces changing from dry to wet season but differing also between years that can be “dry” with rain in order on order on  $317.5 \text{ mm year}^{-1}$  (2009) but also “wet” with rain in order of  $744.6 \text{ mm year}^{-1}$  (2010). Regarding spatial patterns, the spatial variability of groundwater fluxes was large and particularly distinct when applying spatio-temporally variable driving forces inputs; as compared to temporally variable but spatially uniform driving forces,  $\Delta S$  and  $ET_g$ , increased by 62.3 % and 61.9 % respectively while  $R_g$ ,  $q_g$  and  $Exf_{gw}$  decreased by 8.6

%, 14.8 % and 36.8 % respectively. The spatial variability of input driving forces, enhanced spatial variability of groundwater fluxes

The numerical implementation of the stratiform hydrological conceptual model provided realistic solution although in contrast to one of the assumptions of that concept, it resulted in larger hydraulic conductivity in the shallow saprolite layer than in deeper fissured layer.

Key words: Hard-rock aquifer, groundwater, stratiform hydrogeological conceptual model, steady-state and transient model calibration, groundwater fluxes

## ACKNOWLEDGEMENTS

First of all thanks to God who gave me the power, patience and knowledge to finish this study successfully with full health.

I offer my sincere appreciation for the scholarship opportunities provided by Joint Japan/World Bank Graduate Scholarship Program (JJ/WBGSP) to study at university of Twente, ITC. I am also grateful to Ministry of Agriculture Maekel zone branch, Ministry of agriculture the state of Eritrea and Maekel zone administration for allowing me to participate in this M.Sc. program.

I would like to extend my warm and heartfelt appreciation to my supervisor, Dr Maciek Lubczynski, for his relentless, invaluable and critical comments, advice and encouragement during the study and his assistance and guidance during the field work. I would like also to express my appreciation for my second supervisor, Dr. Robert Becht.

This study could not have been accomplished without the support of Richard B. Winston from USGS the developer of Modelmuse GUI, GW-chart and Listing analyst, for his effort in answering technical questions regarding the models, in pin out problems and finding solutions to my model to the successful model run and simulation.

My thanks also goes to the following individuals: Alain Pascal Francés for providing me raw data and the conceptual model that assisted me during this study; Tanvir Hassan Research Fellow from Bangladesh in providing data related to my research and helping when I faced problem in running the model; Richard Niswonger from USGS in giving some technical support about MODFLOW-NWT and Modelmuse GUI; Amr EL Zehairy, Assistant Lecturer, Mansoura University Mansoura, Egypt who gave me some comments on Modelmuse; Philipo Hezron from Tanzania and Mshindo Omar from Zanzibar former students of ITC in giving comments for successful run of the model; Patrick Lachassagne from France in providing me with journals and technicalities related to hydrological conceptual model of hard-rock aquifers and SuriNaidu L. from India in answering technical questions.

I am grateful to Mr Arno van Lieshout, the Course Director of the Department of Water Resources and Environmental Management in allowing to purchase latest book “Applied groundwater Modeling”, staffs members of Water Resources and Environment Management (WREM) Department and student affairs for their technical and administrative support.

My special thanks go to the members of Habesha community who make my stay in ITC very enjoyable and unforgettable, I felt with them as if I am with my friends back home.

At last but not least, I would like express my heartfelt love and gratitude to my family: my mother, father, brothers and sisters for their moral encouragement when I stay away home.

# TABLE OF CONTENTS

---

1.	INTRODUCTION .....	1
1.1.	General bckground .....	1
1.2.	Modeling of hard-rock aquifers .....	3
1.3.	Research setting.....	4
1.3.1.	Research objective.....	4
1.3.2.	Research question.....	4
1.3.3.	Research hypothesis and assumptions .....	4
1.3.4.	Novelty of the study .....	5
1.4.	Description of the study area .....	5
1.4.1.	Study area.....	5
1.4.2.	Monitoring network.....	6
1.4.3.	Climate .....	6
1.4.4.	Topography and Land cover .....	7
1.4.5.	Hydrogeology and drainage.....	8
1.4.6.	Groundwater level (potentiometric head) .....	9
2.	Research method and materials .....	10
2.1.	Methodolgy flow chart .....	10
2.2.	Data collection and model input preparation.....	11
2.2.1.	Precipitation .....	11
2.2.2.	Potential evapotranspiration.....	11
2.2.3.	Stream discharge.....	12
2.2.4.	Interception.....	12
2.2.5.	Infiltration rate.....	13
2.2.6.	Runoff.....	13
2.3.	Conceptual hydrogeological model .....	13
2.4.	Numerical model.....	14
2.4.1.	Software selection.....	15
2.4.2.	Aquifer geometry and grid setup .....	15
2.4.3.	Boundary conditions.....	16
2.4.4.	Hydraulic properties .....	19
2.4.5.	Head observations (HOB).....	19
2.5.	Water budget.....	19
2.6.	Model calibration and driving forces .....	21
2.6.1.	Steady-state model calibration.....	21

2.6.2.	Warming-up period for transient model calibration.....	22
2.6.3.	Transient model calibration.....	22
2.7.	Error assessment and sensitivity analysis .....	22
2.7.1.	Error assessment .....	22
2.7.2.	Sensitivity analysis .....	23
2.8.	Post-calibration.....	23
2.8.1.	Validation.....	23
2.8.2.	Transient simulation with spatio-temporally variable UZF1 driving forces.....	24
3.	RESULT AND DISCUSSION.....	25
3.1.	Meteorological and Hydrological analysis result .....	25
3.1.1.	Metrological data analysis.....	25
3.1.2.	Infiltration rate.....	25
3.2.	Steady-state model calibration.....	26
3.2.1.	Calibrated head and error assessment.....	26
3.2.2.	Hydraulic conductivities.....	28
3.2.3.	Water budget of the steady-state simulation.....	30
3.2.4.	Groundwater fluxes spatially .....	33
3.2.5.	Sensitivity analysis .....	34
3.3.	Transient state model calibration.....	36
3.3.1.	Calibrated heads and error assessment .....	37
3.3.2.	Hydraulic conductivity.....	40
3.3.3.	Specific yield and specific storage.....	41
3.3.4.	Groundwater budget.....	42
3.3.5.	Temporal variability of groundwater fluxes .....	43
3.3.6.	Yearly transient and steady-state groundwater fluxes for the entire model domain .....	45
3.3.7.	Mean Mass water balance for the entire transient model .....	45
3.3.8.	Sensitivity analysis .....	47
3.4.	Validation.....	49
3.4.1.	Calibrated head and error assessment.....	49
3.4.2.	Transient simulation with spatio-temporally variable UZF1 driving forces.....	49
4.	CONCLUSION AND RECOMMENDATION.....	53
4.1.	Conclusion.....	53
4.2.	Recommendation .....	54

## LIST OF FIGURES

---

Figure 1: The classical concept of discontinuous aquifer.....	2
Figure 2: Stratiform conceptual model of the structure and hydrogeological properties of hard rock aquifers.....	3
Figure 3: Location of Sardon catchment.....	5
Figure 4: Monitoring systems and ADAS stations of study area .....	6
Figure 5: Daily precipitation ( $P$ ), reference evapotranspiration ( $ET_0$ ) and mean temperature of Sardon catchment.....	7
Figure 6: Topographic maps of Sardon catchment: (a) Elevation map and (b) Digital Elevation Model (DEM) .....	8
Figure 7: Calibrated heads .....	9
Figure 8: Flow chart for methodologies applied and the processes followed during the study.....	10
Figure 9: Schematic cross-section of the Sardon catchment .....	14
Figure 10: Schematic cross-section transversal to the main, Sardon catchment valley hydrogeological conceptual model of the Sardon catchment.....	14
Figure 11: Boundary condition of Sardon catchment.....	16
Figure 12: Schematic representation of MODFLOW-NWT that integrates UZF1 and SFR2 packages ...	18
Figure 13: Precipitation ( $P$ ), infiltration rate ( $Inf$ ), interception loss rate ( $I$ ) and potential evapotranspiration ( $PET$ ) .....	25
Figure 14: Relationship between simulated and observed head in the Sardon catchment for steady-state condition of 12 observation points averaged for hydrologic year of 2008 to 2014.....	26
Figure 15: Residuals vs. observed head of the steady-state simulation .....	27
Figure 16: Calibrated head distribution (a) first layer and (b) second layer of the steady-state model simulation.....	28
Figure 17: Calibrated horizontal hydraulic conductivity ( $K_H$ ) distribution map: (a) first layer and (b) second layer after calibration in steady-state condition [ $m\ day^{-1}$ ].....	29
Figure 18: Schematic representation volumetric budget for the entire model of Sardon catchment for steady-state model simulation [all units are $mm\ day^{-1}$ ].....	32
Figure 19: Groundwater evapotranspiration map of Sardon catchment for calibrated steady-state condition.....	33
Figure 20: Groundwater exfiltration map of Sardon catchment for steady-state condition; non-zero individual cells within the outcrops represent direct exfiltration from the fissured layer.....	33
Figure 21: Gross recharge ( $R_g$ ) map of the Sardon catchment at steady-state model simulation .....	34
Figure 22: Sensitivity of model for horizontal hydraulic conductivity ( $K_H$ ) and vertical hydraulic conductivity ( $K_V$ ) for steady-state model simulation .....	35
Figure 23: Sensitivity of model for UZF1 package parameter and driving force.....	35
Figure 24: Sensitivity of model for UZF1 package variables.....	36

Figure 25: Scatter plot of the mean of daily differences between observed and simulated heads for the transient model simulation in the period from 01 October 2008 to 30 September 2013 for 12 groundwater monitoring points.....	37
Figure 26: Calibrated head distribution (a) first layer and (b) second layer of the transient model simulation.....	38
Figure 27: 7-year, transient model simulation consisting of 3 steps .....	40
Figure 28: Specific yield after transient model calibration for the first layer for simulation period 01 October 2007 to 30 September 2013.....	41
Figure 29: Schematic representation of groundwater budget for the entire model of Sardon catchment obtained as a result of transient model calibration within the period 01 October 2007-30 September 2013 (all units are mm day <sup>-1</sup> ).....	43
Figure 30: The transient calibrated groundwater exfiltration ( $Exf_{gw}$ ), groundwater evapotranspiration ( $ET_g$ ), gross recharge ( $Rg$ ) and net recharge ( $Rn$ ) groundwater fluxes for 6-year periods from 01 October 2007 to 30 September 2013.....	44
Figure 31: The transient calibrated unsaturated zone evapotranspiration ( $ET_m$ ) and groundwater evapotranspiration ( $ET_g$ ) for 6-year periods (01 October 2007 to 30 September 2013).....	44
Figure 32: Yearly volumetric change of ground storage within six hydrological years (01 October 2007 to 30 September 2013): (a) yearly groundwater storage; (b) cumulative change in storage.....	45
Figure 33: Sensitivity analysis of hydraulic parameters on head of groundwater through the change of Root Mean Square Error (RMSE).....	47
Figure 34: Sensitivity analysis of storage coefficients on head of groundwater through the change of Root Mean Square Error (RMSE).....	47
Figure 35: Sensitivity analysis of UZF1 package inputs on head of groundwater through the change of Root Mean Square Error (RMSE).....	48
Figure 36: Sensitivity analysis of UZF1 (a) Brooks-Corey-Epsilon, (b) saturated water content and (c) Maximum unsaturated vertical conductivity.....	49
Figure 37: Scatter plot between observed and simulated heads for validation of model for one year (01 October 2013 to 30 September 2014) for 7 groundwater monitoring points.....	49
Figure 38: Temporal variability of groundwater fluxes for fixed and variable inputs for 1-year model simulation.....	50
Figure 39: Groundwater gross recharge map for the last stress period 30 September 2014: (a) Spatially and temporally variable driving forces (b) spatially fixed driving forces [mm day <sup>-1</sup> ].....	51
Figure 40: Groundwater evapotranspiration map for the last stress period 30 September 2014: (a) Spatially and temporally variable driving forces (b) spatially fixed driving forces [mm day <sup>-1</sup> ].....	51
Figure 41: Groundwater exfiltration map for the last stress period 30 September 2014: (a) Spatially and temporally variable inputs (b) spatially fixed inputs [mm day <sup>-1</sup> ].....	52

## LIST OF TABLES

---

Table 1: Parameters of the hydrogeological conceptual model.....	19
Table 2: Observed and simulated head with calculated error assessment for 12 piezometers in meters ....	27
Table 3: Statistical analysis of hydraulic conductivity for steady-state simulation period of the first and second layers of Sardon catchment.....	29
Table 4: Total water balance of Sardon catchment aquifer at steady-state condition.....	30
Table 5: Water balance of land surface and unsaturated zone in steady-state condition ( $\text{mm day}^{-1}$ ).....	30
Table 6: Water balance of groundwater (saturated zone) in steady-state condition ( $\text{mm day}^{-1}$ ) .....	31
Table 7: Groundwater fluxes for steady-state condition for the first and second layer ( $\text{mm day}^{-1}$ ).....	32
Table 8: Statistical analysis result for 6-year transient model simulation for 12 groundwater monitoring points (hydrological years 1 October 2007 to 30 September 2013) [ meters] .....	38
Table 9: Statistical analysis of hydraulic conductivity in the transient model simulation for the first and second layer of Sardon catchment .....	41
Table 10: Groundwater budget of the entire model obtained as a result of the transient model calibration within the period (01 October 2007 to 30 September 2013).....	42
Table 11: Water balance yearly means as a result of 7-year MODFLOW-NWT.....	46
Table 12: Water balance for entire model, unsaturated and saturated zones for transient model simulation for six hydrological years (01 October 2007 to 30 September 2013) [all units are in $\text{mm year}^{-1}$ ] .....	46
Table 13: Groundwater budget for spatially uniform and spatio-temporally variable driving forces for the entire model domain (all units $\text{m day}^{-1}$ ).....	50

## LIST OF ABBREVIATIONS

---

$\Delta S$	Change in storage
ADAS	Automated Data Acquisition System
b.g.s	Below ground surface
DA	Discrete Fracture
DEM	Digital elevation Model
DP	Dual Porosity
EPM	Equivalent Porous Medium
ERT	Electrical Resistivity Tomography
ET <sub>g</sub>	Groundwater evapotranspiration
ET <sub>o</sub>	Reference Evapotranspiration
ET <sub>ss</sub>	Subsurface evapotranspiration
ET <sub>Un</sub>	Unsaturated zone evapotranspiration
ETXWC	Extinction water content
Exf <sub>gw</sub>	Groundwater Exfiltration
EXTDP	Extinction depth
FAO	Food and Agriculture Organization
GHB	General Head Boundary
GSFLOW	Groundwater and Surface Flow
GUI	Graphical User Interface
GW	Groundwater
HOB	Head Observation package
HRA	Hard-Rock Aquifer
I	Canopy Interception
K <sub>c</sub>	Crop Coefficients
K <sub>H</sub>	Horizontal Hydraulic Conductivity
K <sub>V</sub>	Vertical Hydraulic Conductivity
m a.s.l	Meters above sea level
MAE	Mean Absolute Error
ME	Mean Error
MODFLOW	MODulr three dimensional finite difference groundwater Flow model
NWT	Newtonian
PET	Potential Evapotranspiration
q	Stream discharge at the outlet of the catchment
q <sub>g</sub>	Lateral groundwater outflow across the northern catchment outlet
q <sub>gs</sub>	Stream discharge from groundwater to stream
<i>Qi</i>	<i>Quercus ilex</i>

$q_{in}$	Lateral groundwater inflow across the northern catchment outlet
$Qp$	<i>Quercus pyrenaica</i>
$q_{sg}$	Stream discharge from stream to groundwater
Rg	Gross recharge (UZF recharge)
RMSE	Root Mean Square Error
SA	Stratiform Aquifer
SFR2	Stream Flow Routing 2
SS	Specific Storage
SY	Specific Yield
UPW	Upstream Weighting Package
UZF	Unsaturated-Zone Flow package of MODFLOW
VES	Vertical Electrical Sounding
WTD	Water Table Depth

# 1. INTRODUCTION

## 1.1. General background

Hard-rock aquifers (HRA) are complex due to their heterogeneity, anisotropy and discontinuity of the flow system (Meijerink et al., 1999; Hassan et al., 2014). These factors make complicated to understand the flow behaviour of groundwater in hard-rocks. Reliable and representative conceptual model of such rock areas is vital for groundwater assessment in general and for HRA in particular, pertaining its complexity.

The classical conceptual model developed for HRA considers HRA aquifers as discontinuous systems. In the classical conceptual model, fractured materials are represented either by Equivalent Porous Medium (EPM), Dual Porosity (DP) or Discrete Fractures (DF) models (Anderson & Woessner, 1992). In EPM approach, the heterogeneity of fractured rock systems is modelled using a small number of regions rather than treating individually (Nyende et al., 2013). The DP models apply to rock matrix with significant primary permeability (Anderson & Woessner, 1992). This approach assumes, the medium separated into two distinct superpositioned pore systems, these are fractured pore system and less permeable matrix pore system. The pore systems are treated as homogeneous media with separate hydraulic property and they interact by exchanging water in response to pressure head (Gerke & Van Genuchten, 1993). The DF models apply to fractured media with low primary porosity assuming water moves only through the fracture network (Anderson & Woessner, 1992). The recently developed hydrological conceptual model of Stratiform Aquifer (SA) (Courtois et al., 2010; Dewandel et al., 2006), emphasizes on the importance of the individual weathered and fissured/fractured layers of crystalline rocks in conjunction with their hydrodynamic properties. The hydrodynamic properties of stratiform HRA are an aggregation of hydrodynamic properties of each layer in the composite aquifer. This study applied the hydrological conceptual model of stratiform aquifer in the Sardon catchment, Spain.

Groundwater and surface water is considered as one management unit in hydrologic cycle and integrated models (Ala-aho et al., 2015). They are interrelated and interact in a different ways in the physiographic and climatic landscapes (Sophocleous, 2002). Surface water that recharges groundwater and the groundwater that exfiltrates or evaporates to the surface, are important interaction aspects of the hydrologic cycle. Hence, an understanding of the basic principles of interactions between groundwater and surface water is needed for effective management of water resources. Surface-groundwater interaction is a hydrologic process that occurs through vertical and lateral exchange of fluxes between surface water and groundwater systems through unsaturated zone. The interactions can also occur through flows in fractures or solution channels in the case of fractured rocks or karst (Sophocleous, 2002).

Hard-rock aquifers (granites and metamorphic rocks) cover large areas in the world (Lachassagne et al., 2008) and typically occupy the first 100 meters from the ground surface (Taylor & Howard, 2000). These aquifers are characterized by insignificant primary porosity and their hydraulic properties are mainly controlled by secondary porosity which is developed due to weathering and fracturing (Shikhar, 2011). Even though the discharge from HRAs per productive well is small (from 2 to 20 m<sup>3</sup> h<sup>-1</sup>), they are good source of water supply in arid and semi-arid areas where the surface water resources are limited (Lachassagne et al., 2014; Ahmed et al., 2008; Lachassagne et al., 2008).

Numerical distributed models are developed as tools to understand groundwater systems and to guide and support the decision making process on water resources management (Meijerink et al., 1999; Lubczynski & Gurwin, 2005; Yao et al., 2015). Numerical groundwater modeling begins with a conceptual understanding of the physical problem (Anderson & Woessner, 1992). Conceptual models have been developed for HRAs. The classical concept, which is developed in the seventies is known as concept of discontinuous aquifer ( Lachassagne et al., 2008 after Detay et al., 1989) (Figure 1). The discontinuity is due to the discrete hydraulic conductivity and considers the water bearing zones as tectonic open fractures (Courtois et al., 2010; Lachassagne et al., 2008).

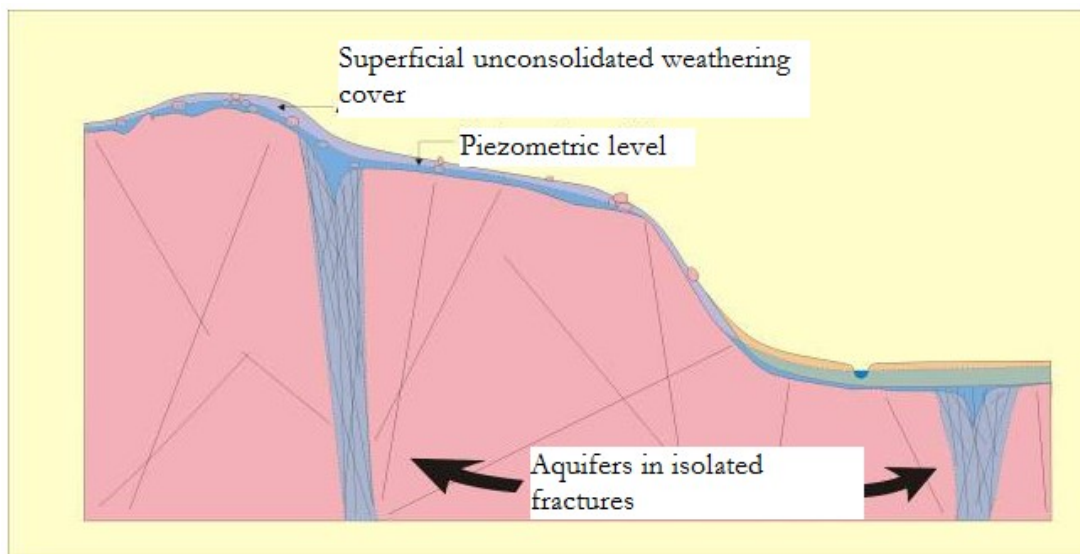


Figure 1: The classical concept of discontinuous aquifer , after Lachassagne et al. (2008)

Continuum approach is adapted recently to HRA. The new concept developed based on the continuity of fractures/fissures resulted from weathering process. Weathering process creates a typical weathering profile which comprises laterite, saprolite and fissured layer (Figure 2). The saprolite has typically a storage function and the underlying fissured layer has a transmissive function (Dewandel et al., 2006; Wyns et al., 2004). The fissured layer is generally characterized by dense horizontal fissures and depth-decreasing sub-horizontal and vertical fissures (Lachassagne et al., 2011).

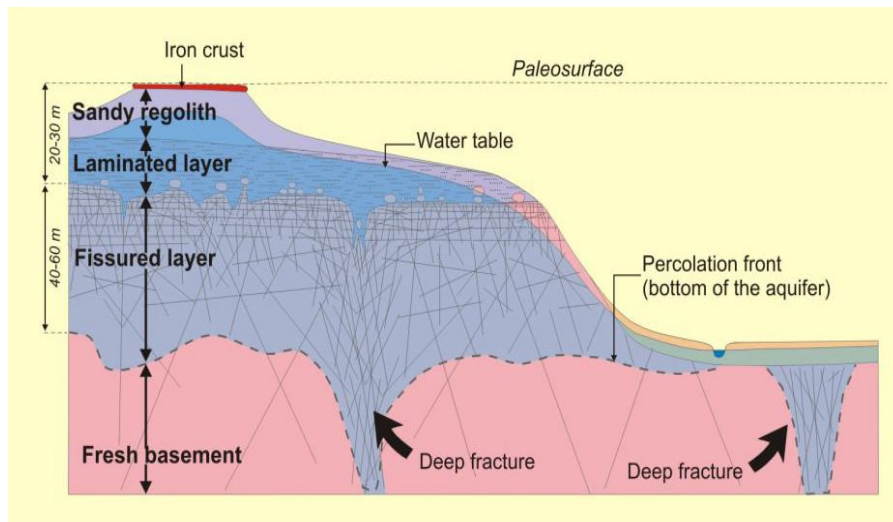


Figure 2: Stratiform conceptual model of the structure and hydrogeological properties of hard rock aquifers , after Wyns et al. (2004)

The Sardon catchment, is selected as study area because of its small size, well defined physical boundaries, low human impact, semi-arid conditions, typical fractured granite rocks and land cover with standard hard-rock hydrology problems (Lubczynski & Gurwin, 2005). This study is to develop integrated hydrological numerical model of the Sardon hard rock aquifer based on the stratiform hydrological conceptual model proposed by Francés et al. (2014) throughout 7-year period (hydrological years 01 October 2007 to 30 September 2014).

## 1.2. Modeling of hard-rock aquifers

Groundwater flow in HRA attracts attention as a source of potable water mainly in water scare areas. Starting recently, researches are undergoing to investigate the groundwater flow and to quantify the groundwater resources in these types of aquifers and its link with weathering profile. Sekhar et al. (1994) proposed a double-porosity model based on an aquifer-water table aquitard concept for HRA to compare the result with classical DP model and to investigate the potential use of the proposed model for parameter identification in an isotropic fracture aquifer system. A study conducted in Brittany (France), showed 80% groundwater reserve found in the fissured zone and 20% in unconsolidated laterite layer (Wyns et al., 2004). It has also been tried to prove that fracture permeability of HRA is due to weathering processes (Dewandel et al., 2011; Lachassagne et al., 2011) and to link the hydrodynamics properties of HRA with this weathering processes (Courtois et al., 2010; Dewandel et al., 2006). These researches were based on geological and geophysical surveys, hydraulic tests and a generalized 3-D geological and hydrogeological conceptual model.

Francés et al. (2014) proposed a multi-techniques methodology based on a downward approach that combines remote sensing, hydrogeophysics and hydrogeological field data acquisition to contribute to the design of hydrogeological conceptual models of HRAs in Sardon catchment. They proposed

methodology, which is particularly suitable for data scarce areas. Hassan et al. (2014) applied a transient, integrated hydrologic model in GSFLOW (Groundwater and Surface water FLOW) to evaluate the surface-groundwater interactions calibrated with 18 years of daily groundwater head and stream discharge data. Based on their result, hydrological observations for the Sardon catchment and more generally for hard-rock systems, were made. The study by Hassan et al. (2014) and Lubczynski & Gurwin (2005) applied EPM concept assuming the average flow resembles flow through a porous medium with equivalent, statistically distributed hydraulic parameters represented in the groundwater flow equation by averaging highly fractured and interconnected rocks over a large volume. Nyende et al. (2013) applied MODFLOW-NWT under Modelmuse graphical user interface (GUI). The fractured environment was modelled as a porous medium and concluded that groundwater resources in hard-rocks are associated with weathered and fractured zones and the flow to fractured zones is controlled by their transmissivity or by their structure. A three dimensional ground water flow model was applied for the Osmansagar and Himayathsagar catchments in India with two conceptual layers under transient conditions using visual MODFLOW to quantify the input and output of the groundwater flow in the area (Varalakshmi & Tejaswini, 2012).

In this study, stratiform hydrological conceptual model following conceptual model presented by Frances et al. (2014) was applied to the weathering profile of the HRA of the study area using the MODFLOW-NWT (MODular three dimensional finite difference groundwater Flow ) model (Niswonger et al., 2011) under ModelMuse graphical user interface (Winston, 2009).

### **1.3. Research setting**

#### **1.3.1. Research objective**

To understand dynamics of surface-groundwater interactions in HRAs applying stratiform hydrological conceptual model with specific objectives of setting up numerical distributed model following that concept, calibrate it in steady-state and in transient model and finally to quantify groundwater budget.

#### **1.3.2. Research question**

Does the stratiform hydrological conceptual model provide reliable basis for quantification of HRAs applying numerical modelling technique?

#### **1.3.3. Research hypothesis and assumptions**

It is hypothesized that the calibration of integrated transient numerical model applying stratiform concept could give realistic estimate of the groundwater flow and groundwater budget of HRA provided that the following assumptions are met:

- The interaction between the Sardon catchment aquifer and streams can be realistically simulated using SFR2 (Stream Flow Routing) package of MODFLOW-NWT;

- The fluxes interacting between surface and groundwater domains, i.e. recharge, groundwater evapotranspiration and groundwater exfiltration, can be realistically simulated using the UZF1 (Unsaturated-Zone Flow) package of MODFLOW-NWT.

### 1.3.4. Novelty of the study

The findings of this thesis will augment the existing data and will contribute to the understanding of HRA of the study area by including the following novelties.

1. Application of new concept of continuous stratiform aquifer in hard-rock modelling of subsurface water flow not tested in the Sardon catchment study area yet. All previous studies applied the classical hard-rock conceptual model;
2. Application of modelling tool that was not used before in the Sardon catchment study area; so far MODFLOW under PMWIN environment, Earth and GSFLOW were used. In this study MODFLOW-NWT under ModelMuse environment is applied;
3. Use of recent head data for model calibration that earlier was not used for model calibration.

## 1.4. Description of the study area

### 1.4.1. Study area

The Sardon catchment is located in the Central-Western part of Spain 40 km to the west of Salamanca, Spain. It is bounded in between  $6^{\circ}07' - 6^{\circ}13'$  W longitudes and  $41^{\circ}01' - 41^{\circ}08'$  N latitudes with an altitude ranging from 730 m a.s.l. at the northern boundary (Sardon River outlet) to 870 m a.s.l. at the southern catchment boundary. The catchment is part of the Rio Tormes river basin with estimated area coverage of  $\sim 80 \text{ km}^2$  (Figure 3) (Lubczynski & Gurwin, 2005).

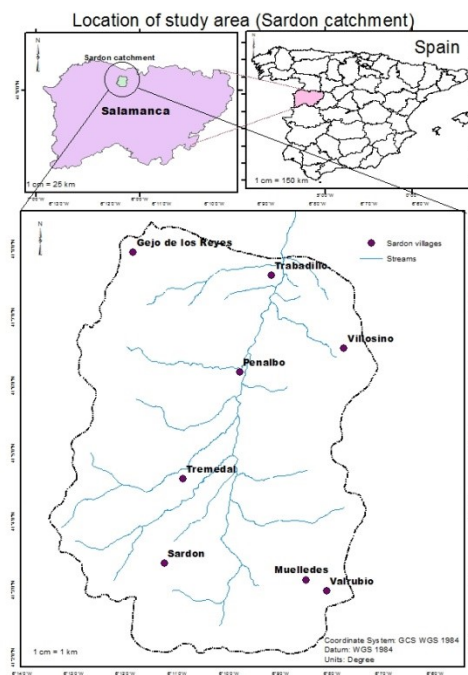


Figure 3: Location of Sardon catchment (data extracted from <http://www.diva-gis.org/Data>)

#### 1.4.2. Monitoring network

The hydrological variables, including climate, stream discharge and groundwater table are monitored by automated hydrological monitoring network (Figure 4). In the Sardon catchment, Automated Data Acquisition System (ADAS) is installed in two locations, in the upper catchment (Trabadillo) and in the lower catchment (Muelledes), to collect climatic data (rainfall, temperature, wind speed, relative humidity, incoming and outgoing radiation). Groundwater levels are monitored by automated groundwater head monitoring water level recorders, such as Tirta, Nivolog and Keller, that record data in an hourly interval. The groundwater levels have been monitored since 1994 and now their number increased with a wider distribution of groundwater level time series data (Francés et al., 2014; Hassan et al., 2014; Lubczynski & Gurwin, 2005). Stream flow at the northern catchment outlet was monitored on an hourly basis from 1997–2001 using steel flume with a capacity of measuring flows  $<145 \text{ l.s}^{-1}$ . To correlate the flow measured by the flume and the fluctuation of groundwater level, a piezometer was installed as adjacent to the flume. The extrapolated from the piezometric records, low flows (baseflow  $<145 \text{ l.s}^{-1}$  are available from 2008 to 2011 on an hourly basis (Hassan et al., 2014).

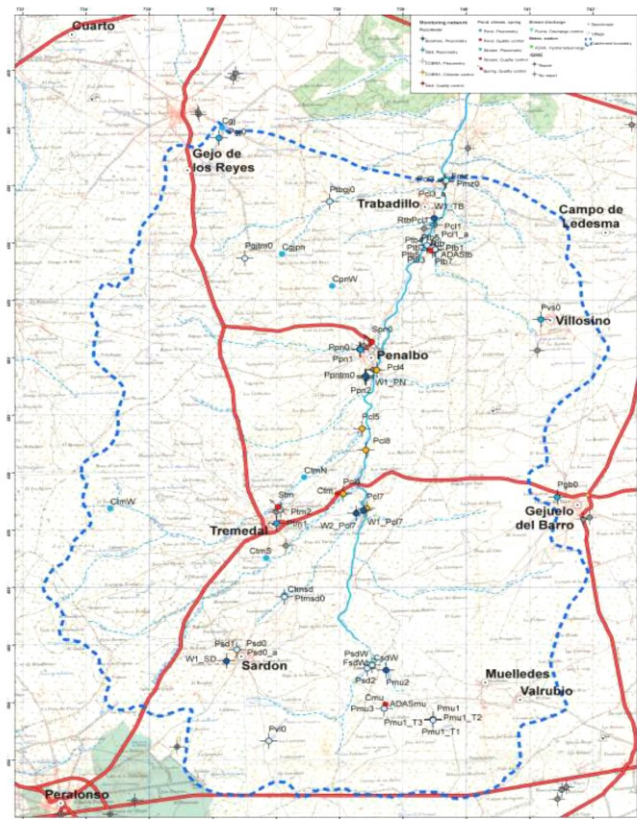


Figure 4: Monitoring systems and ADAS stations of study area , after Francés (2015).

#### 1.4.3. Climate

The climate in the study area is semi-arid, Mediterranean, typical for the central Iberian Peninsula. According to 23-year rainfall estimate obtained from Spanish meteorological institute, based on six rain gauges located in the surroundings of the study area, the Sardon area receives on average  $\sim 500 \text{ mm}$  of

rainfall annually. July and August are identified as the warmest and the driest months with the average temperature of  $\sim 22$  °C, Potential Evapotranspiration ( $PET$ ) on average  $\sim 5$  mm  $day^{-1}$  and rainfall is less than 20 mm  $month^{-1}$ . January and February are the coldest months with an average temperature of 5 °C and the lowest  $PET$  of 0.5 mm  $day^{-1}$  and November and December are the wettest months with precipitation above 100 mm  $month^{-1}$  (Lubczynski & Gurwin, 2005). Figure 5 shows the mean monthly precipitation [mm  $month^{-1}$ ], mean monthly temperature [°C] and  $ET_o$  [mm  $month^{-1}$ ] for the study period at Trabadillo station.

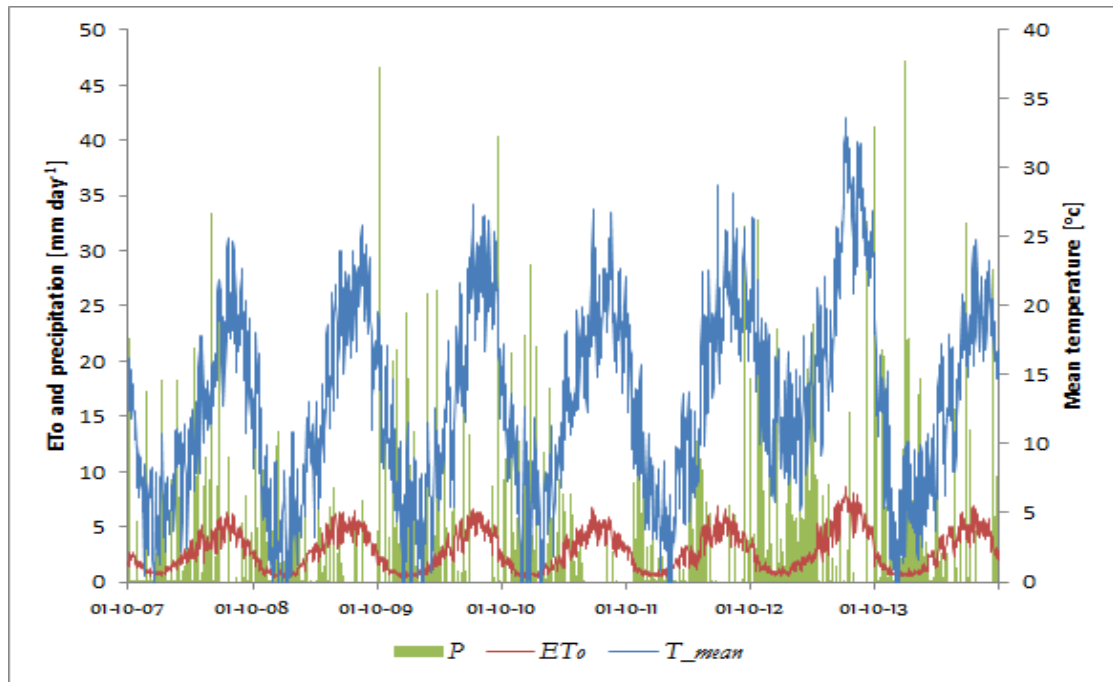


Figure 5: Daily precipitation ( $P$ ), reference evapotranspiration ( $ET_o$ ) and mean temperature of Sardon catchment - Data collected from Trabadillo station for 7 hydrological years from 1 October 2007 to 30 September 2014

#### 1.4.4. Topography and Land cover

Sardon catchment is characterized by undulating topography with elevation ranging from 730 m a.s.l. along the main fault zone to 870 m a.s.l. at the watershed divides of the catchment (Figure 6 a and b). There are ridges and dense network of narrow valleys that resulted from geological structures and weathering processes along the lineaments and intense joint systems in the granitic rock (Rwarinda, 1996). The south, south-east and south-west part of the area, are high elevated areas and in the central part where the major drainage channel is located, the elevation is the lowest. The elevated areas, including catchment boundaries, are composed of quartzite dykes (eastern boundary), massive or fractured granitic outcrops eventually are overlain by thin soil layers. The depression area has thick alluvial and colluvial materials (T'esfai, 2000).

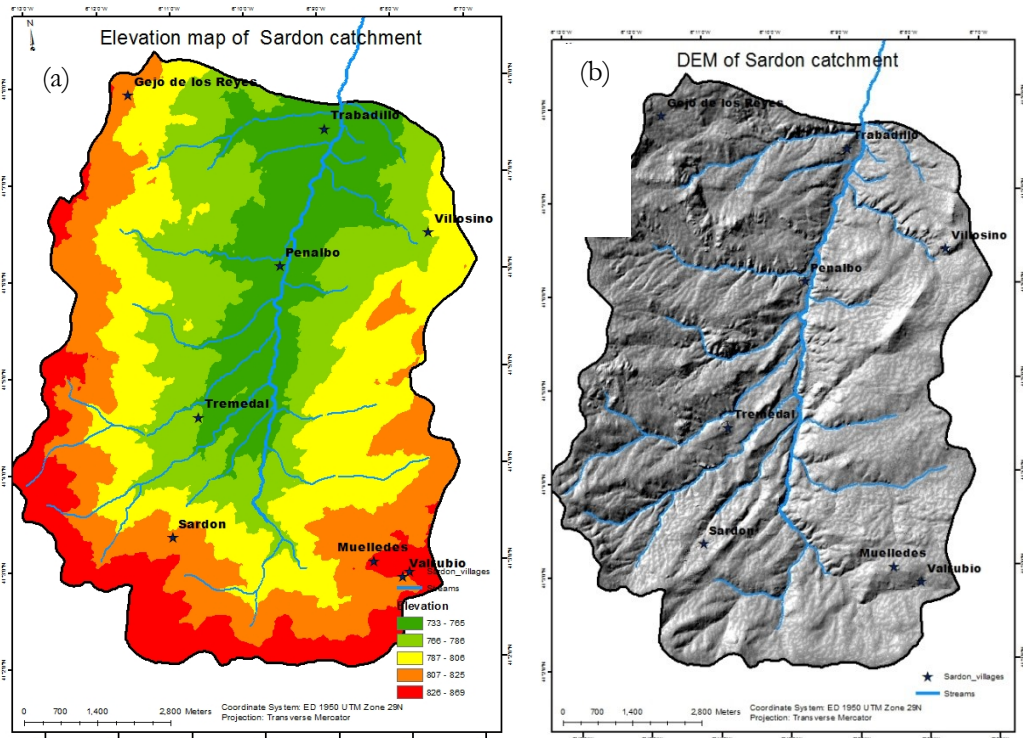


Figure 6: Topographic maps of Sardon catchment: (a) Elevation map and (b) Digital Elevation Model (DEM)

Land use of the study area includes built-up areas, cultivated land, natural vegetation cover and pasture land. The vegetation of the area is characterized by sparsely distributed natural woody-shrub broad leaved vegetation dominated by two types of tree species, namely, evergreen oak *Quercus ilex* (*Q.i*) and broad-leaved, deciduous oak *Quercus pyrenaica* (*Q.p*). There is also shrub known as Scotch Broom (*Cytisus scoparius*) (Lubczynski & Gurwin, 2005). Majority of the area is covered by grasses that start to germinate in March-May, wilt in June and disappears afterwards due to the drying soil and cattle grazing (Francés, 2015). The area is unsuitable for agriculture as the soil is dominated by weathered granite, which has low fertility (Hassan et al., 2014)

#### 1.4.5. Hydrogeology and drainage

The hydrology of Sardon catchment is strongly influenced by weathering and fracturing process. Three hydrogeological layers have been recognized in the area, the top unconsolidated layer (L1), the second fractured granite layer (L2) and impervious massif layer. The unconsolidated, water bearing (saprolite) layer is composed of weathered and alluvial deposits with a thickness of on average 0-5 m up to 10 m with limited spatial extent. It is thick at the valley of Sardon and thin or does not exist in high elevation areas where the outcrops of massif rocks are dominant. The second layer has a thickness of ~ 60 m and is considered as transmissive layer. The third is a massive granite layer of the basement (Lubczynski & Gurwin, 2005). The width of the fault zones is between 30 m and 600 m and the fracture spacing is between few centimetres to several meters (Francés et al., 2014).

The drainage network is dense and largely influenced by the intermittent river Sardon. The rivers are dry from mid-June to mid-October and for the rest of the year perform a role of a drain, mainly for direct and groundwater runoffs. Along the river Sardon course, there is a regional brittle fault zone named as the Sardon fault. The channel-fill structure along that fault, acts as a groundwater drain all year round (Lubczynski & Gurwin, 2005).

#### 1.4.6. Groundwater level (potentiometric head)

The monitoring dataset consists of daily head measurements averaged from hourly measurements at 12 observation points including 4 piezometers (PSDO, PTB2, PPNO and PJGTMO), 3 wells (PGBO, PGJO and PMU1) and 5 deep boreholes (W1TB, W1PN, W1SD, W1PCL7 and W2PCL7). The groundwater table level is not uniform in the entire catchment as measured from the ground surface. It is shallow in the river valleys ranging from 0 to 3 m below ground surface (b.g.s) and deeper at the catchment divides, ranging from 1 to 10 m. Groundwater table has similar potentiometric pattern in both, layers. As unconfined, the water table in the surficial, layer follows the topography of the study area. The hydraulic head distribution has a concentric pattern influenced by the Sardon fault drainage line (Hassan et al., 2014; Lubczynski & Gurwin, 2005) (Figure 7).

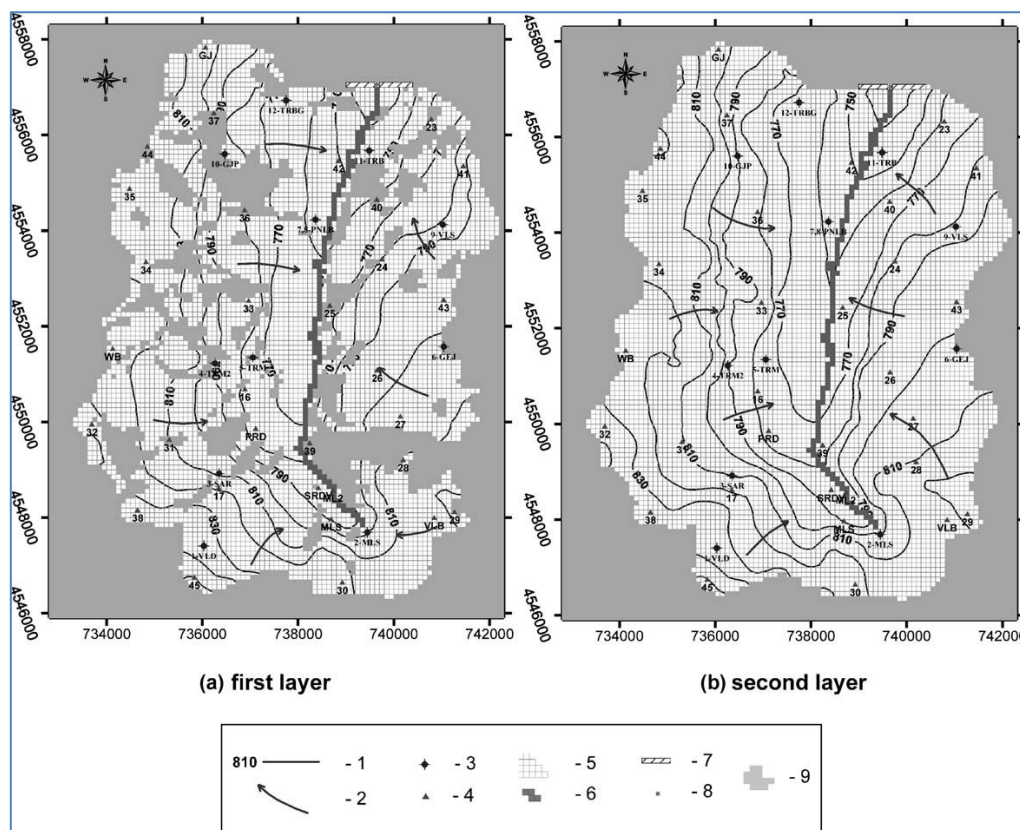


Figure 7: Calibrated heads after Lubczynski & Gurwin (2005): 1–piezometric head; 2–direction of groundwater flow; 3–groundwater monitoring point; 4–groundwater table measurement point; 5–model grid; 6–DRAIN boundary cell; 7–GHB-general head boundary cell; 8– $H = \text{constant}$  cell in transient solution converted to drain boundary; 9–inactive cells.

## 2. RESEARCH METHOD AND MATERIALS

### 2.1. Methodology flow chart

The methodology applied to answer research question and to come-up with the targeted objective is summarized in the flow chart in Figure 8-a and the model calibration process step followed (Figure 8-b).

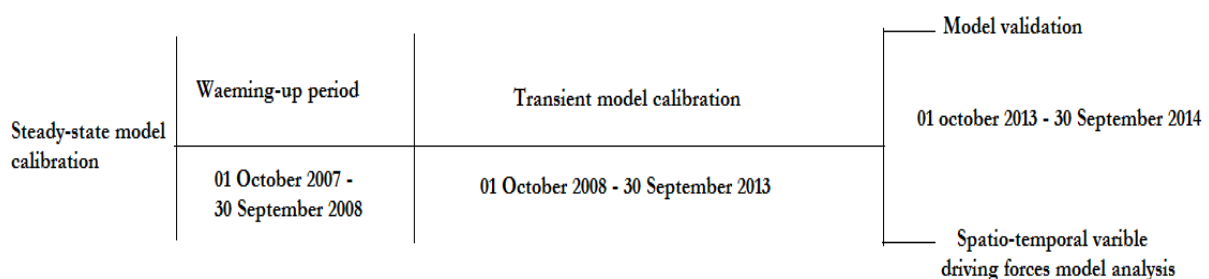
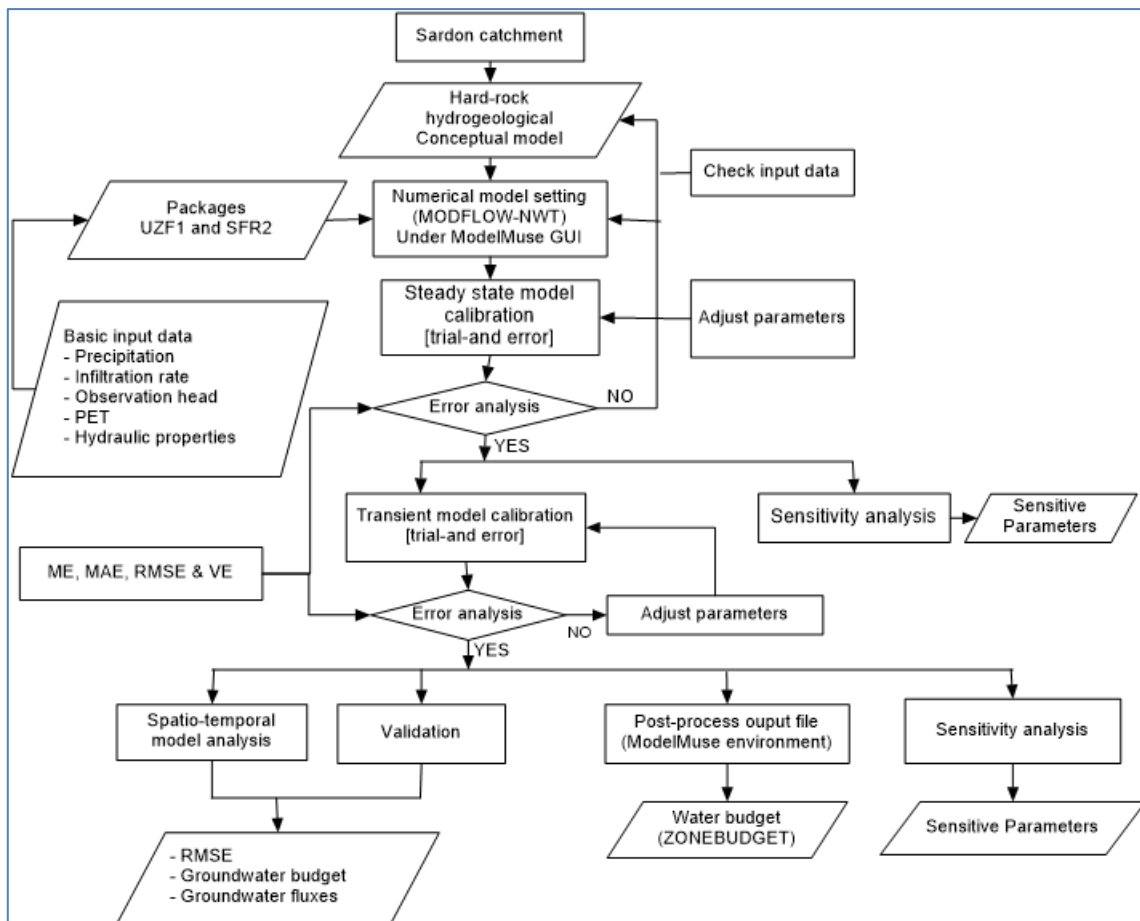


Figure 8: Schematic diagram (a) Flow chart for methodologies applied and the processes followed during the study, (b) model calibration process

## 2.2. Data collection and model input preparation

Data analysis and input preparation is a pre-calibration activity, which is needed to provide the base for effective model simulation. Meteorological and hydrogeological data were collected, analysed and pre-processed according to the model requirement to facilitate model simulation. The model was simulated in daily time steps for 7 hydrological years from 01 October 2007 to 30 September 2014. The sources for these data were the Trabadillo ADAS station and logger-based water level recorders installed in piezometers, dug wells and shallow and deep boreholes (Figure 4).

### 2.2.1. Precipitation

Precipitation is the most important input for hydrological models. Precipitation at land surface is partitioned in UZF1 package (Niswonger et al., 2006) into runoff, infiltration, evapotranspiration, unsaturated-zone storage, and recharge. The tipping bucket rain gauge installed in the Trabadillo station was used to estimate the daily precipitation on hourly basis. This data was aggregated to daily time step in order to match the UZF1 package input requirement. The precipitation collected from Trabadillo ADAS station is considered as representative of the rainfall pattern of Sardon catchment (Lubczynski & Gurwin, 2005)

### 2.2.2. Potential evapotranspiration

McMahon et al. (2013) defined PET as the rate at which evapotranspiration would occur from a large area completely and uniformly covered with growing vegetation which has access to an unlimited supply of soil water, and without advection or heat storage effects. PET is one of the driving forces in the applied modelling solution involving UZF1 package. In UZF1, the PET is applied at the land surface and decreases linearly with depth down to the assigned extinction depth where evapotranspiration no longer occurs (Allander et al., 2014).

There are two methods to convert  $ET_0$  to PET. The first is the single crop coefficient, in which the evapotranspiration differences between reference grass and crop is combined into one single coefficient and depends only on crop characteristics, crop type and growth stage. The second is the dual crop coefficient which requires detailed data of the crop and soil. In this approach, the crop coefficient is split into two factors describing separately the differences in evaporation and transpiration between the crop and reference surface (Allen et al., 1998). Since detailed data about the crop/vegetation and soil of the area is not available, the single crop coefficient ( $K_c$ ) method was applied in this study. Following that method, PET is calculated using Equation 1.

$$PET = ET_0 * K_c \tag{1}$$

Where:  $ET_0$  - reference evapotranspiration [ $\text{mm day}^{-1}$ ] and  $K_c$  - crop coefficient [-]

$ET_0$  for the study year was estimated by general FAO Penman-Montieth equation (Allen et al., 1998) (Equation 2).

$$ET_0 = \frac{0.408\Delta(R_n - G) + \gamma \frac{900}{T + 273} u_2 (e_s - e_a)}{\Delta + \gamma(1 + 0.34u_2)} \quad (2)$$

Where:  $R_n$  - net radiation at the crop surface [ $MJ\ m^{-2}day^{-1}$ ],  $G$  - soil heat flux density [ $MJ\ m^{-2}day^{-1}$ ],  $T$  - mean daily air temperature at 2 m height [ $^{\circ}C$ ],  $U_2$  - wind speed at 2 m height [ $m\ s^{-1}$ ],  $e_s$  - vapour pressure [kPa],  $e_a$  - actual vapour pressure [kPa],  $e_s - e_a$  saturation vapour pressure deficit [kPa],  $\Delta$  - slope of vapour pressure curve [ $kPa\ ^{\circ}C^{-1}$ ],  $g$  - psychrometric constant [ $kPa\ ^{\circ}C^{-1}$ ].

The general FAO Penman-Montieth equation is the recommended approach to calculate  $ET_0$  by the scientific community (Wang et al., 2012). The  $K_c$  value to convert  $ET_0$  to  $PET$  was estimated for the study area in two steps in order to account for the land use and vegetation type. Firstly, the combined  $K_c$  for grass and bare soil was determined by weighted average of the two, weighting their areal contributions based on the dominance in one year time. Grass is dominant for three months of a year (25%) and the rest nine months (75%) is bare soil (Francés, 2015). The  $K_c$  of grass was taken as 0.75 and for bare soil as 0.61 (average of the minimum and maximum for dry and wet soil condition) (Allen et al., 1998). The combined, weighted  $K_c$  value for bare soil and grass was 0.65. The second step was to estimate  $K_c$  for the entire area based on weights of all contributing land covers so, including trees. The combined weight of bare soil/grass and trees was also assigned according to their areal coverage ratio with respect the total area of the Sardon catchment. The tree covers 7% of Sardon catchment and the grass/bare soil 93 % of (Reyes-Acosta & Lubczynski, 2013). The  $K_c$  of trees was assigned as 1 (Allen et al., 1998). The final weighted  $K_c$  of Sardon area was 0.67. That  $K_c$  and applied to Equation 1 convert to  $ET_0$  to  $PET$ . Such  $PET$  was finally applied in each cell of the model as spatially uniform in the steady-state model calibration and as temporary variable in transient model calibration.

### 2.2.3. Stream discharge

Sardon stream flow data for the year 1997 to 2001 was obtained on hourly basis from trapezoidal, calibrated flume installed at the northern outlet of the Sardon catchment equipped with automatic data recorders. The flume was capable to measure flows  $\leq 145\ l\ sec^{-1}$  (Hassan et al., 2014). A relationship was developed by Hassan et al. (2014) between the flume measured stream flow data and groundwater level fluctuation measured by piezometer installed nearby from 2008-2011 on hourly basis.

### 2.2.4. Interception

Precipitation might reach the ground, as direct rain fall and as stem flow, or can be retain and be evaporated by vegetation canopy interception. The interception rate depends on the type and density of vegetation cover. The interception rate was determined for the sparse tree canopy cover of the two major species in the area  $Q.i$  and  $Q.p$ , which represent  $\sim 7\%$  of the Sardon catchment (Reyes-Acosta &

Lubczynski, 2013). The interception loss rate of  $Q_i$  was taken as 29.6 % of gross precipitation (Pereira et al., 2009) and of  $Q_p$  as 15.95 % of gross precipitation (Berhe, 2010). The tree weighted average interception loss was estimated as 18.5 % of gross precipitation assuming that  $Q_i$  comprises 18.6 % and  $Q_p$  81.4 % of the total canopy coverage in the catchment. The interception loss rate by the rest land cover, grass and other land use, estimated as 3 % of gross precipitation (Berhe, 2010). The interception loss then calculated by Equation 3.

$$I = P * (I_f * A_f + I_{other} * A_{other}) \quad (3)$$

Where  $I$  - canopy interception per grid cell [ $\text{mm day}^{-1}$ ],  $P$  - precipitation  $I_f$  and  $I_{other}$  - interception loss rate by forest and other land use coverage respectively expressed in [%] of precipitation and  $A_f$  and  $A_{other}$  - ratios of area coverage of forest and other land use areas respectively.

### 2.2.5. Infiltration rate

Infiltration rate is the amount of water per surface area per time that percolates to the soil. It is an input for UZF1 package applied at the surface. The infiltration rate was calculated as the difference between precipitation and interception loss as a required by UZF1 package (Niswonger et al., 2006). The average infiltration rate over the 7-year simulation period applied for steady-state was  $1.41 \text{ mm day}^{-1}$ . In the transient model, the infiltration rate input was calculated as daily variable for each time step in order to account for the temporal variability of subsurface fluxes.

### 2.2.6. Runoff

Runoff is a result of precipitation in the form of excess infiltration and saturation excess (rejected infiltration) runoff that flow into the streams (Niswonger et al., 2006) and as groundwater discharged through seepage faces, hereafter referred as groundwater exfiltration, when groundwater levels are above land surface (Viridi et al., 2013). In MODFLOW-NWT, runoff is an input to the SFR2 MODFLOW-NWT package where stream flow is simulated. The UZF1 Package of MODFLOW-NWT provides a method in which daily-averaged values of overland runoff and saturation excess runoff can be simulated (Niswonger et al., 2006). "The routing of discharge to streams and lakes" (IRUNFLG) option was selected in UZF1 in order to route discharge to streams as runoff.

## 2.3. Conceptual hydrogeological model

Conceptual model of groundwater system as defined by Anderson & Woessner (1992) is a pictorial representation of that system. The hydrostratigraphic unit, flow system and water budget are the basics steps to set up the conceptual model. Hydrostratigraphic units are geologic units with similar hydrogeological properties. The study area has two hydrostratigraphic units identified by Lubczynski & Gurwin (2005), the unconfined saprolite upper layer and the confined fissured second layer (Figure 9).

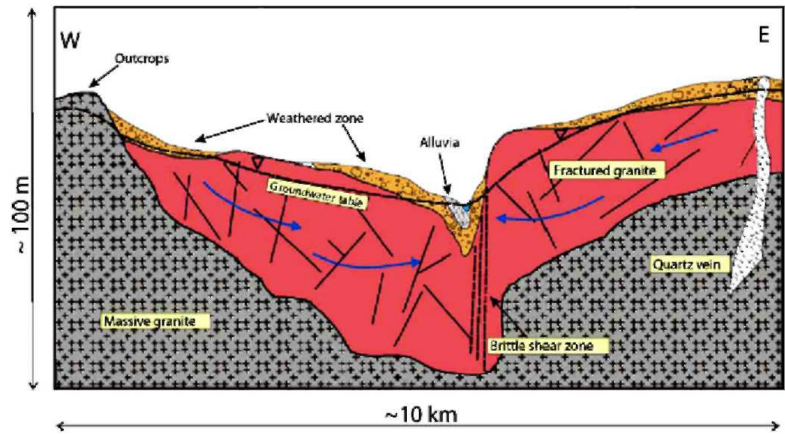


Figure 9: Schematic cross-section of the Sardon catchment , after Lubczynski & Gurwin (2005)

Francés et al. (2014) further identified six types of internally uniform zones in the saprolite and fissured layers that control the dynamics of the hydrogeological system at the catchment scale along the faults (F1) and (F2). These zones are L1-F1: saprolite along the F1 fault zone; F2/3: saprolite along the F2/F3 fault sets; L1: saprolite outside the fault zones; F1fissured layer along the F1 fault zone; F2/3: fissured layer along the F2/F3 fault sets; L2: fissured layer outside the fault zones (Figure 10). This conceptual model was applied in this study to understand the dynamics of the fractured hard-rocks system of the area.

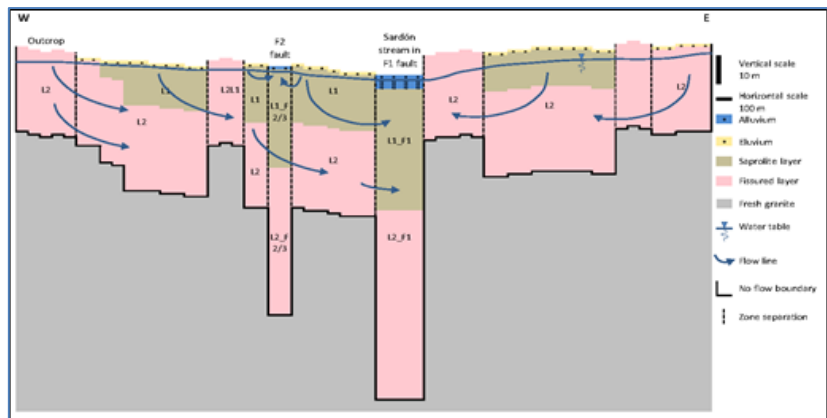


Figure 10: Schematic cross-section transversal to the main, Sardon catchment valley hydrogeological conceptual model of the Sardon catchment , after Francés et al. (2014).

Precipitation is the only external source of the groundwater recharge in Sardon catchment. Part of this precipitation evaporates, some drains to the Sardon streams and the rest recharges to the aquifer. The groundwater flow direction is toward the Sardon-fault zone from all directions and it has a concentric pattern (Figure 7), is being influenced by the Sardon fault-river drainage line (Lubczynski & Gurwin, 2005).

## 2.4. Numerical model

Groundwater and surface water are interrelated components of the hydrologic system through different physiographic and climatic conditions. The interaction process occurs through vertical and lateral

exchange of fluxes between surface water and groundwater systems through unsaturated zone and infiltration to or exfiltration from saturated zone (Sophocleous, 2002).

#### **2.4.1. Software selection**

The groundwater flow was simulated with the three dimensional finite difference block centred groundwater model code MODFLOW-NWT (Niswonger et al. 2011). MODFLOW-NWT with SFR2 and UZF1 is among the models in which there is dynamic that link between groundwater and surface water through the unsaturated zone. The model was applied under the ModelMuse Graphical User Interface (GUI) (Winston, 2009) to pre-process input data and post-process output. The MODFLOW-NWT is a Newton formulation of MODFLOW-2005 and an independent groundwater modelling program intended to solve problems involving drying and rewetting nonlinearities of the unconfined groundwater-flow equation. It has an advantage over the previous models (MODFLOW-2005, MODFLOW 2000 and GSFLOW) because it enables to simulate water flow and storage in the unsaturated zone and to partition flow into evapotranspiration and recharge (Niswonger et al., 2011) and it can better to achieve convergence and computational efficiency (Niswonger et al., 2011). The model incorporates the Unsaturated Zone Flow (UZF1) (Niswonger et al., 2006) and Stream flow Routing (SFR2) (Niswonger & Prudic, 2005) packages among others. The Newton solver (NWT) was selected to solve the finite difference equations in each step of a MODFLOW-NWT stress period. The tolerance values for NWT solver were changed from recommended values by Niswonger et al. (2011) due to convergence problem in the model. “The head tolerance” was set to 0.01 m and the flux tolerance was 200,000 m<sup>3</sup> day<sup>-1</sup>. The recommended values in the manual are 0.001 m and 500 m<sup>3</sup> day<sup>-1</sup> (Niswonger et al., 2011) for head tolerance and flux tolerance respectively. The model units of length and time were assigned as metres and days respectively.

#### **2.4.2. Aquifer geometry and grid setup**

The structural aquifer boundaries of hydrostratigraphic layers and their thickness were adopted from Hassan et al. (2014) and Lubczynski & Gurwin (2005). The land surface was represented by Digital Elevation Model (DEM). The model consisted of two permeable layers, the upper unconsolidated porous layer (saprolite) and the lower fractured (fissured) layer (Figure 9). The size of grid was set based on data availability, modelling process and element of conceptual model (Varalakshmi et al., 2012). The model grid discretized vertically into two layers and horizontally into 95 columns and 131 rows (12,445 cells) with equally sized square grid cell set to 100 × 100 m area taking into account the dense fracture distribution, topography and size of the area. The active cells of the model are 7,531 (75.31 sq.km) and 7,935 (79.35 sq.km) for the first and second layer respectively. The inactive cells are 404 (0.4 sq. km). The first layer was set as convertible between confined and unconfined condition; the second layer also set as convertible to account for the outcrops.

### 2.4.3. Boundary conditions

The boundaries were categorized into internal and external model boundary conditions. The external model boundary conditions were simulated through the no-flow and head-dependent flux boundary (Figure 11). The boundary condition set by Lubczynski & Gurwin (2005) was adopted in this study except for the simulation for the Sardon river. The external boundary of the catchment is assigned along watershed divides which are marked by locally outcropping and shallow sub-cropping massive non-fractured rocks composed of granites and impermeable schists at the southern, western, and northern boundaries and quartzite intrusion in granite along the eastern boundary (Hassan et al., 2014). All the external boundaries of the aquifer were, therefore, simulated as no-flow boundaries that allow no lateral flow into or out of the model except small section at the northern boundary where there is saprolite layer and underlain crushed fault zone as investigated by Electrical Resistivity Tomography (ERT) in combination with Vertical Electrical Sounding (VES) and lateral groundwater outflow takes place (Lubczynski & Gurwin, 2005). This boundary, at the outlet of the Sardon stream, is represented by the 1.3 km long boundary section assigned as Drain Boundary in both active layers. The conductance was defined based on the field data and adjusted during the model calibration.

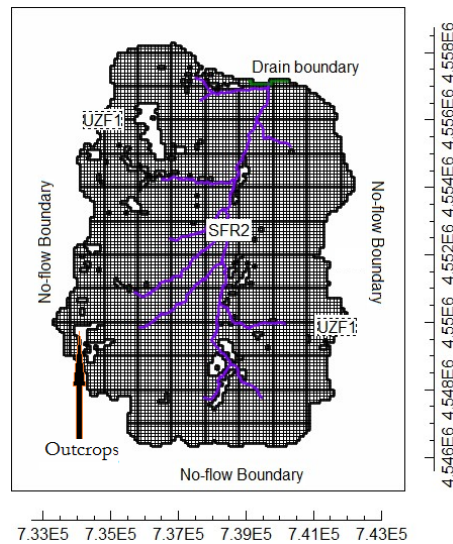


Figure 11: Boundary condition of Sardon catchment adopted from Lubczynski & Gurwin (2005) with addition of UZF1 and SFR2 packages as internal boundary conditions

The model internal boundary condition was head-dependent flux boundaries and simulated through UZF1 and SFR2 packages respectively (Figure 11). UZF1 package is recently developed package that replaces the Recharge and Evapotranspiration Packages of MODFLOW-2005 (Niswonger et al., 2006). It uses a kinematic-wave approximation of vertical, 1D variably saturated flow by applying the kinematic-wave approximation equation

$$\frac{\partial \theta}{\partial t} + \frac{\partial K(\theta)}{\partial z} + a = 0 \quad (4)$$

Where:

$\theta$  - the volumetric water content ( $L^{-3}L^{-3}$ );  $t$  is time (T),  $Z$  - the distance in the vertical direction (L);  $K(\theta)$  - unsaturated hydraulic conductivity ( $LT^{-1}$ );  $a$  - evapotranspiration rate per unit length of roots ( $T^{-1}$ ); and L and T denote length and time units.

UZF1 calculates groundwater evapotranspiration ( $ET_g$ ), unsaturated zone evapotranspiration ( $ET_{um}$ ), gross recharge ( $R_g$ ), storage change ( $\Delta S$ ) and groundwater exfiltration ( $Exf_{gw}$ ) as a function of the inputs assigned to the package including extinction water content (EXTWC), extinction depth (EXTDP),  $PET$  and infiltration rate. UZF1 recharged groundwater from precipitation after satisfying the evapotranspiration demand based on the given input values of EXTWC, EXTDP and  $PET$  (Viridi et al., 2013). The infiltration rate was assigned as  $1.41 \text{ mm day}^{-1}$ ; the evapotranspiration demand ( $PET$ )  $2.1 \text{ mm day}^{-1}$ ; extinction water content was fixed to  $0.05 \text{ m}^{-3}\text{m}^{-3}$  as spatially uniform to all cells and the extinction depth, below which no more water will be removed by evapotranspiration, was assigned as weighted average of 1.6 m. The weight of extinction depth is given according to the areal coverage ratio of the land covers and vegetation of the total area of the Sardon catchment. The land cover and vegetation type identified are bare soil, grass, outcrops and  $Q.i$  and  $Q.p$ . The extinction depth of outcrops was taken as 0 m (Hassan et al., 2014); the extinction depth of grass and bare soil was determined based on the dominant soil type of the area. The soil of the area is weathered granite, the value for sand soil is taken as representative of the area. The extinction depth of the bare soil and grass was assigned after Shah et al. (2007) as 1.45 and 0.5 m b.g.s respectively. The extinction depth for  $Q.i$  and  $Q.p$  was taken as 15 and 10 m b.g.s respectively after Francés (2015).

The infiltration rate and  $PET$  values for steady-state simulation were assigned as the average values for the 7 years of simulation period and for the transient state, time series data aggregated on daily basis was applied. The “Number of trailing waves” (NTRAIL2) was set to 16 (the recommendable range is between 10 and 20) and “Number of wave sets” (NSETS2) was set to 20 since the infiltration rate varies with time and also options “Route discharge to streams and lakes” (IRUNFLG) and “Simulate evapotranspiration” (IETFLG) were selected. The Brooks-Corey-Epsilon was assigned as 3.5 which defines the relation between unsaturated hydraulic conductivity and water content (Niswonger & Prudic, 2005); spatially uniform maximum unsaturated vertical hydraulic conductivity  $0.35 \text{ m day}^{-1}$  and saturated water content  $0.3 \text{ m}^{-3}\text{m}^{-3}$  were assigned to all cells. The model top was taken as the land surface where the infiltration was applied. “The recharge and discharge location option” (NUZTOP) was selected as “Top active cell”.

The Sardon river that flows along the major fault zone and the main tributaries were simulated by the SFR2 package. The SFR2 stream segments are hydraulically connected with groundwater as confirmed by field observation (Lubczynski & Gurwin, 2005). The SFR2 package, used to simulate stream interactions with groundwater, gives good and realistic results as it can simulate volumetric water exchanges between the two. The SFR2, allows different options to calculate the stream water depth; it allows the user to add or subtract water from streams due to runoff, precipitation, and evapotranspiration (Niswonger & Prudic,

2005). The flow in a stream is routed instantaneously downstream or to lakes and the unsaturated flow beneath streams can also be simulated. The unsaturated zone properties specified in SFR2 include, saturated and initial water contents; saturated vertical hydraulic conductivity; and the Brooks-Corey exponent. These variables were defined independently for each stream reach (Niswonger & Prudic, 2005).

Regarding the SFR2 package input, prior to setting up the model, the maps of stream segments and reaches for the main streams and tributaries, were prepared in ArcGIS. Each stream segment is composed of number of reaches and segments were assigned in sequential order from upstream to downstream. In the model, the streams were represented by 19 segments which made up of 920 reaches. The map was validated with existing stream map (Hassan et al., 2014) and imported as shape file to ModelMuse and the SFR2 parameters were set in order to achieve the desired result in the model simulation accordingly. “Number of trailing wave increments” (NSTRAIL) set to 20, “Maximum number of trailing waves” (NSFRSETS) to 30, “Maximum number of cells to define unsaturated zone” (ISUZN) to 10 were set. The stream reaches were set to a constant width of 3 meters and the length ranged from 2.5 m to 157.8 m in the cells. “The stage calculation” (ICALC=1) were simulated by rectangular section, the stream bed thickness for all streams was assumed equal to 0.2 m, “Streambed top” (STRTOP) was assigned between 2-4 m and adjusted during model calibration, the Manning coefficient (channel roughness) was assumed equal to 0.035 since there was vegetation along the natural streams (Fetter, 2001), “the stream bed  $K_V$ ” (STRHC1) was set as one-tenth of the horizontal hydraulic conductivity assigned to the  $K_H$ -zone and adjusted during model calibration (Niswonger & Prudic, 2005). Stream depth was also adjusted for each stream while unsaturated-zone variables were kept constant among all stream reaches.

The interaction of surface-groundwater under MODFLOW-NWT model including the UZF1 and SFR2 packages is shown schematically in (Figure 12).

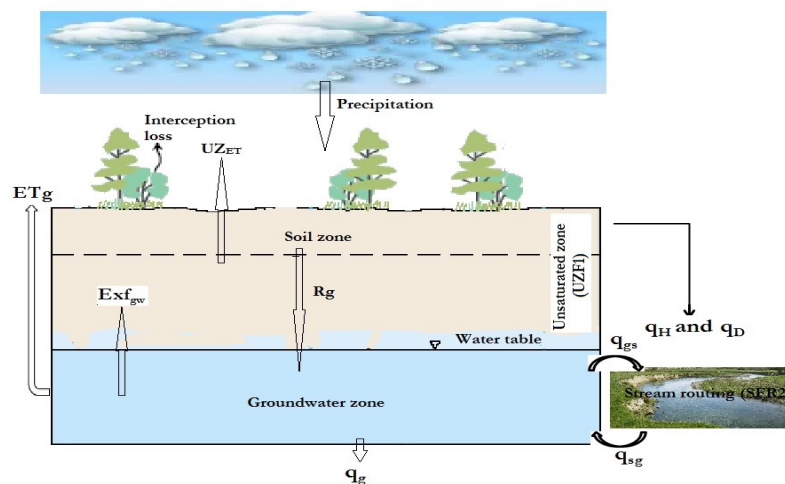


Figure 12: Schematic representation of MODFLOW-NWT that integrates UZF1 and SFR2 packages where  $ET_g$  (groundwater evapotranspiration),  $ET_{un}$  (unsaturated zone evapotranspiration),  $R_g$  (gross recharge),  $q_H$  (Hortonian runoff),  $q_D$  (Dunnian saturated-excess runoff),  $q_{gs}$  (stream leakage from groundwater),  $q_{sg}$  (stream leakage to groundwater) and  $q_g$  (lateral groundwater outflow across the northern catchment boundary)

Horizontal hydraulic conductivity ( $K_H$ ), vertical hydraulic conductivity ( $K_V$ ), specific storage (SS), specific yield (SY) in the MODFLOW-NWT were defined using the upstream weighting package (UPW) in MODFLOW-NWT and Newton Solver (NWT) was applied (Niswonger et al., 2011). The units for all inputs were in meters for length and in days for time.

#### 2.4.4. Hydraulic properties

The hydraulic properties including  $K_H$ , SS and SY data was obtained from hydraulic tests performed in situ measurements. These test values given by Francés (2014) were used as initial values and adjusted during the model calibration (Table 1). The drain conductance and stream conductance were calculated from calibrated  $K_H$  values.

Table 1: Parameters of the hydrogeological conceptual model , after Francés (2015)

Zone	Thickness			K (m.d <sup>-1</sup> )			T (m <sup>2</sup> .d <sup>-1</sup> )			Sy (-)			Se (-)		
	int.	min.	max.	int.	min.	max.	int.	min.	max.	int.	min.	max.	int.	min.	max.
L1_F1	45.0	20.0	75.0	$1.6 \times 10^{-4}$	$2.3 \times 10^{-5}$	$1.8 \times 10^{-5}$	$7.4 \times 10^{-3}$	$4.6 \times 10^{-4}$	$1.4 \times 10^{-1}$	1.9	0.8	4.6			
L1_F2/3	35.0	5.0	50.0				$5.8 \times 10^{-3}$	$1.2 \times 10^{-4}$	$9 \times 10^{-2}$						
L1_nf	20.0	1.0	40.0				$3.3 \times 10^{-3}$	$2.3 \times 10^{-5}$	$7.2 \times 10^{-2}$						
L2_F1	67.5	30.0	112.5	$1.6 \times 10^{-3}$	$2.3 \times 10^{-5}$	$1.8 \times 10^{-2}$	$1.1 \times 10^{-1}$	$6.9 \times 10^{-3}$	2.0	0.5	0.1	1.0	$1 \times 10^{-3}$	$4 \times 10^{-4}$	$3 \times 10^{-3}$
L2_F2/3	52.5	7.5	75.0				$8.6 \times 10^{-2}$	$1.7 \times 10^{-3}$	1.4				$1 \times 10^{-4}$	$4 \times 10^{-4}$	$3 \times 10^{-3}$
L2_nf	30.0	1.0	60.0				$4.9 \times 10^{-2}$	$3.5 \times 10^{-4}$	1.1				$4 \times 10^{-4}$	$2 \times 10^{-4}$	$7 \times 10^{-5}$

#### 2.4.5. Head observations (HOB)

The locations of head observation points were imported as shape file to ModelMuse and the piezometer ID, time step and observed heads were assigned as an input to each piezometer representing point object. The observed heads were used as reference in model calibration to graph the observed versus simulated head during steady-state, transient model calibration and validation.

#### 2.5. Water budget

Water budget shows the fluxes of groundwater within the aquifer system. In the steady-state model, the average water budget of 7-year simulation periods was estimated. In the transient model, water budget was estimated for each time step, i.e. daily. No external source of groundwater recharge other than direct from rainfall was considered except for leakage from streams. In water budget assessment, the incoming and outgoing flux should balance exactly or within acceptable limit at the end of simulation period. After each run, the MODFLOW-NWT model gives only the overall budget of the model, not for the individual model layers. ZONEBUDGET (Harbaugh, 1990) was applied to calculate budget for individual layers, in steady-state simulation but also in transient for each stress period. ZONEBUDGET calculates sub-regional water budgets using results from the groundwater flow model under ModelMuse GUI. It uses cell-by-cell flow data saved by the model in order to calculate the budgets.

The water balance of the entire Sardon catchment and the daily fluxes for the surface, unsaturated and saturated zone were calculated using the following equations:

Water balance of the entire catchment (aquifer) was calculated using Equation 5 , modified after Hassan et al. (2014)

$$P = ET + q + q_g \pm \Delta S \quad 5$$

Where  $P$ -precipitation;  $ET$  - total evapotranspiration;  $q$ - stream discharge at the outlet of the catchment;  $q_g$  - lateral groundwater outflow across the northern catchment boundary and  $\Delta S$  is the change in the catchment storage. All units are in mm day<sup>-1</sup>.

The  $ET$  and  $\Delta S$  component of Equation 5 was explained in detail in Equations 6 and 7.

$$ET = ET_g + ET_{Un} + I \quad 6$$

$$\Delta S = \Delta S_g + \Delta S_{Un} \quad 7$$

Where  $ET_g$  - groundwater evapotranspiration,  $ET_{un}$  - unsaturated zone evapotranspiration from UZF1 package,  $\Delta S_g$  - change of storage in the saturated zone,  $\Delta S_{un}$  - change of storage in the unsaturated zone and  $I$  - canopy interception. All units are in mm day<sup>-1</sup>.

The water balance of the land surface and the unsaturated zone is expressed in Equation 8

$$P + EXf_{gw} = I + R_o + R_g + ET_{un} + \Delta S_{un} \quad 8$$

Where  $EXf_{gw}$  - groundwater exfiltration,  $R_o$  - the total runoff to streams and  $R_g$  - gross recharge  
Actual infiltration rate in unsaturated zone and gross recharge can be computed as (Equation 9):

$$P + Exf_g = I + R_o + P_e \quad 9$$

Where  $P_e$  the actual infiltration rate and can be further divided into (Equation 10):

$$P_e = R_g + ET_{un} \pm \Delta S_{un} \quad 10$$

The water balance of the groundwater (saturated) zone is expressed as (Equation 11)

$$R_g + q_{sg} = ET_g + EXf_{gw} + g_{gs} + q_g \pm \Delta S_g \quad 11$$

Where  $q_{sg}$  - stream leakage into the groundwater,  $q_{gs}$  - groundwater leakage into the stream and  $\Delta S_g$  - change in the groundwater storage.

Net groundwater recharge controls the sustainability of groundwater resources and enables to understand the behaviour of changes in groundwater storage better than using the total recharge (Hassan et al., 2014; Sophocleous, 2005) and it is estimated by Equation 12:

$$R_n = R_g - EXf_{gw} - ET_g \quad 12$$

Where  $R_n$  - net recharge,  $R_g$  - total recharge,  $EXf_{gw}$  - groundwater exfiltration and  $ET_g$  - groundwater evapotranspiration.

The net recharge is the actual amount of water that recharges the groundwater after the loss of water by evapotranspiration and exfiltration. Groundwater net recharge originates from precipitation that reaches the water table through the unsaturated zone and was applied in the model using UZF1.

## **2.6. Model calibration and driving forces**

Model calibration is the modification of model input data to match observed and simulated heads and flows (Reilly & Harbaugh, 1999), so to minimize average error in calibration (Anderson & Woessner, 1992). The calibration process of the model was completed in three different but interrelated processes. Initially steady-state model calibration was undertaken, followed by warming-up period and at last, the transient model calibration was conducted. Groundwater heads were monitored at 12 observation points. In this study, the steady-state and transient model calibration was performed using the trial-and-error adjustment method. In some aspects, that type of calibration is advantageous as compared to automated calibration as it is much faster and enables to understand the model behaviour during the calibration process and in consequence to incorporate hydro(geo)logical knowledge of the area in the calibrated model (Hassan et al., 2014).

The results of calibration runs after parameter adjustment were evaluated applying Root Mean Square Error (RMSE). The trial-and-error adjustment was conducted till the RMSE became small and no more model improvement was observed.

The driving forces in this study area were rainfall and potential evapotranspiration; the state variables were heads and the calibrated variables are  $K_H$ ,  $K_V$ , SY and SS. Additionally, the water table was controlled whether in any cell, it does not rise above the topographic surface and also the budget consistency and realism was assessed in every model run.

### **2.6.1. Steady-state model calibration**

A steady-state model was calibrated based on the average of the hydrological conditions in the study years, including observation head, precipitation, PET and infiltration rate. Twenty five internally homogenous, uniform  $K_H$  zones were defined for both layers based on groundwater heads in observation points and hydrogeological knowledge of the area particularly related to main and secondary faults, categorized as main fault zones, secondary fault zone and non-fractured zones. The vertical hydraulic conductivity for steady-state calibration was assigned by defining 6 internally homogeneous  $K_V$  -zones for both first and second layer. The  $K_H$  and  $K_V$  were assigned initially on the basis of the surface geology and field tests. The values indicated in Table 1 and values from Hassan et al., (2014) were used as a guideline for model calibration. These values were assigned in UPW pane and adjusted during model calibration till model error assessment criteria suggested by Anderson & Woessner (1992) and Mason & Hipke (2013) was met. The maximum absolute value of model residuals should be less than 10 % , MAE less than 2 % ,

all MAE less than 5 %, RMSE less than 2 % and the ratio of RMSE to the the total observed head difference should be lower than 10 % the total observed head difference.

### **2.6.2. Warming-up period for transient model calibration**

Warming-up period is a way of minimizing the influence of initial state conditions on the transient simulation (Navarro & Playan, 2007). 365 time steps of one hydrologic year (1 October 2007 to 30 September 2008) piezometric records were applied as warming-up period. The steady-state simulation head was used as initial head for the warming-up period.

### **2.6.3. Transient model calibration**

Transient model simulation was applied to examine the behaviour of the aquifer over time. It produced set of heads for each time step (Anderson & Woessner, 1992). The simulation period was for hydrological years starting from 1 October 2008 and ending 30 September 2013. The head from last stress period of the model warming-up (30 September 2008) was used as initial head for transient model simulation. Time series data of head observation to Head Observation package (HOB), infiltration and PET to UZF1 package and stream flow to SFR2 package were assigned as input. The initial input parameter ( $SS$ ,  $SY$ ,  $K_H$  and  $K_V$ ) were obtained from previous studies (Francés, 2015; Hassan et al., 2014), and adjusted in transient model calibration.  $SS$  was assigned as spatially uniform for the first and second layer. Regarding  $SY$ , the shallow aquifer was divided into 9 internally uniform zones based on soil sampling and shallow geophysical investigation (Hassan et al., 2014). The  $K_H$  and  $K_V$  zones were defined in steady-state model simulation and used for the transient state model simulation. Listing analyst (Winston & Paulinski, 2014) was used to facilitate analysis of listing files for the transient model calibration as the output files were large and this program was capable to organize and display large ModelMuse output files quickly. Groundwater chart (GW\_Chart) (Winston, 2000) was used to export water budget files to Microsoft Excel for further analysis.

## **2.7. Error assessment and sensitivity analysis**

In this study error assessment was carried out to evaluate the performance of the calibrated model.

### **2.7.1. Error assessment**

Error assessment of the model calibration was demonstrated by statistical and graphical comparisons of simulated and observed data. The observed time series data set of groundwater levels in 12 piezometers was used as reference to compare with simulated heads. The residual error was analysed by Mean Error (ME), Mean Absolute Error (MAE) and Root Mean Square error (RMSE) (Anderson & Woessner, 1992) and the ratio of the RMSE to the total head loss (less than 10 % error) was also used for further assessment of the errors. Equations 13 to 15 were used to facilitate the error assessment analysis. Scatter plot of observed head versus simulated head was used for graphical comparison of the model simulation result.

$ME$  that is the difference between the observed head ( $Head_{obs}$ ) [m] and model calculated ( $Head_{sim}$ ) [m] result and calculated as (Equation 13):

$$ME = \frac{1}{n} \sum_{i=1}^n (Head_{obs} - Head_{sim})_i \quad (13)$$

Mean absolute value is the mean of the absolute differences of the observed head ( $Head_{obs}$ ) [m] and model calculated ( $Head_{sim}$ ) [m] result and calculated as (Equation 14):

$$MAE = \frac{1}{n} \sum_{i=1}^n |(Head_{obs} - Head_{sim})_i| \quad (14)$$

Root means square error ( $RMSE$ ) is calculated as (Equation 15):

$$RMSE = \left[ \frac{1}{n} \sum_{i=1}^n (Head_{obs} - Head_{sim})_i^2 \right]^{0.5} \quad (15)$$

Where  $n$  is the number of calibration values

Discrepancy error in volumetric budget was assessed for error analysis of the water balance closure. In most cases percent discrepancy of 0.1% is recommended and it was applied in this study (Konikow, 1996).

## 2.7.2. Sensitivity analysis

The uncertainty in calibrated model caused by uncertainty in the estimate of aquifer parameters, observation data, conceptual model, stress and boundary conditions are analysed by sensitivity analysis (Anderson & Woessner, 1992; Wu & Zeng, 2013). The model's ability to estimate a parameter value during calibration is related to the sensitivity of the changes in the model output relative to changes in the parameter value (Doherty, 2004; Reilly & Harbaugh, 1999). A model is said to be sensitive if the response of the model is high for small change in parameters (Bear & Cheng, 2010).

The model input parameters were evaluated for their effect on head. The sensitivity analysis was conducted by altering one parameter value at a time in the range of  $\pm 10\%$  increment to the calibrated parameters. The sensitivity of the following parameters, driving forces and variables were tested:  $K_H$ ,  $K_V$ , EXTWC, EXTWD, PET, infiltration rate, maximum unsaturated conductivity ( $K_{Vun}$ ), Brooks-Corey-Epsilon (BCE) and saturated water content ( $WC_{sat}$ ) in the steady-state and transient model calibration. In transient simulation additionally storage parameters (SY and SS) were analysed.

## 2.8. Post-calibration

### 2.8.1. Validation

Validation is a post-calibration process to verify the representativeness of the optimum parameter set during the model calibration. Validation shows whether a model is applicable for another set of data

which had not been already used in the calibration stage. Calibrated model was validated using independent one year data (1 October 2013 to 30 September 2014) applying in seven piezometers (five deep boreholes which started to record in 2010 and 2 shallow boreholes) without changing model parameters. The last stress period of the transient model simulation (30 September 2013) was used as initial head for model validation. The hydrographs and RMSE of the validation result was compared with hydrographs and RMSE of transient model simulation to check the validity of the model for another set of data.

### **2.8.2. Transient simulation with spatio-temporally variable UZF1 driving forces**

The inputs of UZF1 package: crop coefficient ( $K_c$ ), interceptions rate ( $I$ ) and root extinction depth (EXTDP) applied in the transient model simulation were assumed as if spatially and temporarily invariant. The spatio-temporal UZF1 driving forces were analyzed to observe the effect on entire groundwater budget and groundwater fluxes. These driving forces affect the spatio-temporal inputs of UZF1 package:  $PET$  and infiltration rate.  $PET$  (Equation 1) is a product of temporal variable  $ET_0$  and spatially variable  $K_c$  and infiltration rate (Equation 3) is a product of temporal variable precipitation and spatially variable interception loss rate. The variation of these driving forces is due to the difference in land covers and vegetation types and their impact on water loss. Landcover classes were prepared based on tree classification map by Reyes-Acosta & Lubczynski (2013) and hydrologic response units (HRUs) (Hassan et al., 2014). The gross rainfall interception loss of  $Q_i$  was taken as 29.6 % (Pereira et al., 2009),  $Q_p$  without leaves, 11.9 % (November-April) and 18 % with leaves (May-October) and the interception of the rest of the land cover was estimated as 3 % (Berhe, 2010). The extinction depth of the bare soil and grass was assigned after Shah et al. (2007) as 0.5 and 1.45 m b.g.s respectively. The extinction depth for the dominant trees  $Q_i$  and  $Q_p$  were assigned as 15 and 10 m b.g.s (Francés, 2015). The EXTWC was set as  $0.05 \text{ m}^3\text{m}^{-3}$  spatially uniform for all cells. The simulation period for validation was set as 1-year (hydrological year from 01 October 2013 to 30 September 2014). The spatio-temporal driving forces in the UZF1 package were adjusted. The groundwater fluxes and groundwater budget of the spatio-temporal driving forces analysis and validation were compared to assess the difference in the simulation.

### 3. RESULT AND DISCUSSION

#### 3.1. Meteorological and Hydrological analysis result

##### 3.1.1. Metrological data analysis

The only external source of recharge in Sardon catchment is precipitation that falls as rain. The estimated mean annual precipitation for the study period from 01 October 2007 to 30 September 2014 was 540 mm year<sup>-1</sup>, so the daily average was 1.48 mm day<sup>-1</sup>. The highest monthly rate of rainfall was observed in the months of March, May and December. The largest monthly rainfall of 147 mm month<sup>-1</sup> was in March 2013. July-August are recognized as the driest months with no or small amount of rainfall. High temperature corresponds with high  $ET_0$  as shown in Figure 5. The  $ET_0$  during the study period was in the range of 2-2.5 mm day<sup>-1</sup>; the temperature ranged from a minimum of 3 °C during the months of December-February (coldest months) to maximum temperature of 29 °C during the months of July-August (driest and warmest months) (Figure 5). The metrological data collected and analysed for the 7-year simulation period was similar to the 23-year data from Spanish Meteorological Institute (Lubczynski & Gurwin, 2005).

##### 3.1.2. Infiltration rate

The average interception loss by the forest canopy was  $6 \times 10^{-2}$  mm day<sup>-1</sup>. High infiltration rate was observed during the periods with high rate of precipitation, the estimated infiltration was the highest in March 2013 with 4.5 mm day<sup>-1</sup> (Figure 13). The estimated infiltration rate ranged from 0 to 4.5 mm day<sup>-1</sup> with an average of 1.41 mm day<sup>-1</sup>. That infiltration rate was applied in the steady-state model calibration.

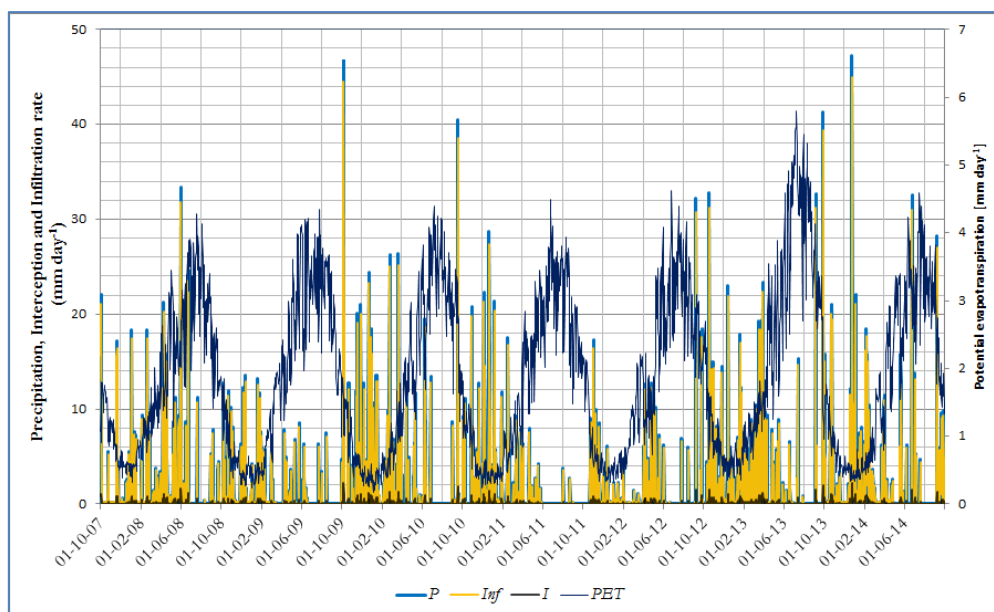


Figure 13: Precipitation ( $P$ ), infiltration rate ( $Inf$ ), interception loss rate ( $I$ ) and potential evapotranspiration ( $PET$ ) for 7-year periods (hydrologic years 2008 to 2014) for the study area

### 3.2. Steady-state model calibration

#### 3.2.1. Calibrated head and error assessment

The steady-state simulated and observed heads were examined for correlation using a scatter plot and by calculating coefficient of correlation ( $r$ ). A quantitative comparison of the head data in all the observation points indicates a good match between the observed and simulated head values (Figure 14). The scatter plot depicts that the observation points are randomly distributed and fall close to the 1:1 solid line, which represents a perfect fit between observed and simulated head changes. The residuals calculated as the difference between observed and simulated heads in all observation points are indicated in Table 2 and the coefficient of correlation was high ( $r=0.9999$ ) as shown in Figure 14. The residual varied from the lowest  $-0.83$  m at W1PCL7 piezometer located at Tremedal east to the highest  $0.879$  m at W2PCL7 piezometer located at Tremedal east (Figure 4). The overall residual error was positive that indicates there was slight underestimation of water level rise by the model. The result agrees with the suggestion of Hill (1998) who stated that, when observed heads are plotted against simulated heads they should fall close to a line with a slope of 1 and the correlation between them should be greater than 0.90.

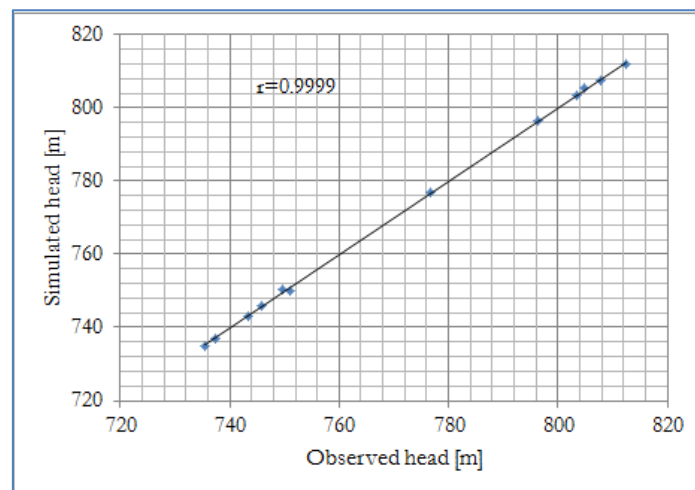


Figure 14: Relationship between simulated and observed head in the Sardon catchment for steady-state condition of 12 observation points averaged for hydrologic year of 2008 to 2014

The error assessment criteria calculated applying equations 13 to 15 were  $0.07$  m,  $0.30$  m and  $0.42$  m for ME, MAE and RMSE respectively and as total observed head difference within the Sardon catchment was  $77$  m as shown in Table 2, the steady-state calibration satisfied the suggested by Anderson & Woessner, (1992) and Mason & Hipke (2013) model error criteria, where the maximum absolute value of model residuals ( $0.88$  m) should be less than 10 % of the total head change ( $7.7$  m); the MAE is less than 2 % of the total head change ( $1.54$  m); all MAE were less than 5 % of the total head difference ( $3.85$ ), the RMSE less than 2 % of the total head difference ( $1.54$  m) and the ratio of RMSE to the total head difference is 0.54 % which is also lower than the 10 % of total head difference ( $7.7$  m). In addition, the errors for observation points have a mean of  $0.07$ , median of  $0.05$  and standard deviation of  $0.5$  as shown in Table 2. These results support the statement of good calibration results of the steady-state model.

Table 2: Observed and simulated head with calculated error assessment for 12 piezometers in meters

Observation points	X-utm	Y-utm	Obs.head	Sim. head	$H_{obs.} - H_{calc}$	$abs[H_{obs.} - H_{calc}]$	$[H_{obs.} - H_{calc}]^2$
W1TB	739493	4556428	735.36	735.07	0.29	0.29	0.08
PTB2	739508	4555882	737.39	736.88	0.51	0.51	0.26
W1PN	738412	4553685	743.40	743.04	0.36	0.36	0.13
PPNo	738316	4551446	745.87	745.99	-0.12	0.12	0.01
W1PCL7	738375	4551345	749.64	750.47	-0.83	0.83	0.69
W2PCL7	738263	4551290	750.94	750.06	0.88	0.88	0.77
PGJTMO	736503	4555731	776.81	776.77	0.04	0.04	0.00
PMU1	739473	4547706	796.32	796.41	-0.09	0.09	0.01
PGBO	741435	4551574	803.53	803.58	-0.05	0.05	0.00
PSDO	736378	4548919	804.93	805.40	-0.47	0.47	0.22
PGJO	736096	4557825	807.74	807.71	0.03	0.03	0.00
W1SD	736215	4548722	812.35	812.04	0.31	0.31	0.10
<b>Sum</b>			9,264.280		0.85	3.96	2.27
		<b>Change of head</b>	<b>77</b>	<b>Calculated</b>	<b>ME</b>	<b>MAE</b>	<b>RMSE</b>
					<b>0.07</b>	<b>0.30</b>	<b>0.42</b>
				Median	<b>0.03</b>	0.30	0.09
				STD	<b>0.45</b>	0.30	0.27
				Min	-0.83	0.03	0.00
				Max	0.88	<b>0.88</b>	0.77

Plotting residuals against hydraulic head helps to check for bias in a groundwater (GW) flow model (Hill, 1998). Figure 15 shows that the residuals randomly and uniformly distributed hence the model was not biased.

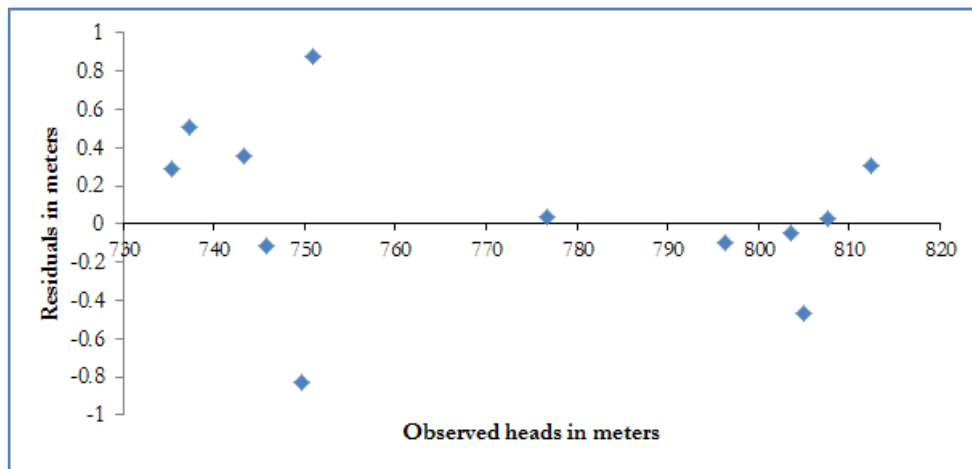


Figure 15: Residuals vs. observed head of the steady-state simulation

Figure 16 shows the distribution of the calibrated heads of the first and second layer after the steady-state model calibration. From the two figures, it can be observed that the water flows from all directions of the catchment towards the main fault zone (central part of the catchment), match the course of the Sardon river. The first and second layers showed nearly the same potentiometric surface. The same observation was made by Lubczynski & Gurwin (2005) and Hassan et al. (2014).

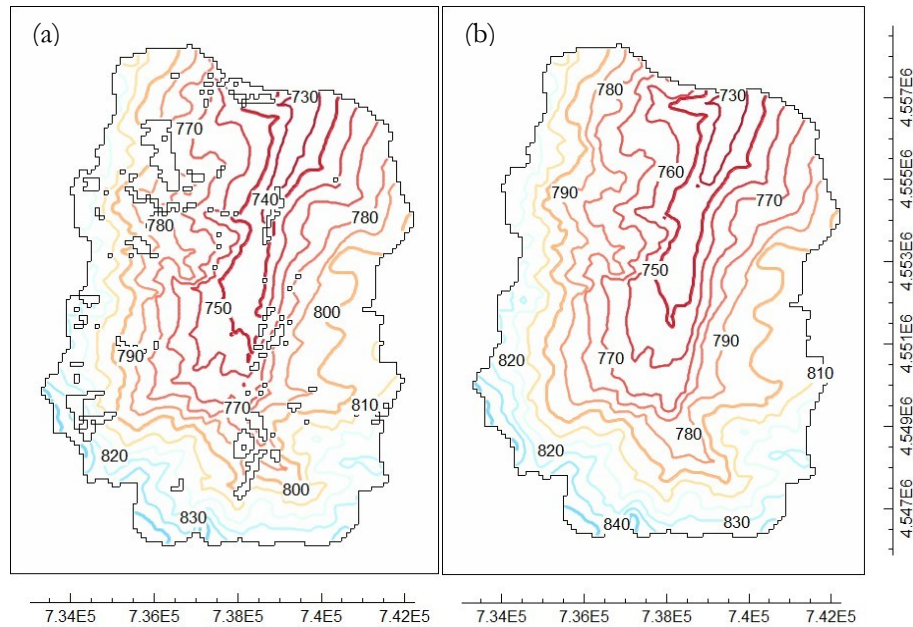


Figure 16: Calibrated head distribution (a) first layer and (b) second layer of the steady-state model simulation

As additional calibration control, the Water Table Depth (WTD) was compared to the topographic surface to check if it did not rise above the ground surface. WTD was calculated as the difference of the “Model-top” and model simulated “head” values for the entire model and for each observation points. In all cells of the model, water table was below the ground surface and the WTD varied from 0.1 m to 10 m depth.

### 3.2.2. Hydraulic conductivities

Figure 17 shows the calibrated  $K_H$  for the first and second layers of the aquifer. Initially, 25 uniform and internally homogeneous K-zones were assigned to the model and through the calibration process the number of zones increased to 30 K-zones. Higher  $K_H$  was observed in most of the K-zones of the first layer as compared to the second layer and in the fault zones as compared to non-fault zones. The  $K_H$  for the first layer of non-fault zones varied from  $1 \times 10^{-3}$  to  $10 \text{ m day}^{-1}$ ; while for fault zones  $K_H$  varied from 0.02 to  $10 \text{ m day}^{-1}$ . For the second layer  $K_H$  of non-fault zones varied from  $6 \times 10^{-4}$  to  $4 \text{ m day}^{-1}$ , and for fault zones from 0.06 to  $1.8 \text{ m day}^{-1}$ . The highest  $K_H$  was observed for both fault and non-fault zones of the first layer. The highest variation of  $K_H$  was observed in the fault zones of the first layer (Table 3).

Table 3: Statistical analysis of hydraulic conductivity for steady-state simulation period of the first and second layers of Sardon catchment

Stastical analysis	Fault zone $K_H$ (m day <sup>-1</sup> )		Non-fault zone $K_H$ (m day <sup>-1</sup> )	
	First layer	Second layer	First layer	Second layer
Mean	3.99	0.54	2.71	0.63
Min	0.02	0.06	$1 \times 10^{-3}$	$6 \times 10^{-4}$
Max	10	1.8	10	4
STD	3.02	0.48	2.72	1.09

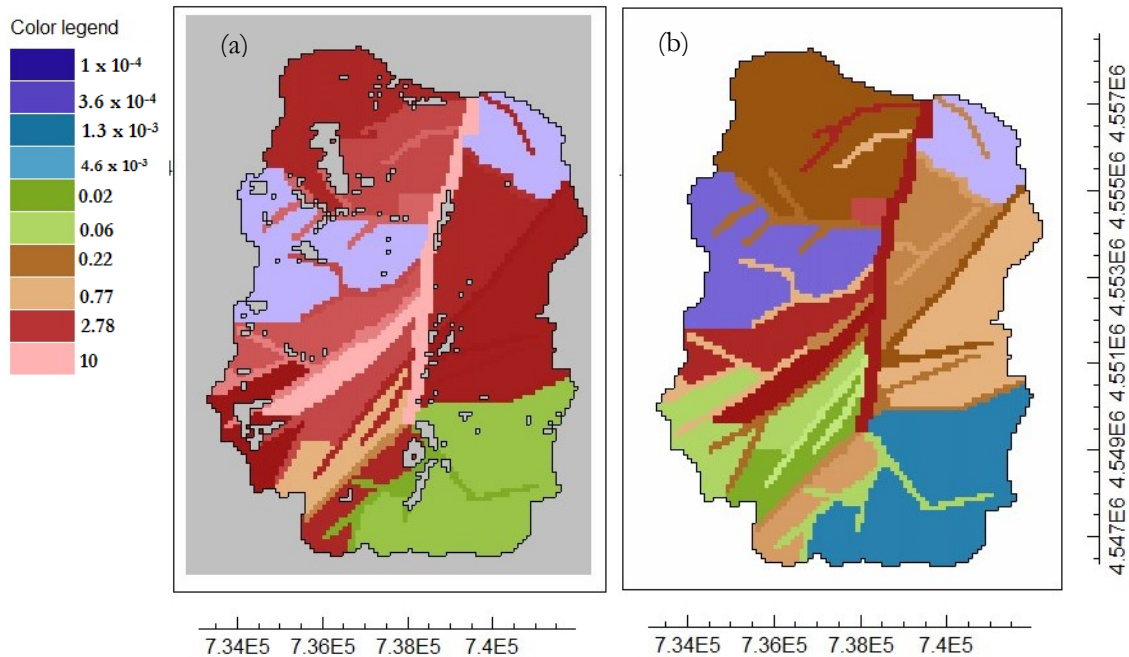


Figure 17: Calibrated horizontal hydraulic conductivity ( $K_H$ ) distribution map: (a) first layer and (b) second layer after calibration in steady-state condition [m day<sup>-1</sup>]

In the first layer, the highest  $K_H$  were observed along the main fault zone and central part of the aquifer. The smallest  $K_H$ , were observed in non-fault zones. These might be attributed to finer grains due to weathering as compared to fault/fractured zone. In the second fissured layer water flows entirely through fractures. The calibrated  $K_H$  value was the same as in the steady-state model of Abubeker (2010) whose  $K_H$  of the first layer ranged from 0.8 to 19 m day<sup>-1</sup> and  $K_H$  of the second layer, from 0.05 to 1.5 m day<sup>-1</sup>.

The vertical hydraulic conductivity ( $K_V$ ) value for the first layer varied from 0.04 to 0.08 m day<sup>-1</sup> and for the second from 0.01-0.08 m day<sup>-1</sup>.  $K_V$  influences the ease how water moves in the vertical direction between the two adjacent layers determining the vertical conductance.

### 3.2.3. Water budget of the steady-state simulation

#### *Water balance of the entire model (2 aquifers combined)*

The daily average water balance of Sardon catchment for steady-state condition was calculated applying Equations 5 to 7 (Table 4). Precipitation was the only component for IN of the water balance of the catchment. The OUT components of water balance: subsurface evapotranspiration contributed 50.7 %, stream discharge at the outlet of the catchment 43.8 %, interception loss 4.4 % and lateral groundwater outflow 1.1 % of the total outflow from the catchment. Unsaturated zone evapotranspiration ( $ET_{un}$ ) is zero since  $PET$  demand is removed from the infiltration rate and groundwater above the extinction depth (Niswonger et al., 2006).

Table 4: Total water balance of Sardon catchment aquifer at steady-state condition  
(mm day<sup>-1</sup>)

Budget component	IN	Budget component	OUT
Precipitation	1.48	Subsurface evapotranspiration ( $ET_{ss}$ )	0.80
		Unsaturated zone ET ( $ET_{un}$ )	0.00
		Interception loss ( $I$ )	0.07
		Stream discharge at the outlet ( $q$ )	0.69
		Lateral groundwater outflow ( $q_g$ )	0.02
<b>Total</b>	<b>1.48</b>	<b>Total</b>	<b>1.57</b>
<b>IN-OUT</b>			<b>-0.09</b>

#### *Water balance of land surface and unsaturated zone*

The water balance of the land surface and the unsaturated zone presented in Table 5 and follows Equation 8. Precipitation contributed the major part 88.6 % and groundwater exfiltration 11.4 % of the total IN for land surface and unsaturated zone water balance. In the OUT budget components gross recharge constituted the major part, 82.6 % followed by total runoff 13.3 % and interception loss by vegetation canopy contributed the lowest 4.1 % of the total OUTFLOW from the land surface and unsaturated zone.

Table 5: Water balance of land surface and unsaturated zone in steady-state condition (mm day<sup>-1</sup>)

Budget component	IN	Budget component	OUT
Precipitation	1.48	Unsaturated zone ET ( $ET_{un}$ )	0.00
GW exfiltration ( $Exf_{gw}$ )	0.19	Interception loss ( $I$ )	0.07
		Gross recharge ( $R_g$ )	1.38
		Total runoff ( $R_o$ )	0.22
<b>Total</b>	<b>1.67</b>	<b>Total</b>	<b>1.68</b>
<b>IN-OUT</b>			<b>-0.01</b>

**Water balance of the saturated zone (2 aquifers combined)**

The water balance of the saturated zone presented in Table 6 follows the Equation 11. That balance is very well closed. Gross recharge contributed 88.1 % and stream leakage to groundwater 18.9 % to the total IN of water in the saturated zone. Groundwater evapotranspiration was the highest component of the OUT budget component with 46.8 %, stream leakage from groundwater 40.2 %, groundwater exfiltration 11.3 % and lateral groundwater outflow at the northern boundary 1.7 % of the total OUT of the water balance of the saturated zone.

Table 6: Water balance of groundwater (saturated zone) in steady-state condition (mm day<sup>-1</sup>)

Budget component	IN	Budget component	OUT
Stream leakage to groundwater ( $q_{sg}$ )	0.32	Groundwater evapotranspiration ( $ET_g$ )	0.80
Gross recharge ( $R_g$ )	1.37	Groundwater exfiltration ( $Exf_{gw}$ )	0.19
		Stream leakage from groundwater ( $q_{gs}$ )	0.68
		Lateral groundwater outflow ( $q_l$ )	0.03
<b>Total</b>	<b>1.69</b>	<b>Total</b>	<b>1.70</b>
<b>IN-OUT</b>			<b>-0.01</b>

The daily average net recharge at steady-state condition as per Equation 12 was 0.39 mm day<sup>-1</sup> which is 28.7 % of the gross recharge and 26.7 % of the total rainfall that fall in the area during the hydrological years of 01 October 2007 to 30 September 2014.

**Water balance of the saturated zone per aquifer**

The steady-state water budget reflects mean water flow as of 7 years (01 October 2007 to 30 September 2014) moving in and out of the Sardon catchment. These are categorized as inflow into and outflow from groundwater. The primary sources of groundwater inflow include: the gross recharge ( $R_g$ ) from precipitation, stream leakage to groundwater ( $q_{sg}$ ); the sources of groundwater outflows are: the groundwater evapotranspiration ( $ET_g$ ), groundwater exfiltration ( $Exf_{gw}$ ), stream leakage out of the groundwater to streams ( $q_{gs}$ ) and the lateral flow out of the aquifers at the drain boundary ( $q_l$ ). These water budget components for first and second layer are shown Table 7. The gross UZF recharge contributes the most for groundwater budget inflow (80.7%), followed by 13% from stream leakage and 6.3 % between the layers of total inflow for first layer. The contribution of the outflow component of the groundwater budget for the first layer were 46.5 % by groundwater evapotranspiration, 23.4 % by stream leakage, 17.9 % between layers, 11.2 % by groundwater exfiltration and only 1 % flow out of the catchment groundwater flow to the drain boundary. The second layer showed lower budget as the interaction with surface was limited to the outcrops. The largest inflow component observed was between layers which was 76.2 % followed by 23.6 % from stream leakage and the gross recharge contributed the lowest with 0.2 % of the total inflow to the second layer. The outflow was dominated by stream leakage (69.8 %) followed by exchange between layers (26.9 %) while the drain boundary contributed (3.1 %) and groundwater exfiltration 0.2 %. In addition, the model simulated stream discharge ( $q$ ) at the northern

outlet of the catchment as  $0.69 \text{ mm day}^{-1}$ , which contributes to the water balance closure of the Sardon catchment.

Table 7: Groundwater fluxes for steady-state condition for the first and second layer ( $\text{mm day}^{-1}$ )

First layer			Second layer		
Budget component	IN	OUT	Budget component	IN	OUT
Head dep bounds	0.00	0.02	Head dep bounds	0.00	0.01
Stream leakage	0.22	0.40	Stream leakage	0.10	0.28
GW ET	0.00	0.80	GW ET	0.00	7.44E-04
UZF recharge	1.38	0.00	UZF recharge	7.63E-04	0.00
GW exfiltration	0.00	0.19	GW exfiltration	0.00	0.00
From layer 1	0.00	0.00	From layer 1	0.31	0.11
From layer 2	0.11	0.31	From layer 2	0.00	0.00
Total IN-OUT	1.71	1.71	Total IN-OUT	0.40	0.40
IN-OUT		0.00	IN-OUT		0.00
Percent Error		0.00	Percent Error		0.00

The water balance of the model is closed and the percent of discrepancy (error) between the inflow and outflow was within the limit of the acceptable range  $\leq 0.1 \%$  (table 4). This indicates that the numerical error in the model was negligible. The water balance of the entire aquifer was closed. The discrepancy 0.0 is within the acceptable range of  $\leq 0.1\%$ .

The schematic diagram (Figure 18) shows the steady-state groundwater budget for the entire catchment model ( $\text{mm day}^{-1}$ ). The leakage from groundwater to stream (OUT) in Table 7 was larger than the stream leakage towards groundwater (IN); the result confirmed that the Sardon stream plays a large role draining groundwater. This river and streams are dry from mid-June to mid-October but otherwise perform a role of a drain, for groundwater and direct runoff (Lubczynski & Gurwin, 2005).

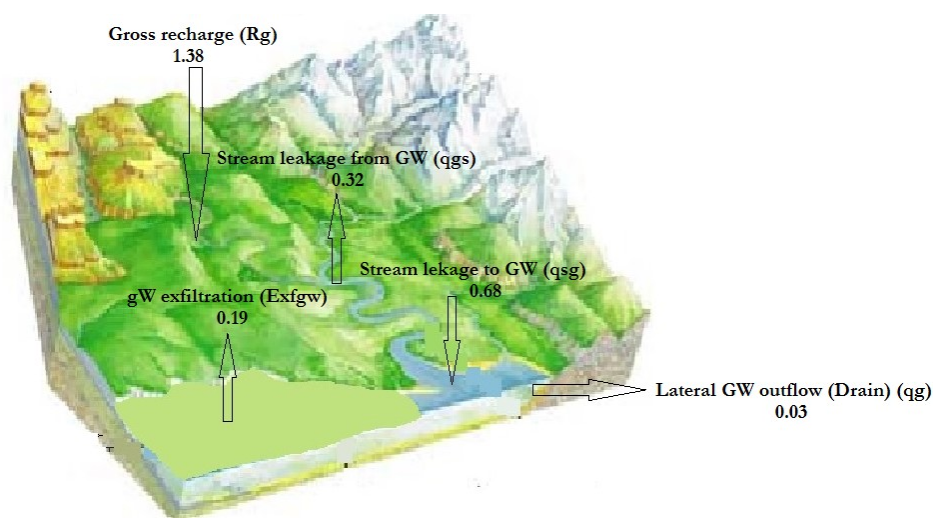


Figure 18: Schematic representation volumetric budget for the entire model of Sardon catchment for steady-state model simulation [all units are  $\text{mm day}^{-1}$ ]

### 3.2.4. Groundwater fluxes spatially

The groundwater fluxes show spatial variation as shown in Figure 19 to Figure 23 for the steady-state model simulation. The simulated  $ET_g$  loss from groundwater in Sardon catchment in the steady-state condition varied from 0 mm day<sup>-1</sup> at the non-fault areas to -1.9 mm day<sup>-1</sup> in the secondary fault zones along the stream channels in east, west and south boundaries of the catchment (Figure 19). Negative sign indicates water is removed from the groundwater budget. Highest  $ET_g$  was observed in the fault zones aligned with stream courses, where the groundwater was the shallowest. Ruwan (2009) has found the same trend of  $ET_g$  along the main fault zone that ranged from 0-0.34 mm day<sup>-1</sup>.

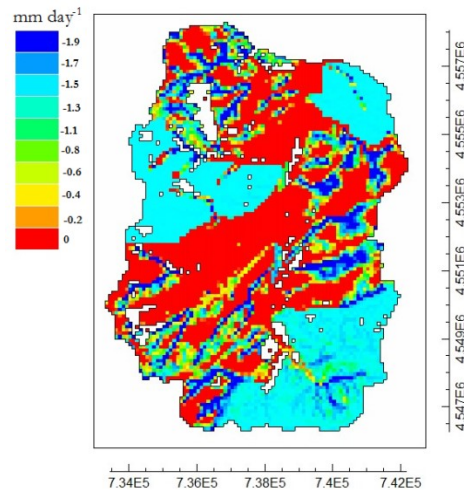


Figure 19: Groundwater evapotranspiration map of Sardon catchment for calibrated steady-state condition

Groundwater discharge to the surface which is described as groundwater exfiltration ( $Exf_{gw}$ ) (Hassan et al., 2014; Lubczynski & Gurwin, 2005) is the highest at the fault zones along river valleys and in upland areas (south west, east and north west) as high as 17.4 mm day<sup>-1</sup>; no groundwater exfiltration was observed at non-fault and low elevated areas (Figure 20). High groundwater exfiltration occurs where water table is shallow such as in the secondary fault zones.

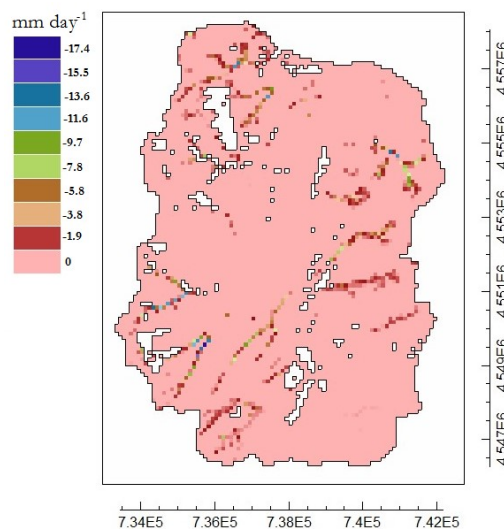


Figure 20: Groundwater exfiltration map of Sardon catchment for steady-state condition; non-zero individual cells within the outcrops represent direct exfiltration from the fissured layer

Groundwater gross recharge for the steady-state mode simulation is shown in Figure 21. The recharge rate was calculated as partition of the actual infiltration rate ( $P_e$ ) in UZF package (Equation 9). However, because in steady state, the  $ET_m = 0$ , the actual infiltration rate was equal to gross recharge (Equation 10). Figure 21 indicates that there is quite uniform distribution of gross recharge in almost of the entire active cells of the model with a maximum recharge rate of  $1.41 \text{ mm day}^{-1}$ . There are cells, especially along the fault/fractures of the aquifer, with lower recharge rate, ranging from  $0 \text{ mm day}^{-1}$  to  $1.21 \text{ mm day}^{-1}$ . In these cells, either the soil was saturated or there was shallow water table level so that part of infiltration rate was routed as saturation-excess (Dunnian) and/or infiltration excess (Hortonian) runoff to the streams with mean total amount of  $16,580.4 \text{ m}^3 \text{ day}^{-1}$ .

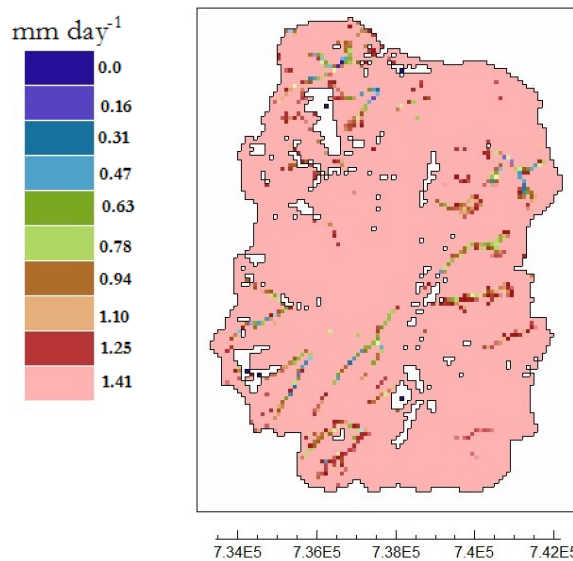


Figure 21: Gross recharge ( $R_g$ ) map of the Sardon catchment at steady-state model simulation ; non-zero individual cells within the outcrops represent direct recharge to the fissured layer.

Stream leakage was observed on the streams along the main and secondary fault zones. Highest stream leakage to groundwater was observed along the main fault zone of the Sardon catchment that ranged from  $3.6 \text{ mm day}^{-1}$  to  $132.5 \text{ mm day}^{-1}$ . Discharge from groundwater was observed at the secondary fault zones that ranged from  $22.2 \text{ mm day}^{-1}$  to  $99.5 \text{ mm day}^{-1}$ .

Despite quite uniform rainfall pattern in the catchment (Lubczynski & Gurwin, 2005), the steady-state model output provided spatially variable fluxes. The variability is due to the variable topographic condition, variable drainage pattern, spatial variability of vegetation types and aquifer heterogeneity (Hassan et al., 2014).

### 3.2.5. Sensitivity analysis

The model performance  $K_H$  and  $K_V$  were analysed as shown in Figure 22. The model was sensitive to change of  $K_H$  and nearly insensitive to changes in  $K_V$ .

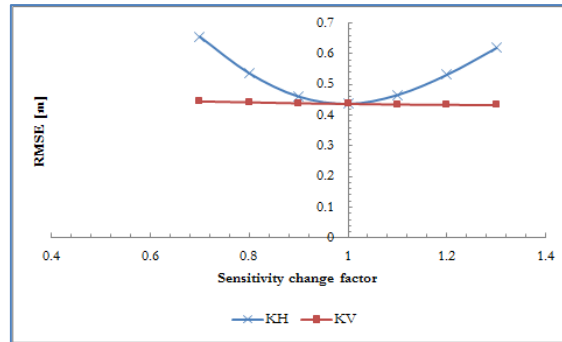


Figure 22: Sensitivity of model for horizontal hydraulic conductivity ( $K_H$ ) and vertical hydraulic conductivity ( $K_V$ ) for steady-state model simulation

The parameters and driving force in the UZF1 package were investigated (Figure 23). The model was sensitive to EXTDP (Figure 23-a), *PET* (Figure 23-b) and infiltration rate (Figure 23-d), the figures show a consistent increase in RMSE as the sensitivity change factor increases for EXTDP and *PET*. The model was insensitive to the EXTWC (Figure 23-c). These result showed that EXTDP, *PET* and infiltration rate are good for model calibration whereas the EXTWC creates uncertainty in the model calibration.

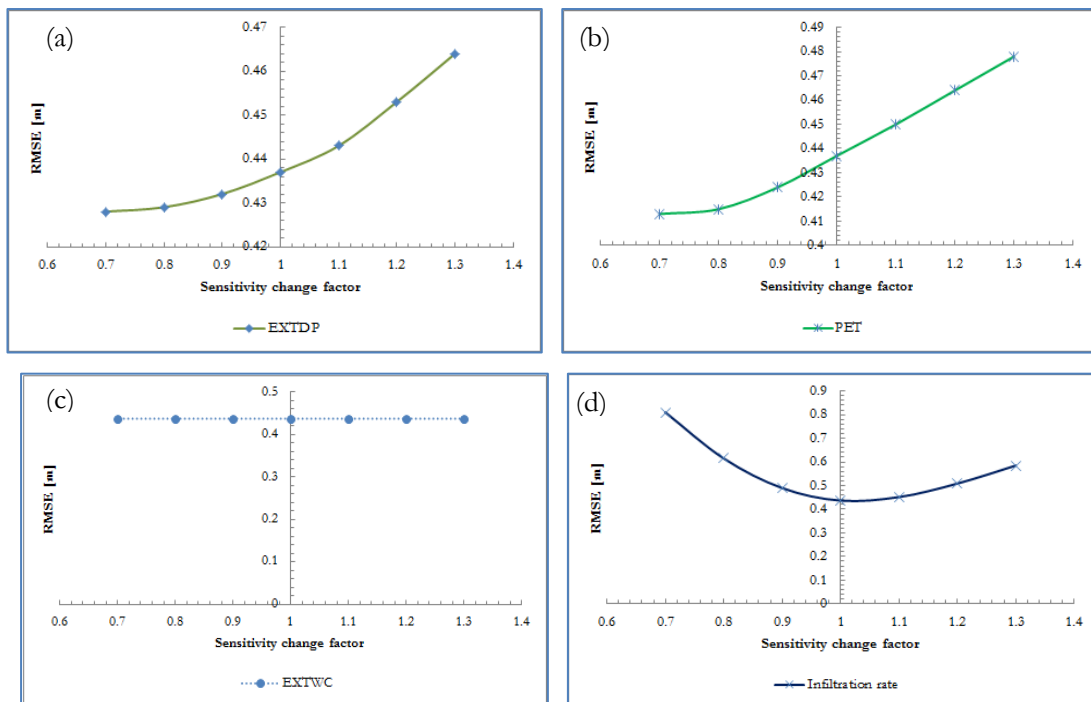


Figure 23: Sensitivity of model for UZF1 package parameter and driving force : (a) extinction depth, (b) potential evapotranspiration, (c) extinction water content and (d) infiltration rate for steady-state model simulation (N.B. There is scale difference)

The model was insensitive to change in UZF1 package variables saturated water content ( $WC_{sat}$ ) (Figure 24-a) and the Brooks-Corey-Epsilon (BCE) (Figure 24-b) and showed less sensitivity to maximum unsaturated hydraulic conductivity ( $K_{Vun}$ ) (Figure 24-c). These variables were assigned as spatially uniform

in each cell of the model in the UZF1 package, as depicted in the figures, the effect of these variables in the model simulation result is minimum.

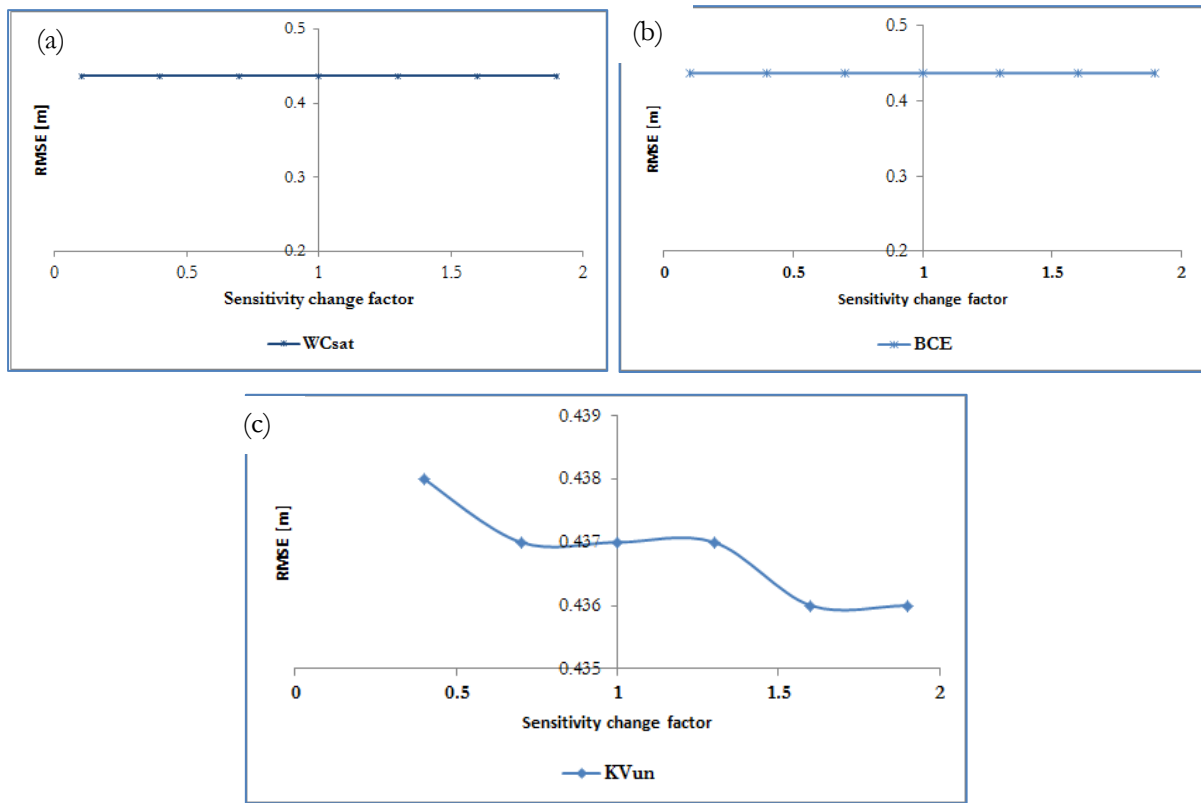


Figure 24: Sensitivity of model for UZF1 package variables : (a) saturated water content, (b) Brooks-Corey-Epsilon, (c) maximum unsaturated vertical conductivity (N.B. there is scale difference)

### 3.3. Transient state model calibration

The transient state model calibration was accomplished by trial-and-error parameter adjustment method. In this calibration, the final steady-state heads were transferred as initial head for the warming up step of transient model simulation. The head distribution obtained at the end of the 1-year warm up period (i.e. on 30/9/2008) was considered as true, initial calibration heads. The calibrated  $K_H$  of the steady-state was adjusted while  $K_V$  values, as non-sensitive (Figure 22) were left intact in the transient model calibration. Also storage parameters (SY and SS) and stream-bed depth were adjusted during model calibration. The transient model calibration was challenging as the parameters and spatial extent of zones affect each other and the results of the model run; the calibration process was time consuming as it each simulation run took up to ~3:00 hours and produced huge output files up to 5 GB. It was difficult to read and analyse these files using the standard Notepad, but the problem was solved by using the Listing Analyst and GW-chart software packages. The output was exported to standard Microsoft Excel for further analysis and interpretation.

### 3.3.1. Calibrated heads and error assessment

The calibrated head in transient model simulation is shown graphically using scatter plot (Figure 25) and statistically Table 8. The scatter plot shows that the observation points are distributed uniformly along the 1:1 line with high coefficient of correlation ( $r=0.9996$ ), this is good indication of good calibration of the model. The correlation result between the observed and simulated head satisfies the condition set by Hill (1998) as the  $r$  is greater than 0.9 and the head residual points fall close to a line with a slope of 1.

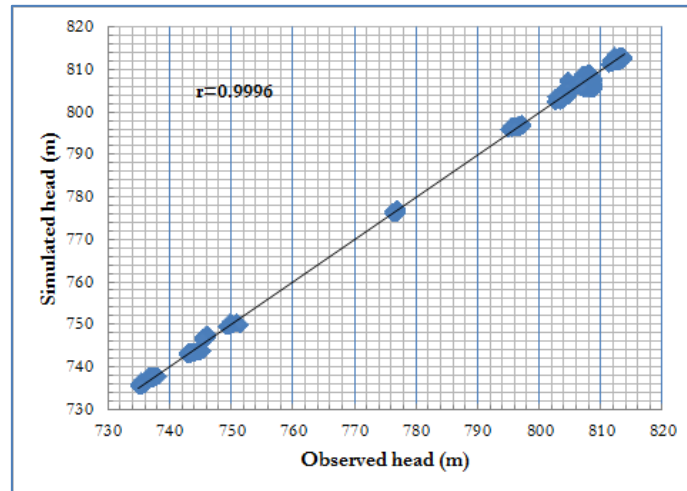


Figure 25: Scatter plot of the mean of daily differences between observed and simulated heads for the transient model simulation in the period from 01 October 2008 to 30 September 2013 for 12 groundwater monitoring points

The error assessment showed that the residuals in all observation points ranged from -1.09 m at piezometer PPNO in Penallbo to 0.76 m at borehole piezometer W1PCL7 in Tremedal. The ME, MAE and RMSE of the overall monitoring points were -0.04 m, 0.62 m and 0.81 m respectively. The RMSE for individual observation points ranged from 0.19 to 1.29 m (Table 8). The overall negative residual shows that there was slight bias towards over prediction of the rise of groundwater table. The RMSE value for individual monitoring points and for the overall of the model was acceptable since it was below 10% of the total head change. The ratio of RMSE to the total head change was also low, 0.01 %, which indicated that the model error represents a small part of the overall model error response. In general, the transient-state calibration satisfies the suggested model error criteria by Mason & Hipke (2013) (See the model criteria in subtopic 3.2.1).

Table 8: Statistical analysis result for 6-year transient model simulation for 12 groundwater monitoring points (hydrological years 1 October 2007 to 30 September 2013) [meters]

Obser. point	ME	MAE	RMSE	STD	Min	Max	N
PMU	-0.16	0.48	0.56	0.54	-1.38	0.79	2193
W1SD	0.20	0.44	0.59	0.56	-0.83	1.59	1102
PSDO	-0.85	0.88	1.05	0.61	-3.15	0.54	1841
W1PCL7	-0.03	0.16	0.19	0.19	-0.36	0.76	1096
W2PCL7	0.75	0.75	0.84	0.36	0.15	1.61	1097
W1PN	0.24	0.47	0.60	0.55	-0.69	2.00	1096
PPNO	-1.11	1.11	1.18	0.40	-1.93	-0.30	870
PTB2	-0.10	0.40	0.50	0.49	-1.40	0.73	703
PGJTMO	0.18	0.38	0.44	0.40	-0.45	1.09	297
W1TB	-0.33	0.38	0.43	0.29	-1.00	0.41	1101
PGJO	0.43	0.94	1.29	1.21	-2.09	3.61	1804
PGBO	0.37	0.62	0.70	0.59	-1.01	1.22	1501

Figure 26 shows the distribution of the calibrated heads of the first and second layer after the transient model calibration. From the two figures, it can be observed that the water flows from all directions of the catchment towards the main fault zone (central part of the catchment). The distribution of the head was almost similar with steady-state calibrated head distribution.

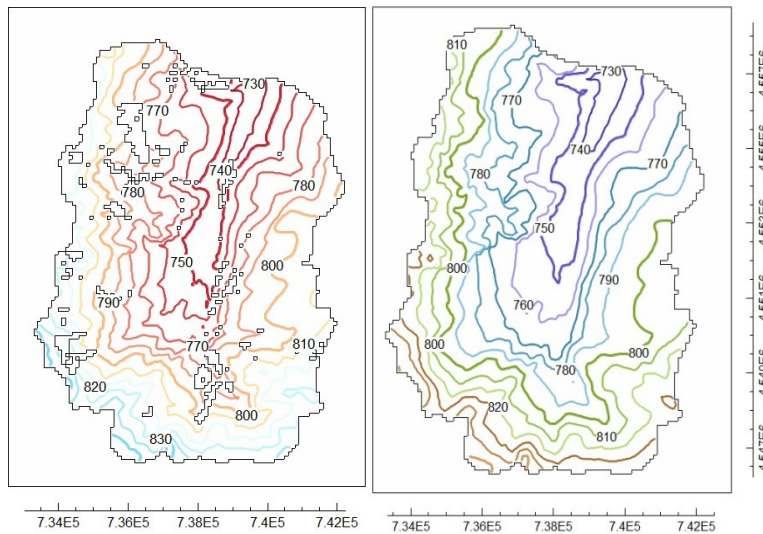


Figure 26: Calibrated head distribution (a) first layer and (b) second layer of the transient model simulation

Figure 27 shows the graphical comparison of hydrographs for observed and simulated groundwater heads for the transient model calibration (six years) and validation (one year). There was fluctuation in rise and recession of the heads in response to the rainfall in most of the monitoring points. The fluctuation of the hydrographs is due to the recharge of the groundwater during the rainy months, January to April in all simulation periods. The graphs also depicts that there is good match in trend of the rise and recession between the simulated and observed heads even though the lines do not match perfectly in some of the monitoring points.

There are different reasons for the mismatch of the observed and simulated heads. This can be caused by poor boundary conditions, poor conceptualization of the geology resulting in incorrect hydraulic properties (vertical and horizontal hydraulic conductivity, specific storage and specific yield), error in numerical solution and problem in parameterization (Konikow & Bredehoeft, 1992). Additional explanation is given by Hassan et al. (2014) that include unaccounted heterogeneity, uncertainty in the measured water level records, unaccounted water extraction, grid size and subgrid-scale altitude variability



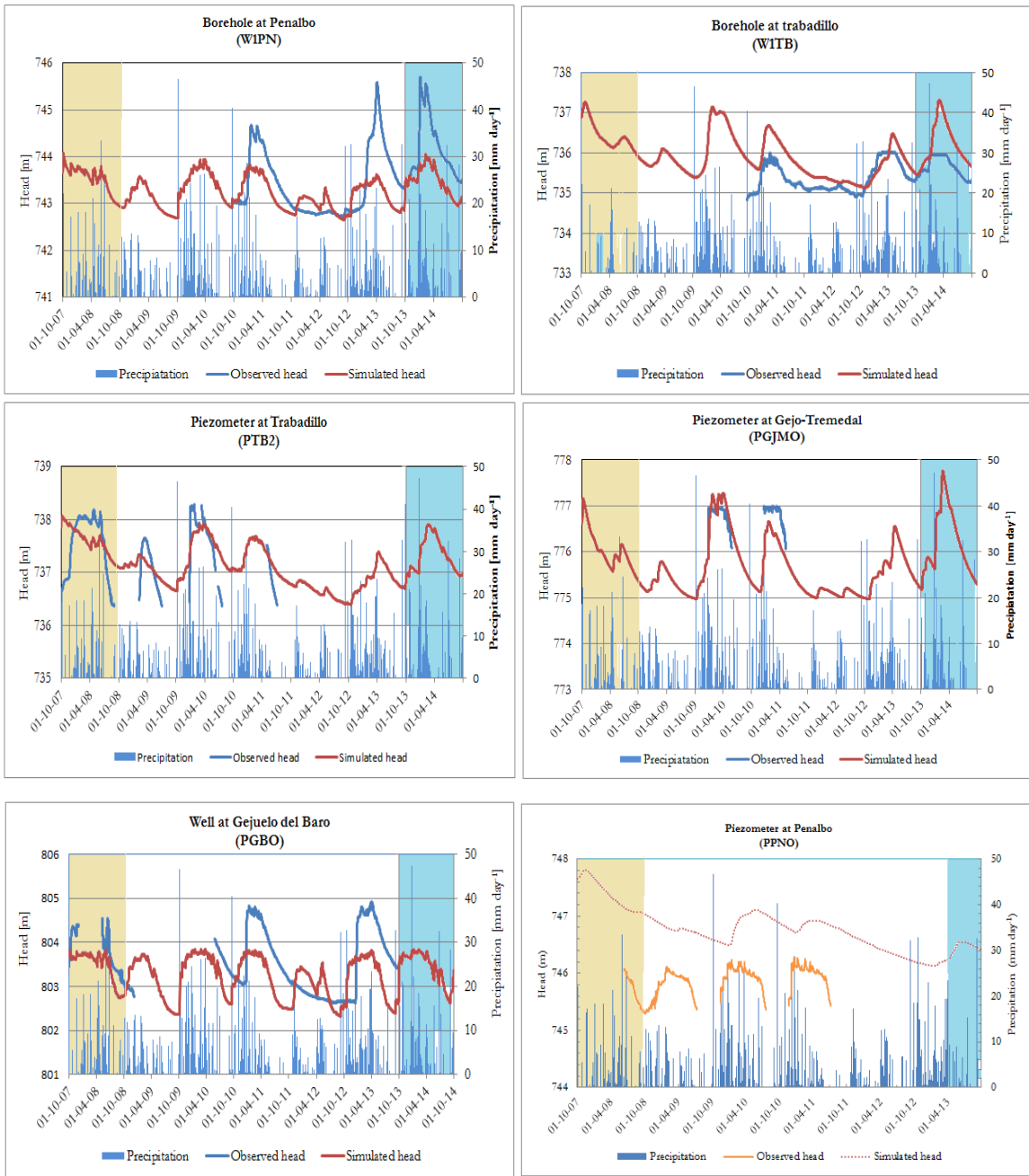


Figure 27: 7-year, transient model simulation consisting of 3 steps : i) 1-year warm up period (01/10/2007 to 30/09/2008) shaded in in light yellow colour; ii) 5-year calibration period (01/10/2008 to 30/09/2013) presented as colour-less; iii) 1 year validation period (01/10/2013 to 30/09/2014) presented as light blue colour. The model is calibrated on daily basis against 12 hydrographs of groundwater heads (3 wells, 5 deep boreholes and 4 piezometers) and validated also on daily basis and validated also on daily basis against 7 monitoring points (5 deep boreholes and 2 wells).

### 3.3.2. Hydraulic conductivity

The spatial distribution of the calibrated in transient  $K_H$  was the same as calibrated  $K_H$  in steady-state simulation (Figure 17). Only minor changes were made, these changes are also visible by comparing statistics of the two calibration modes, i.e. Table 3 (steady-state) with Table 9 (transient).

The calibrated  $K_H$  values in this study were much higher than the  $K_H$  values of the hydrological conceptual model (Table 1) proposed by (Francés, 2015). The calibrated in this study  $K_H$  of the first layer was also slightly larger than the  $K_H$  calibrated in transient GSFLOW mode by Hassan et al. (2014) in the same catchment while for the second layer, the calibrated  $K_H$  were comparable.

The calibrated  $K_H$  values of this study are in the same order of magnitude as in other HRA studies. For example, the  $K_H$  of study is slightly higher than in the Musi River sub-basin, India, where the  $K_H$  was  $0.1 \text{ m day}^{-1}$  for weathered layer and  $0.74 \text{ m day}^{-1}$  for weathered-fractured layer (Massuel et al. 2007) or in north-west Brittany, France, where calibrated  $K_H$  of  $0.07 \text{ m day}^{-1}$  for both weathered and fissured layer (Durand et al., 2015). The results of this model calibration contradicted one of the stratiform concepts, assuming larger  $K$  of the fissured deeper layer than the  $K$  of the shallow saprolite layer.

Table 9: Statistical analysis of hydraulic conductivity in the transient model simulation for the first and second layer of Sardon catchment

Stastical analysis	$K_H$ fault zone ( $\text{m day}^{-1}$ )		$K_H$ Non-fault zone ( $\text{m day}^{-1}$ )	
	First layer	Second layer	First layer	Second layer
Mean	4.11	1.50	3.00	0.66
Min	0.4	0.04	$1 \times 10^{-3}$	$8 \times 10^{-4}$
Max	12	9	10	3
STD	3.59	2.46	3.17	0.94

### 3.3.3. Specific yield and specific storage

The calibrated SY of the first layer ranged from 0.06 to 0.16 (Figure 28) and 0.07 for the whole second layer although active only at the second layer outcrops.

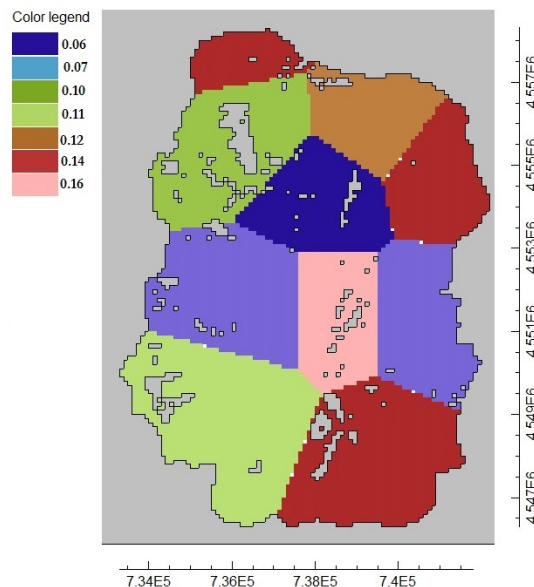


Figure 28: Specific yield after transient model calibration for the first layer for simulation period 01 October 2007 to 30 September 2013

The SY of the first layer was smaller in the central part of the catchment as compared to the elevated areas and was dependent on the soil characteristics and weathering stage. These SY values were slightly higher than in Hassan et al. (2014), which ranged from 0.017 to 0.043 but comparable with SY values observed in other HRA areas: for example in the Musi River sub-basin, India, the SY for the weathered granite layer was 0.16 and for the fractured-weathered layer 0.14 (Massuel et al., 2007) but in the north-west Brittany, France (Durand et al., 2015), the SY was 0.06. In turn, the SY values (Table 1) proposed by Francés (2015) were higher than the calibrated SY value in this study. The SS of the second layer in this study was assigned as uniform value  $1 \times 10^{-6} \text{ m}^{-1}$  for second layer. This value is in agreement with the SS of Hassan et al. (2014).

### 3.3.4. Groundwater budget

Table 10 and Figure 29 show the water budget for the entire model. The water budget components that contribute to the groundwater INPUT are (in % of IN): gross recharge (52.2 %), storage to the groundwater aquifer (43.4 %) and leakage from streams (4.5 %) of the total inflow to the groundwater. The discharges that contribute to groundwater OUTPUT are (in % of OUT): groundwater evapotranspiration (24.8 %), outflow through drain boundary (1.6 %), leakage to streams (23.4) and groundwater exfiltration (24.8 %).

Table 10: Groundwater budget of the entire model obtained as a result of the transient model calibration within the period (01 October 200t to 30 September 2013)

Groundwater fluxes in mm day <sup>-1</sup>		
Budget component	IN	OUT
Storage change ( $\Delta S$ )	0.61	0.53
Head dependent bounds ( $q_d$ )	0.00	0.02
Stream leakage	0.06	0.33
Groundwater evapotranspiration ( $ET_g$ )	0.00	0.35
Gross recharge ( $R_g$ )	0.73	0.00
GW exfiltration ( $Exf_{gw}$ )	0.00	0.17
Total IN=OUT	1.40	1.40
IN-OUT		0.00
% Error		0.00

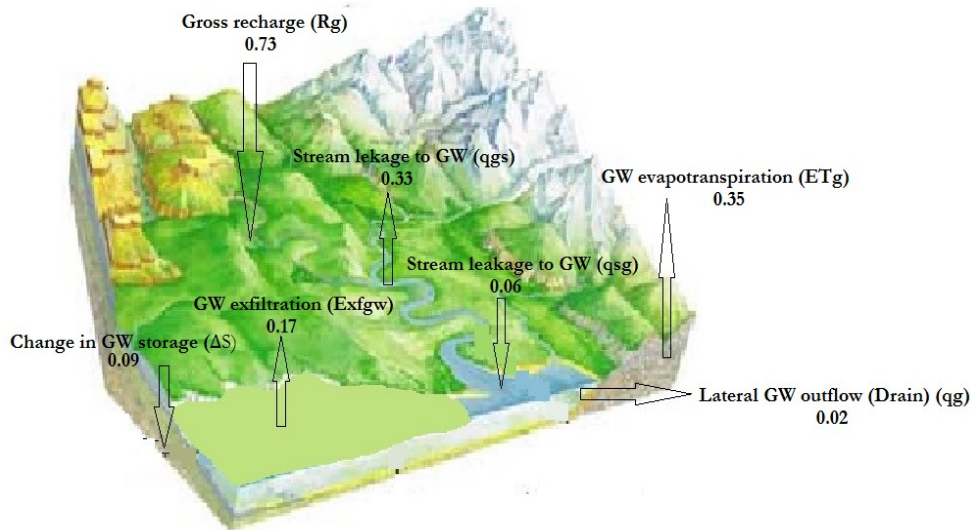


Figure 29: Schematic representation of groundwater budget for the entire model of Sardon catchment obtained as a result of transient model calibration within the period 01 October 2007-30 September 2013 (all units are  $\text{mm day}^{-1}$ )

The analysis of the transient model simulation showed that the gross recharge represented 49.3 %, net recharge 14.2 % (was positive), groundwater evapotranspiration 23.5 % and drain boundary 1.6 % of the total annual rainfall. The average discrepancy in all stress periods was  $\leq 0.1$  % with maximum of 0.21 % and minimum of -0.11 %.

### 3.3.5. Temporal variability of groundwater fluxes

The gross recharge, groundwater evapotranspiration, groundwater exfiltration, and the resultant (Equation 12) net recharge, all showed large temporal variability (Figure 30). The gross recharge and groundwater exfiltration indicated the same trend, i.e. their peaks were simultaneous but with opposite sign. Therefore, the difference between the two is referred (Hassan et al. 2014) as effective recharge ( $R_e = R_g - Exf_{gw}$ ). During the wet month (e.g. November), when  $R_g$  and  $Exf_{gw}$  reached their peaks and  $ET_g$  was negligible, the  $R_e$  and  $R_n$  were reaching their positive maxima. In contrast, during dry months (e.g. July and August),  $ET_g$  was high but because of no rainfall, also  $Exf_{gw}=0$  and therefore net recharge used to reach nonnegative maxima being equal to  $ET_g$ .

Summarizing groundwater flux variability within the simulated period (01 October 2007 to 30 September 2013): the  $ET_g$  ranged from  $-0.03 \text{ mm day}^{-1}$  in November to  $-1.34 \text{ mm day}^{-1}$  in June with an average of  $-0.34 \text{ mm day}^{-1}$ ; the  $Exf_{gw}$  ranged from  $0.00 \text{ mm day}^{-1}$  in dry months to  $-3.15 \text{ mm day}^{-1}$  in February with an average of  $0.17 \text{ mm day}^{-1}$ ; the  $R_g$  ranged from  $0.00 \text{ mm day}^{-1}$  in dry months to  $> 9 \text{ mm day}^{-1}$  with an average of  $0.73 \text{ mm day}^{-1}$ ; the  $R_n$  ranged from  $-1.13 \text{ mm day}^{-1}$  in dry months to  $> 10.13 \text{ mm day}^{-1}$  with an average of  $0.21 \text{ mm day}^{-1}$  (Figure 30).

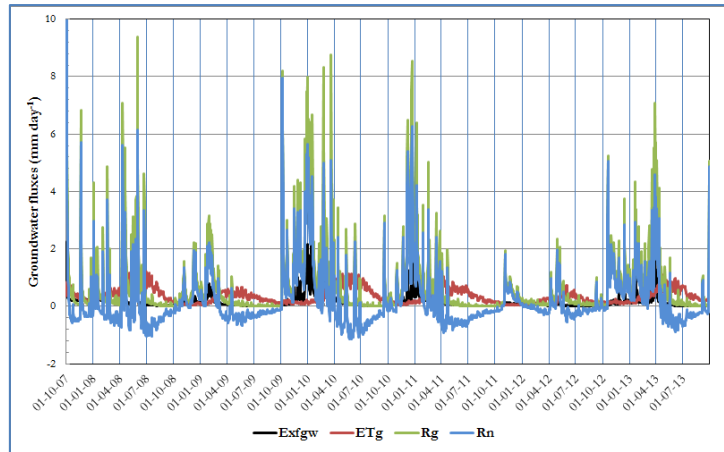


Figure 30: The transient calibrated groundwater exfiltration ( $Ex_{fgw}^c$ ), groundwater evapotranspiration ( $ET_g$ ), gross recharge ( $R_g$ ) and net recharge ( $R_n$ ) groundwater fluxes for 6-year periods from 01 October 2007 to 30 September 2013.

The  $ET_g$  and  $ET_{un}$  rates from UZF1 output showed a daily variability as shown in Figure 31. The maximum  $ET_{un}$  of  $\sim 2.7$  mm day<sup>-1</sup> was observed in September and the minima (0 mm day<sup>-1</sup>) in the months of June-October. The graph shows also that the  $ET_{un}$  was typically higher than  $ET_g$  during the months of October to March when  $PET$  demand was satisfied by the available soil moisture of unsaturated zone preventing or at least restricting  $ET_g$ . Evapotranspiration simulated over a specified depth in the unsaturated zone. The rate of groundwater evapotranspiration is dependent on the quantity of water stored in the unsaturated zone above the assigned extinction depth and on extinction water content. The  $ET_g$  reached peak during the month July when the unsaturated zone moisture failed to satisfy the  $PET$  demand. The  $ET_g$  of this study (0.01 mm day<sup>-1</sup> to 1.34 mm day<sup>-1</sup>) is almost the same as in the transient model results of the previous study by Lubczynski Gurwin, (2005) that ranged from  $< 0.05$  mm day<sup>-1</sup> in wet season up to 0.8 mm day<sup>-1</sup> in dry season.

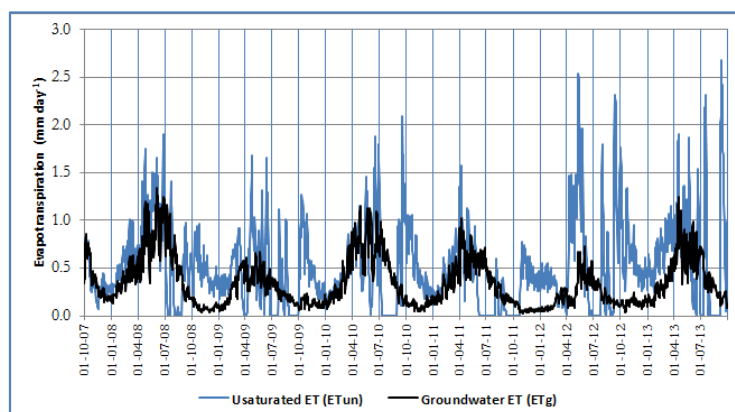


Figure 31: The transient calibrated unsaturated zone evapotranspiration ( $ET_{un}$ ) and groundwater evapotranspiration ( $ET_g$ ) for 6-year periods (01 October 2007 to 30 September 2013).

Figure 32-a and b show the yearly and cumulative change in volumetric groundwater storage of the two Sardon aquifers' system during the 6-year simulation periods. The positive change of groundwater storage

(increase) occurred in “wet” years 2008, 2009, 2011 and 2012, i.e. when infiltration exceeded the annual evapotranspiration rate. The negative change of groundwater storage (decrease) occurred in “dry” years 2010 and 2013, i.e. when evapotranspiration exceeded infiltration (Figure 32-a).

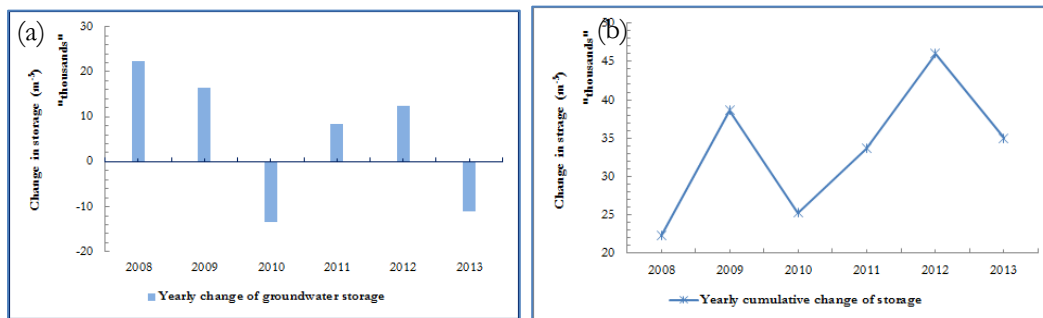


Figure 32: Yearly volumetric change of ground storage within six hydrological years (01 October 2007 to 30 September 2013): (a) yearly groundwater storage; (b) cumulative change in storage

### 3.3.6. Yearly transient and steady-state groundwater fluxes for the entire model domain

Table 11 shows the summarized analysis of transient model simulation and driving forces (precipitation and  $PET$ ), infiltration, groundwater fluxes ( $ET_g$ ,  $Exf_{gw}$ ,  $q$ ,  $q_{gs}$  and  $q_{gs}$ ) and UZF package outputs ( $R_g$ ,  $ET_{um}$  and  $R_o$ ) for the steady-state and 6-year transient model simulation (hydrological years extended from 01 October 2007 to 30 September 2013). It can be observed that there is annual variability in fluxes and also there is difference in fluxes simulated by the steady-state and transient model.  $ET_{um}$  and  $\Delta S$  was simulated for the transient state only. The steady-state model simulation does not consider the change in storage and unsaturated zone evapotranspiration. The steady-state and transient model simulation results were comparable with mean of the 6-year simulation periods for some of the groundwater fluxes including outflow at the drain boundary and stream leakage to groundwater. There is, however, variation with others fluxes due to the simplification in steady-state model simulation. In steady-state the applied infiltration is assigned in total as recharge to the groundwater table whereas in transient state, it is partitioned as effective recharge ( $Pe$ ) according to Equations 9 and 10.

The  $ET_g$  in steady-state was higher than the average of the transient model simulation since the unsaturated zone evapotranspiration was neglected in steady-state model simulation and considered as a loss from the total recharge to the groundwater.

### 3.3.7. Mean Mass water balance for the entire transient model

The MODFLOW-NWT numerical model simulates the surface groundwater interaction. The water balance was calculated for unsaturated, saturated zone and for the entire model (Table 12). Equations 5 to 7 used to calculate the water balance for the entire model, Equation 8 for the land surface and unsaturated zone together and Equation 11 for saturated zone. The table shows that the water balance (IN-OUT) was minimal. As shown in Table 12 the difference between IN and OUT ranged from 3.65 to 54.8 mm year<sup>-1</sup> and the discrepancy was close to the allowed limit  $\leq 0.1\%$ .

Table 11: Water balance yearly means as a result of 7-year MODFLOW-NWT steady-state model calibration (7-year average), transient model calibration (2008-2013) and validation (2014) for the Sardon catchment calculated according to the equations 5-12; each hydrological years starts from 01 October of the previous year and ends 30 September of the year as listed (All units are in m year<sup>-1</sup>)

	$P$	$PET$	$I$	$Inf$	$R_n$	$q_g$	$R_g$	$q_g$	$q_g$	$R_o$	$ET_g$	$Exf_{gp}$	$\Delta S_g$	$R_o$	$P_e$	$ET_m$	$\Delta S_m$
Stead-state model	540.2	681.9	25.3	501.2	162.0	17.7	498.8	10.2	169.5	261.5	75.3	0.0	88.9	498.8	0.0	0.0	0.0
2008	540.2	666.9	25.3	515.5	20.4	21.6	295.4	9.3	140.6	192.8	82.2	107.9	116.3	479.9	215.7	-30.1	-30.1
2009	317.2	683.1	14.9	302.3	11.2	24.3	139.4	8.1	106.6	91.3	36.9	79.3	45.2	293.1	151.2	2.8	2.8
2010	744.1	636.7	34.9	709.3	195.2	20.3	459.9	9.1	141.8	151.6	113.0	-64.6	170.0	650.2	186.5	4.8	4.8
2011	440.8	644.0	20.7	420.2	68.8	22.3	261.4	8.6	123.1	121.8	70.8	40.6	99.4	390.3	138.8	-9.6	-9.6
2012	333.6	660.7	15.6	318.0	13.0	25.7	102.3	7.3	91.2	70.1	19.2	59.8	22.9	313.3	189.2	22.3	22.3
2013	671.5	818.1	31.5	640.0	151.7	22.8	340.7	7.9	113.1	132.3	56.7	-53.4	86.0	608.9	246.1	22.8	22.8
Validation (2014)	726.4	664.3	32.9	693.5	80.3	18.3	430.7	11.0	171.6	189.8	160.6	84.0	244.6	613.2	186.2	-3.7	-3.7
Spatio-temporal	726.4	664.3	32.9	693.5	-18.3	21.9	394.2	7.3	127.8	310.3	102.2	138.7	153.3	580.4	204.4	-18.3	-18.3
Minimum	317.2	636.7	14.9	302.3	11.2	20.3	102.3	7.3	91.2	70.1	19.2	0.2	22.9	293.1	138.8	-30.1	-30.1
Maximum	744.1	818.1	34.9	709.3	195.2	25.7	459.9	9.3	141.8	192.8	113.0	-0.1	170.0	650.2	246.1	22.8	22.8
Average	507.9	684.9	23.8	484.2	76.7	22.8	266.5	8.4	119.4	126.7	63.1	0.1	90.0	456.0	187.9	2.2	2.2
Standard deviation	176.0	67.3	8.2	167.8	79.1	1.9	131.8	0.8	19.8	43.6	33.4	-0.1	52.3	150.3	39.8	20.1	20.1

Table 12: Water balance for entire model, unsaturated and saturated zones for transient model simulation for six hydrological years (01 October 2007 to 30 September 2013) [all units are in mm year<sup>-1</sup>]

Balance component	$PPT$	$ET_g$	$ET_m$	$Exf_{gp}$	$q_g$	$R_g$	$R_o$	$I$	$q$	$q_g$	$\Delta S_g$	$\Delta S_m$	IN-OUT	% Discrepancy
Entire aquifer	540.2	-127.8	-189.8					-25.6	-171.55	-7.3	32.9	3.7	54.8	0.19
Land surface and unsaturated zone	540.2		-189.8	62.1		-266.5	-87.6	-25.6				3.7	36.5	0.12
Saturated zone		-127.8		-62.1	21.9	266.5				-7.3	32.9		3.65	0.02

Where  $P$  is precipitation,  $PET$  is potential evapotranspiration,  $ET_g$  is groundwater evapotranspiration,  $Exf_{gp}$  is exfiltration,  $q_g$  is stream leakage toward the groundwater aquifer,  $q_g$  is stream leakage from groundwater,  $R_g$  is gross recharge,  $R_o$  is runoff,  $I$  is infiltration,  $Inf$  is actual infiltration,  $P_e$  is actual infiltration,  $q$  is stream discharge at the northern outlet,  $q_g$  is the later out flow at rain boundary,  $\Delta S_g$  is change in groundwater storage,  $\Delta S_m$  is storage change in unsaturated zone

### 3.3.8. Sensitivity analysis

A sensitivity analysis was conducted to understand the uncertainty of parameters:  $K_H$ , SY, SS and UZF1 package parameters (EXTDP, EXTWC, *PET* and infiltration rate). The model was sensitive to change in  $K_H$ . The increase of RMSE was observed when the  $K_H$  was less than - 10 % and greater than +10 % of calibrated  $K_H$  (Figure 33).

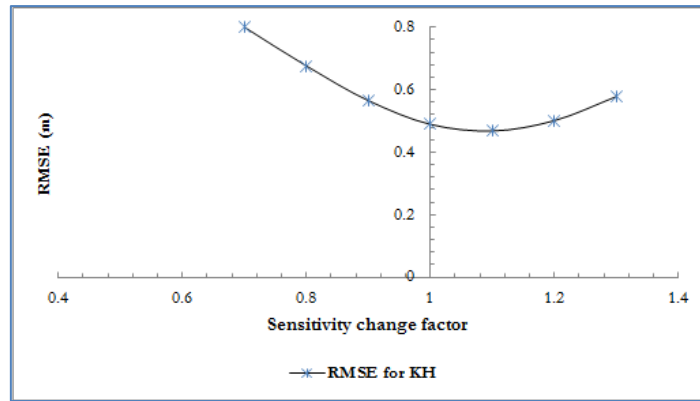


Figure 33: Sensitivity analysis of hydraulic parameters on head of groundwater through the change of Root Mean Square Error (RMSE).

RMSE value was increased as the SY value increased (Figure 34-a), this indicates that the difference between simulated and observed head is high and the hydrographs will not match. As shown in the Figure 34-b, the SY values control the amplitudes of the fluctuations in the water table at observation point. Higher values of the SY had a damping effect and lower values increased the amplitude. For low values of SY, the model failed to converge. Regarding SS sensitivity presented in Figure 34-c, the model was practically irresponsive.

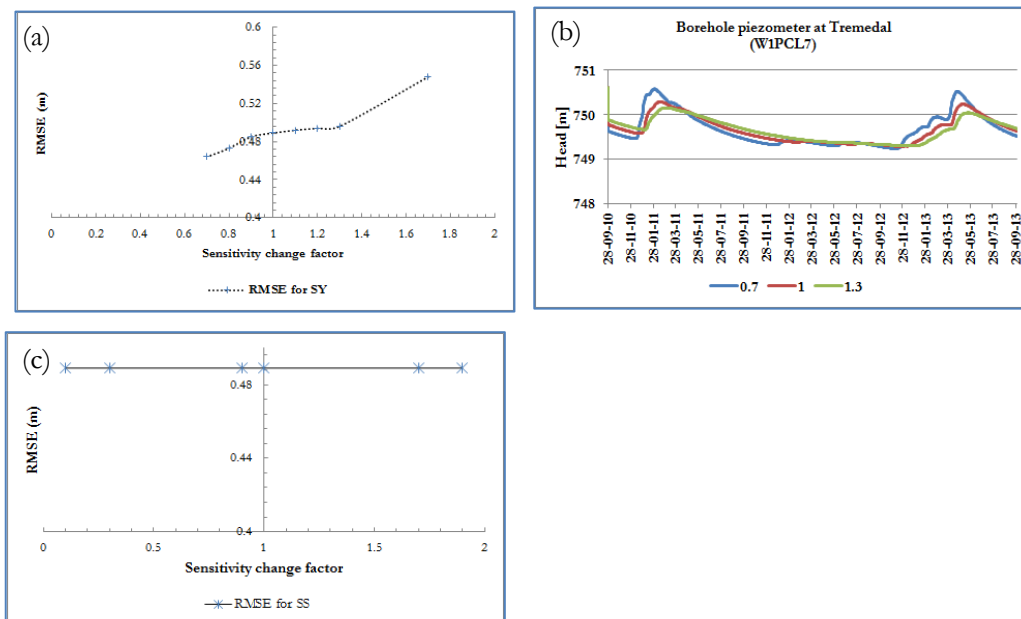


Figure 34: Sensitivity analysis of storage coefficients on head of groundwater through the change of Root Mean Square Error (RMSE)

The model was sensitive to changes in UZF1 driving forces, *PET*, EXTWD and Infiltration (Figure 35 a-c) while it was insensitive for EXTWC (Figure 35-d). The sensitivity pattern for EXTDP and *PET* was the same since *PET* and EXTDP are interrelated in groundwater loss by groundwater evapotranspiration. *PET* is the driving for loss of water from the groundwater up to the extinction depth of roots. The sensitivity analyses for both the steady-state and transient model simulation showed almost similar results.

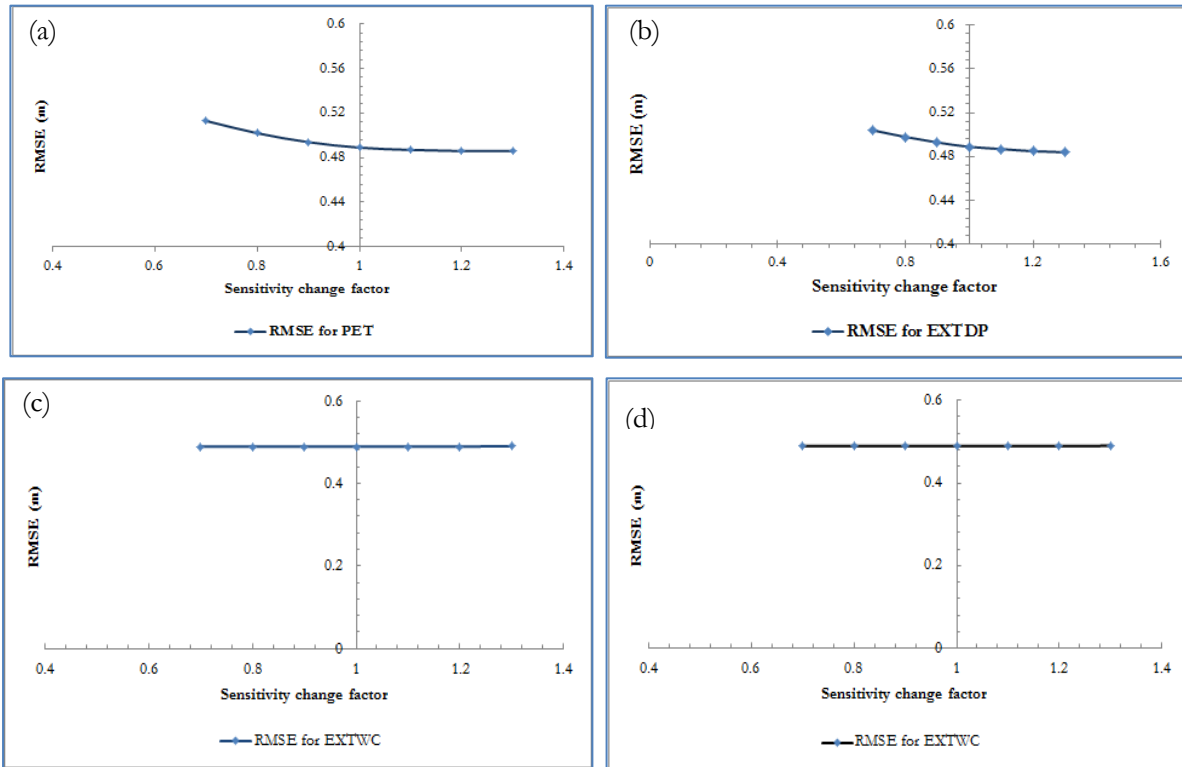
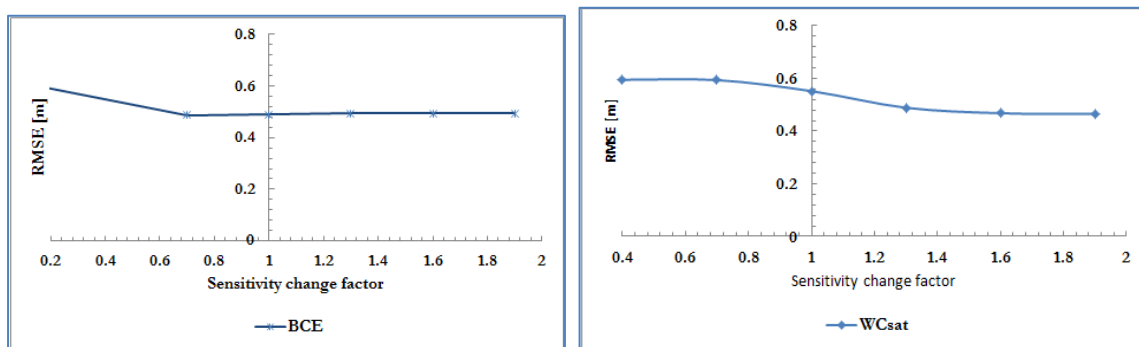


Figure 35: Sensitivity analysis of UZF1 package inputs on head of groundwater through the change of Root Mean Square Error (RMSE)

The sensitivity analysis of UZF1 parameters as shown in Figure 36 revealed that Brooks-Corey-Epsilon (Figure 36a), saturated water content (Figure 36-b) and maximum unsaturated vertical conductivity (Figure 36-c) are less sensitive to change of the assigned variables. Note that for Brooks-Corey-Epsilon below -30 % change of the assigned 3.35, the model encountered solver convergence problem.



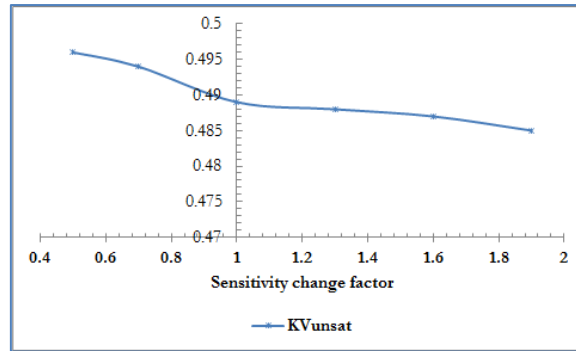


Figure 36: Sensitivity analysis of UZF1 (a) Brooks-Corey-Epsilon, (b) saturated water content and (c) Maximum unsaturated vertical conductivity

### 3.4. Validation

#### 3.4.1. Calibrated head and error assessment

The head validation in transient model simulation provided for year 2014, is shown graphically using scatter plot Figure 37. This plot shows that the observation points are scattered uniformly along the 1:1 line with high correlation coefficient ( $r=0.9997$ ). In general, there is good match between the trend of hydrographs of the simulated head and observed head (Figure 27). The RMSE of the validated model was 0.94 which is comparable with the RMSE of the transient model calibration (0.81) this means that the calibration of the model was well validated.

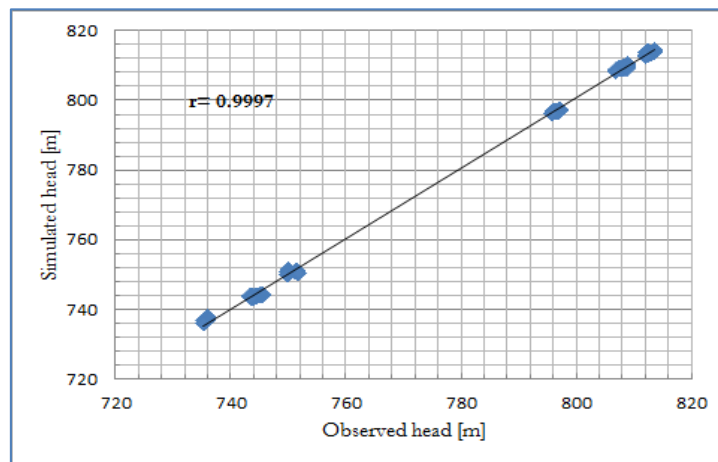


Figure 37: Scatter plot between observed and simulated heads for validation of model for one year (01 October 2013 to 30 September 2014) for 7 groundwater monitoring points

#### 3.4.2. Transient simulation with spatio-temporally variable UZF1 driving forces

An additional, 1-year (2014) transient model simulation in which infiltration rate, PET, EXTDP changed temporally and spatially, demonstrated that the groundwater budget was different as compared to similar run but with spatially uniform driving forces. Higher groundwater evapotranspiration and change in groundwater storage was observed whereas the groundwater exfiltration, gross recharge, stream leakage

and outflow at the drain boundary were lower in the spatio-temporally variable driving forces (Table 13) as compared to spatially uniform driving forces. The water budget was closed for both model simulation and the discrepancy for both was within the acceptable range  $\leq 0.1\%$ .

Table 13: Groundwater budget for spatially uniform and spatio-temporally variable driving forces for the entire model domain (all units  $\text{m day}^{-1}$ )

Budget components	Spatio-temporally variable driving forces		Spatially uniform driving forces	
	IN	OUT	IN	OUT
Change in storage	1.06	0.68	0.93	0.70
Head dep bounds	0.00	0.02	0.00	0.03
Stream leakage	0.06	0.35	0.05	0.47
GW Evaporation	0.00	0.85	0.00	0.52
Gross recharge	1.08	0.00	1.18	0.00
GW Exfiltration	0.00	0.28	0.00	0.44
Total IN-OUT	2.19	2.19	2.16	2.16
IN-OUT		0.00		0.00
Percent Error		0.00		0.00

The groundwater evapotranspiration contributed 38.7 % of the total outflow in the simulation with spatio-temporally variable driving forces while as compared to the spatially fixed inputs which was 27.7 % of the total outflow. The gross recharge constitutes lower 49.2% contribution to the total IN in the simulation with spatio-temporally variable driving forces, as compared to 54.4 % in the simulation with spatially uniform driving forces (Table 13). Figure 38 shows the temporal variability of the groundwater fluxes, with uniform (a) and spatio-temporally variable (b) driving forces. Both simulation showed the same trend in temporal variability.

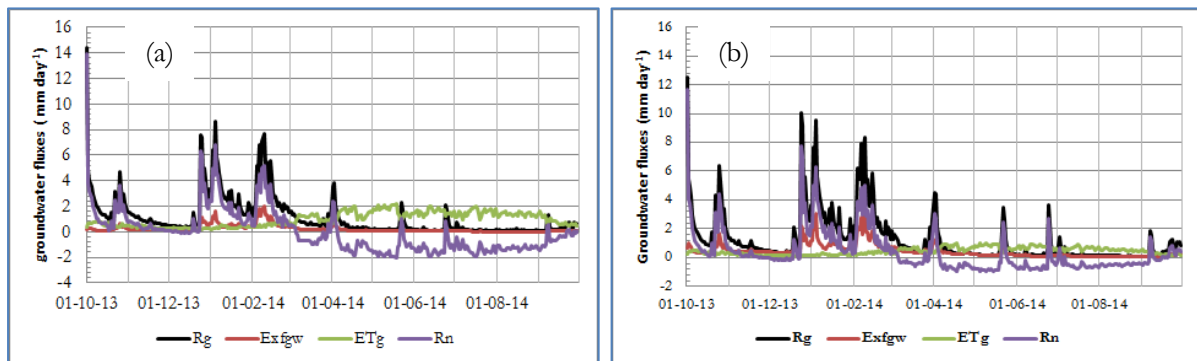


Figure 38: Temporal variability of groundwater fluxes for fixed and variable inputs for 1-year model simulation (a) fixed driving force and (b) variable driving forces

The spatial variability of input driving forces, enhanced spatial variability of groundwater fluxes. There is spatial variation of gross recharge between the two simulations. The gross recharge ranged from 0 to 5.41 mm day<sup>-1</sup> (Figure 39-a) for spatio-temporal variable driving forces which is lower than the gross recharge range of spatially fixed driving forces simulation 0-3.65 mm day<sup>-1</sup> (Figure 39-b).

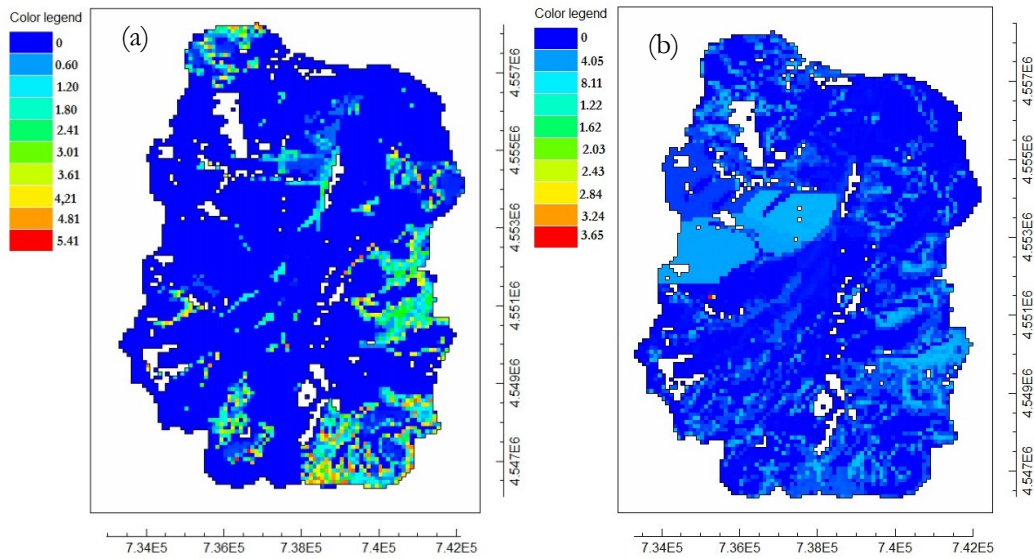


Figure 39: Groundwater gross recharge map for the last stress period 30 September 2014: (a) Spatially and temporally variable driving forces (b) spatially fixed driving forces [mm day<sup>-1</sup>]

As shown in Figure 40, the  $ET_g$  for the simulation with spatio-temporally variable driving forces was higher, ranging from -1.98 to 0 mm day<sup>-1</sup> (Figure 40-a). For the simulation with spatially uniform driving forces, the  $ET_g$  ranged from -1.33 to 0 mm day<sup>-1</sup> (Figure 40-b). The  $ET_g$  in simulations with spatio-temporally variable driving forces is higher than in simulation with spatially uniform driving forces.

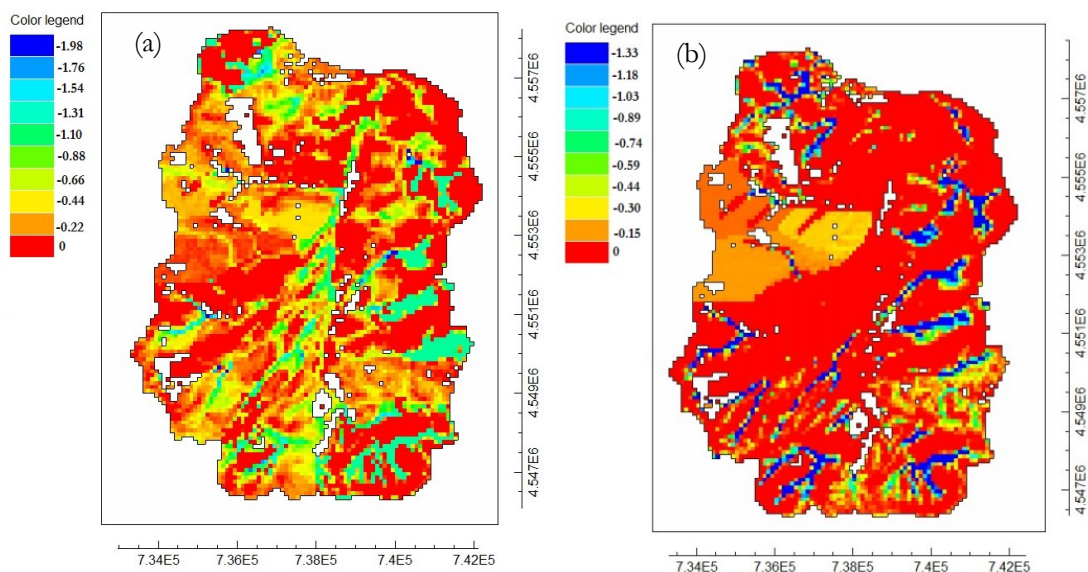


Figure 40: Groundwater evapotranspiration map for the last stress period 30 September 2014: (a) Spatially and temporally variable driving forces (b) spatially fixed driving forces [mm day<sup>-1</sup>]

As shown in Figure 41, the  $Exf_{gw}$  for the simulation with spatio-temporally variable driving forces was higher, ranging from -1.98 to 0 mm day<sup>-1</sup> (Figure 40-a). For the simulation with spatially uniform driving forces, the  $ET_g$  ranged from -1.33 to 0 mm day<sup>-1</sup> (Figure 40-b). The  $ET_g$  in simulations with spatio-temporally variable driving forces is higher than in simulation with spatially uniform driving forces.

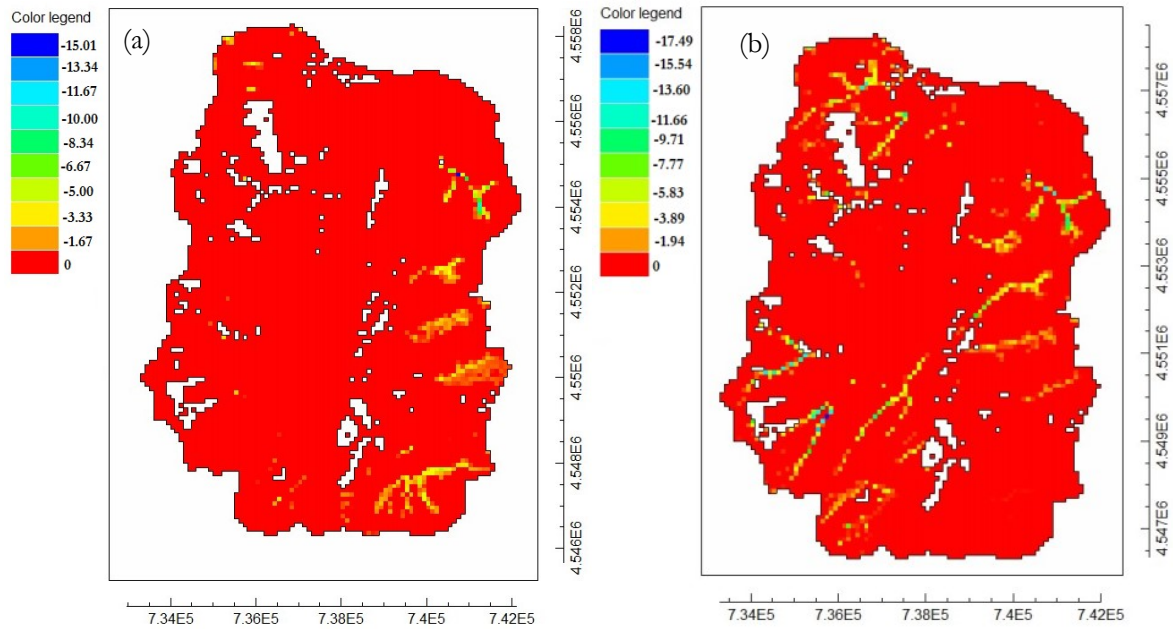


Figure 41: Groundwater exfiltration map for the last stress period 30 September 2014: (a) Spatially and temporally variable inputs (b) spatially fixed inputs [mm day<sup>-1</sup>]

## 4. CONCLUSION AND RECOMMENDATION

### 4.1. Conclusion

The study area, Sardon catchment (~80 km<sup>2</sup>), is a hard-rock aquifer system, with dense fractures and complex, dynamic groundwater-surface interactions. The catchment is nearly not affected by human activities and has long-time meteorological and groundwater monitoring data, perfectly suitable for not only steady state but also transient groundwater modelling including transient model calibration. A number of studies have been conducted to quantify the groundwater and to understand the dynamics of the aquifer considering it as a representative of hard-rock aquifers in arid and semi-arid areas. These studies applied different, stand-alone and coupled models, although none applied stratiform conceptual model in numerical solution.

In this study, the stratiform hydrological conceptual model of Frances et al. (2014) was implemented in the MODFLOW-NWT numerical model utilizing its SFR2 and UZF1 Packages for simulating surface groundwater interactions. The most important findings of this study that satisfy the research objectives and answer the research questions are listed below:

- The calibrated  $K_H$  was higher in the first, saprolite layer than in the fractured/fissured less weathered second layer which contradicts one of the assumptions of the stratiform concept; besides, the  $K_H$  was higher in the fault zones than the non-fault zones. The calibrated  $K_H$  ranged from  $1 \times 10^{-3}$  m day<sup>-1</sup> to 10 m day<sup>-1</sup> in the first layer and from  $4 \times 10^{-3}$  to 11 m day<sup>-1</sup> in the second layer. The  $K_H$  was comparable with other studies in this area and also with studies carried out elsewhere in the world.
- The calibrated SY of the first layer ranged from 0.06 to 0.16 and 0.07 for the entire second layer.
- Steady-state and transient models were calibrated and validated using 7 years of daily hydraulic heads. In the steady-state calibration: gross recharge, contributed 81.4% and stream leakage 18.6% of the total groundwater inflow. The groundwater outflow consisted of groundwater evapotranspiration 46.8%, stream leakage 40.2%, groundwater exfiltration 11.3% and lateral outflow at the northern boundary 1.7%.
- In the transient model calibration, the following 6-year average ( 01 October 2007 to 30 September 2013) groundwater fluxes were obtained: gross recharge 0.73 mm day<sup>-1</sup> (49.3 % of precipitation),  $ET_g$  was 0.35 mm day<sup>-1</sup> (23.7 % of precipitation),  $Exf_{gw}$  0.17 mm day<sup>-1</sup> (11.5 % of the precipitation), net recharge 0.21 mm day<sup>-1</sup> (14.2 % of precipitation),  $\Delta S$  0.09 mm day<sup>-1</sup> (6 % of precipitation),  $q_g$  0.02 mm day<sup>-1</sup> (1.4 % of precipitation).

- In transient model calibration, temporal pattern of flux variability was obtained:  $R_g$  ranged from  $4.5 \times 10^{-5}$  (September) to  $12.8 \text{ mm day}^{-1}$  (October) with an average of  $0.73 \text{ mm day}^{-1}$ ;  $\text{Exf}_{\text{gw}}$  from  $0.01 \text{ mm day}^{-1}$  (August) to  $3.15 \text{ mm day}^{-1}$  (February),  $\text{ET}_g$  from  $0.03 \text{ mm day}^{-1}$  (November) to  $1.34 \text{ mm day}^{-1}$  (June),  $\text{ET}_{\text{un}}$  from  $0 \text{ mm day}^{-1}$  (June-October) to  $2.68 \text{ mm day}^{-1}$  (August) and  $R_n$  from  $-1.1 \text{ mm day}^{-1}$  (May) to  $10.1 \text{ mm day}^{-1}$  (October) with an average of  $0.21 \text{ mm day}^{-1}$ . The groundwater flux variability corresponds mainly with seasonal variability of driving forces changing from dry to wet season but differing also between years that can be “dry” with rain in order on  $317.5 \text{ mm year}^{-1}$  (2009) but also “wet” with rain in order of  $744.6 \text{ mm year}^{-1}$  (2010).
- MODFLOW-NWT with UZF1 and SFR2 in the steady-state model simulation does not have capability to simulate  $\text{ET}_g$  and  $\text{ET}_{\text{un}}$  separately; as a result high  $\text{ET}_g$  was obtained in the steady state model calibration, i.e.  $0.79 \text{ mm day}^{-1}$  (56.8 % of precipitation); this value can be considered as sub-surface evapotranspiration that incorporates the  $\text{ET}_{\text{un}}$  and  $\text{ET}_g$ .
- The 1 year (2014) model validation confirmed appropriateness of the model calibration and its reliability.
- The experiment comparing two model solutions: a) the one with spatially uniform but temporally variable driving forces with b) the one with spatio-temporally driving forces resulted in  $\Delta S$  and  $\text{ET}_g$  increase by 62.3 % and 61.9 % when comparing a and b solutions respectively and decrease of  $R_g$ ,  $q_g$  and  $\text{Exf}_{\text{gw}}$  by 8.6%, 14.8 % and 36.8 % when comparing a and b solutions respectively. The experiment also showed the spatial variability of input driving forces, enhanced spatial variability of groundwater fluxes (check decrease or increase)
- The model applying stratiform hydrological conceptual model could have been calibrated and with more time available could be calibrated even better so it provides valuable alternative to former solutions with classical conceptual model.

#### 4.2. Recommendation

- The numerical implementation of the stratiform hydrological conceptual model is reliable but more spatio-temporal data and smaller grid size (less than  $100 \times 100 \text{ m}$ ) would make that solution better, enabling to understand better the dynamics of the hard-rock aquifers.
- The time for transient model simulation was very long and restricts for further refinement of the model calibration. However, software and/or hardware modifications to address that problem would enable better model calibration and groundwater budget quantification.

## LIST OF REFERENCES

---

- Abubeker, A. M. (2010). *Hydro-Geophysical Assessment of Sub Surface to Improve Groundwater Models: sardon case study, Spain*. Enschede, University of Twente Faculty of Geo-Information and Earth Observation (ITC).
- Ahmed S., Marechal, J. C., Eledoux, & Marsily, G. d. (2008). Groundwater modeling in hard-rock terrain in semi-arid areas: experience from India. In H. Wheater, S. Sorooshian, & K. D. Sharma (Eds.), *Hydrogeological modeling in arid and semi-arid areas*. Cambridge University Press.
- Ala-aho, P., Rossi, P. M., Isokangas, E., & Kløve, B. (2015). Fully integrated surface-subsurface flow modelling of groundwater-lake interaction in an esker aquifer: Model verification with stable isotopes and airborne thermal imaging. *Journal of Hydrology*, 522, 391–406. doi:10.1016/j.jhydrol.2014.12.054
- Allander, K. K., Niswonger, R. G., & Jeton, A. E. (2014). Simulation of the Lower Walker River Basin Hydrologic System , West-Central Nevada , Using PRMS and MODFLOW Models Scientific Investigations Report 2014 – 5190.
- Allen, R., Pereira, L. S., Raes, D., & Smith, M. (1998). Crop evapotranspiration: Guidelines for computing crop requirements. *Irrigation and Drainage Paper No. 56, FAO*, (56), 300. doi:10.1016/j.eja.2010.12.001
- Anderson, M. P., & Woessner, W. W. (1992). *Applied Groundwater Modeling: Simulation of Flow and Advective Transport*. San Diego: Academic press, INC.
- Bear, A. J., & Cheng, H. D. (2010). *Modeling Groundwater Flow and Contaminant Transport*. London: Springer. doi:0.1007/978-1-4020-6682-5
- Berhe, E. T. (2010). *Improving Groundwater Model Reliability by Coupling Unsaturated and Saturated Models: A case study of Sardon catchment, Spain*. Enschede, University of Twente Faculty of Geo-Information and earth Observation (ITC).
- Courtois, N., Lachassagne, P., Wyns, R., Blanchin, R., Bougairé, F. D., Somé, S., & Tapsoba, A. (2010). Large-scale mapping of hard-rock aquifer properties applied to Burkina Faso. *Ground Water*, 48(2), 269–283. doi:10.1111/j.1745-6584.2009.00620.x
- Dewandel, B., Lachassagne, P., Wyns, R., Maréchal, J. C., & Krishnamurthy, N. S. (2006). A generalized 3-D geological and hydrogeological conceptual model of granite aquifers controlled by single or multiphase weathering. *Journal of Hydrology*, 330(1-2), 260–284. doi:10.1016/j.jhydrol.2006.03.026
- Dewandel, B., Lachassagne, P., Zaidi, F. K., & Chandra, S. (2011). A conceptual hydrodynamic model of a geological discontinuity in hard rock aquifers: Example of a quartz reef in granitic terrain in South India. *Journal of Hydrology*, 405(3-4), 474–487. doi:10.1016/j.jhydrol.2011.05.050

- Doherty, J. (2004). PEST: Model-Independent Parameter Estimation. User Manual, 2005.
- Durand, V., Leonardi, V., Marsily, G., & Lachassagne, P. (2015). The two-layer conceptual model of hard-rock aquifers : validation with a deterministic hydrological model. In *Twentieth technical days of the French Hydrogeology Committee International Association of Hydrogeologists . “ Aquifers base : focus on the concepts and operational applications ”* La Roche-sur-Yon. Retrieved from [http://www.cfh-aih.fr/images/DOCS/2-Colloques/Colloque\\_2015\\_socle\\_la\\_roche\\_sur\\_yon/Actes/R\\_etendus/S3\\_P1\\_N6\\_Durand\\_etal\\_IAH-socle-ext-abstract-V3-GdM.pdf](http://www.cfh-aih.fr/images/DOCS/2-Colloques/Colloque_2015_socle_la_roche_sur_yon/Actes/R_etendus/S3_P1_N6_Durand_etal_IAH-socle-ext-abstract-V3-GdM.pdf)
- Fetter, C., W. (2001). *Applied Hydrology* (Fourth Ed.). New Jersey: Prentice-Hall, Inc.
- Francés, A. P. (2015). *Integration of hydrogeophysics and remote sensing coupled with hydrological models*. Enschede, The Netherlands: ITC PHD dissertation.
- Francés, A. P., Lubczynski, M. W., Roy, J., Santos, F. a. M., & Mahmoudzadeh Ardekani, M. R. (2014). Hydrogeophysics and remote sensing for the design of hydrogeological conceptual models in hard rocks – Sardón catchment (Spain). *Journal of Applied Geophysics*, 110, 63–81. doi:10.1016/j.jappgeo.2014.08.015
- Gerke, H., H., & Van Genuchten, M. T. (1993). Dual Porosity. Pdf. *Water Resources Research*, 29(2), 305–319.
- Harbaugh, B. A. W. (1990). *A Computer Program for Calculating Subregional Water Budgets Using Results from the U . S . Geological Survey Modular Three-dimensional Finite-difference Ground-water Flow Model*. U.S. Geological survey, Open-File Report 90-392. Reston, Virginia.
- Hassan, S. M. T., Lubczynski, M. W., Niswonger, R. G., & Su, Z. (2014). Surface-groundwater interactions in hard rocks in Sardon Catchment of western Spain: An integrated modeling approach. *Journal of Hydrology*, 517, 390–410. doi:10.1016/j.jhydrol.2014.05.026
- Hill, M. (1998). Methods and guidelines for effective model calibration: US Geological Survey Water-Resources Investigations Report 98-4005, 90 p. *US Geological Survey, Water Resources Investigations Report 98-4005*, 1–98. Retrieved from [http://ascelibrary.org/doi/pdf/10.1061/40517\(2000\)18](http://ascelibrary.org/doi/pdf/10.1061/40517(2000)18) \n <http://scholar.google.com/scholar?hl=en&btnG=Search&q=intitle:Methods+and+guidelines+for+effective+model+calibration-U.S.+GEOLOGICAL+SURVEY+WATER-RESOURCES+INVESTIGATIONS+REPORT+98-4005#1>
- Konikow, L. F. (1996). Use of numerical models to simulate groundwater flow and transport. *Ground Water Techniques of Water-Res. Invests. of the U.S. Geol. Survey*, (1996), 75–116.
- Konikow, L. F., & Bredehoeft, J. D. (1992). Groundwater Models Cannot Be Validated. *Advances in Water*

*Resources*, 15(1), 75–83. doi:10.1016/0309-1708(92)90033-x

- Lachassagne, P., Dewandel, B., & Wynes, R. (2014). The conceptual model of weathered hard rock aquifers and its practical applications. In J. M. Sharp (Ed.), *Fractured rock hydrology* (p. 408). CRC Press.
- Lachassagne, P., Sh., A., Dewandel, B., Courtois, N., Lacquement, F., J.C., M., ... R., W. (2008). From a new hydrogeological conceptual model for hard rock aquifers to enhanced practical applications (survey, management of the water resource, modeling, protection, etc.). Retrieved from [http://www.iwra.org/congress/2008/resource/authors/abs506\\_article.pdf](http://www.iwra.org/congress/2008/resource/authors/abs506_article.pdf)
- Lachassagne, P., Wyns, R., & Dewandel, B. (2011). The fracture permeability of Hard Rock Aquifers is due neither to tectonics, nor to unloading, but to weathering processes. *Terra Nova*, 23(3), 145–161. doi:10.1111/j.1365-3121.2011.00998.x
- Lubczynski, Maciek, W., & Gurwin, J. (2005). Integration of various data sources for transient groundwater modeling with spatio-temporally variable fluxes—Sardon study case, Spain. *Journal of Hydrology*, 306(1-4), 71–96. doi:10.1016/j.jhydrol.2004.08.038
- Mason, D., & Hipke, W. (2013). Regional groundwater flow model of the Tucson Active Management Area, Arizona, (24), 97. Retrieved from <http://www.azwater.gov/azdwr/default.aspx>
- Massuel, S., George, B., Gaur, A., & Nune, R. (2007). Groundwater Modeling for Sustainable Management in the Musi Catchment , India Resource. *MODSIM-2007, Christchurch*, 1429–1435.
- McMahon, T. A., Peel, M. C., Lowe, L., Srikanthan, R., & McVicar, T. R. (2013). Estimating actual, potential, reference crop and pan evaporation using standard meteorological data: a pragmatic synthesis. *Hydrology and Earth System Sciences*, 17(4), 1331–1363. doi:10.5194/hess-17-1331-2013
- Meijerink, A. M. J., Lubczynski, M., & Wolski, P. (1999). Remote sensing, hydrological analysis and hydrotopes. *Regionalization in Hydrology, LAHS*.
- Navarro, P. G., & Playan, E. (2007). *Numerical Modelling of Hydrodynamics for Water Resources: Proceedings of the Conference on Numerical Modelling of Hydrodynamic Systems (Zaragoza, Spain, 18-21 June 2007)* (Vol. 1). CRC Press. Retrieved from <https://books.google.com/books?id=GPEKQhfZhuQC&pgis=1>
- Niswonger, R. G., Panday, S., & Ibaraki, M. (2011). MODFLOW-NWT , A Newton Formulation for MODFLOW-2005. *Ground Water - Modeling Techniques*, 56.
- Niswonger, R. G., & Prudic, D. E. (2005). Documentation of the Streamflow-Routing (SFR2) Package to Include Unsaturated Flow Beneath Streams—A Modification to SFR1. *U.S. Geological Survey*, (Techniques and Methods 6-A13), 50. Retrieved from <http://pubs.er.usgs.gov/publication/tm6A13>
- Niswonger, R. G., Prudic, D. E., & Regan, S. R. (2006). Documentation of the Unsaturated-Zone Flow

(UZF1) Package for Modeling Unsaturated Flow Between the Land Surface and the Water Table with MODFLOW-2005. *Book 6, Modeling Techniques, Section A, Ground Water*, 71.

Nyende, J., Van, T., & Vermeulen, D. (2013). Conceptual and Numerical Model Development for Groundwater Resources Management in a Regolith-Fractured-Basement Aquifer System. *J Earth Sci Clim Change*, 4(5). doi:10.4172/2157-7617.1000156

Pereira, F. L., Gash, J. H. C., David, J. S., David, T. S., Monteiro, P. R., & Valente, F. (2009). Modelling interception loss from evergreen oak Mediterranean savannas: Application of a tree-based modelling approach. *Agricultural and Forest Meteorology*, 149(3-4), 680–688. doi:10.1016/j.agrformet.2008.10.014

Reilly, B. T. E., & Harbaugh, A. W. (1999). Guidelines for Evaluating Ground-Water Flow Models Different Modeling Approaches to Address. Retrieved from <http://pubs.usgs.gov/sir/2004/5038/PDF/SIR20045038part2.pdf>

Reyes-Acosta, J. L., & Lubczynski, M. W. (2013). Mapping dry-season tree transpiration of an oak woodland at the catchment scale, using object-attributes derived from satellite imagery and sap flow measurements. *Agricultural and Forest Meteorology*, 174–175, 184–201. doi:10.1016/j.agrformet.2013.02.012

Ruwan Rajapakse, R. R. G. (2009). *Numerical Groundwater Flow and Solute Transport Modelling : A Case Study of Sardon Catchment in Spain*. Enschede, ITC. Retrieved from [http://www.itc.nl/library/papers\\_2009/msc/wrem/rajapakse.pdf](http://www.itc.nl/library/papers_2009/msc/wrem/rajapakse.pdf)

Rwarinda, E. (1996). *Hydrological investigation in Sardon catchment; a part of the lower Rio Tormes basin, Salamanca province, Spain*. MSc,ITC.

Sekhar, M., Mohan Kumar, M. S., & Sridharan, K. (1994). A Leaky Aquifer Model For Hard Rock Aquifers. *Hydrogeology Journal*, 2(3), 32–39. doi:10.1007/s100400050039

Shah, N., Nachabe, M., & Ross, M. (2007). Extinction depth and evapotranspiration from ground water under selected land covers. *Ground Water*, 45(3), 329–338. doi:10.1111/j.1745-6584.2007.00302.x

Shikhar Kumar. (2011). What are Hard Rock Aquifers? Retrieved January 1, 2015, from <http://www.waterandmegacities.org/what-are-hard-rock-aquifers/>

Sophocleous, M. (2002). Interactions between groundwater and surface water: The state of the science. *Hydrogeology Journal*, 10(1), 52–67. doi:10.1007/s10040-001-0170-8

Sophocleous, M. (2005). Groundwater recharge and sustainability in the High Plains aquifer in Kansas, USA. *Hydrogeology Journal*, 13(2), 351–365. doi:10.1007/s10040-004-0385-6

Taylor, R., & Howard, K. (2000). A tectono-geomorphic model of the hydrogeology of deeply weathered crystalline rock: evidence from Uganda. doi:10.1007/s100400050015

- Tesfai, B. H. (2000). *Subsurface characterization of Granitic basement from structural and resistivity data: A case study from sardon catchment area, Salamanca, Spain*. University of Twente faculty of Geo-information and Earth Observation (ITC).
- Varalakshmi, V., Rao, B. V., SuriNaidu, L., & Tejaswini, M. (2012). Ground Water Flow Modelling of an Hard Rock Aquifer - a Case Study. *Journal of Hydrologic Engineering*, 430. doi:10.1061/(ASCE)HE.1943-5584.0000627
- Virdi, M. L., Lee, T. M., Swancar, A., & Niswonger, R. G. (2013). Simulating the effect of climate extremes on groundwater flow through a lakebed. *Ground Water*, 51(2), 203–18. doi:10.1111/j.1745-6584.2012.00969.x
- Wang, Y. L., Wang, X., Zheng, Q. Y., Li, C. H., & Guo, X. J. (2012). A Comparative Study on Hourly Real Evapotranspiration and Potential Evapotranspiration during Different Vegetation Growth Stages in the Zoige Wetland. *Procedia Environmental Sciences*, 13(2011), 1585–1594. doi:10.1016/j.proenv.2012.01.150
- Winston, R. B. (2000). Graphical User Interface for MODFLOW , Version 4: Open-File Report 00-315, 34.
- Winston, R. B. (2009). ModelMuse: A Graphical User Interface for MODFLOW-2005 and PHAST: U.S. Geological Survey Techniques and Methods 6–A29, 52. Retrieved from <http://pubs.usgs.gov/tm/tm6A29/tm6A29.pdf>
- Winston, R. B., & Paulinski, S. (2014). ListingAnalyst: A Program for Analyzing the Main Output File from MODFLOW. *Groundwater*, 52(2), 317–321. doi:10.1111/gwat.12054
- Wu, J., & Zeng, X. (2013). Review of the uncertainty analysis of groundwater numerical simulation. *Chinese Science Bulletin*, 58(25), 3044–3052. doi:10.1007/s11434-013-5950-8
- Wyns, R., Baltassat, J. E. a N. I., Lachassagne, P. A., & Legchenko, a N. (2004). Application of proton magnetic resonance soundings to groundwater reserve mapping in weathered basement rocks ( Brittany , France ). *Bull. Soc. Géol. France*, 175(August 2015), 21–34. doi:10.2113/175.1.21
- Yao, Y., Zheng, C., Liu, J., Cao, G., Xiao, H., Li, H., & Li, W. (2015). Conceptual and numerical models for groundwater flow in an arid inland river basin. *Hydrological Processes*, 29(6), 1480–1492. doi:10.1002/hyp.10276

# APPENDICES

---

Appendix 1: Some photos from study site

